PREDICTING EMISSIONS USING AN ON-ROAD VEHICLE PERFORMANCE SIMULATOR

Prabeshan Govindasamy

Submitted in partial fulfilment
of the requirements for the degree of
MScEng.

School of Bioresources Engineering and Environmental Hydrology
University of Natal
Pietermaritzburg

2002

ABSTRACT

South Africa is coming under increasing pressure to conform to the rest of the world in terms of emissions regulations. The pressure is caused by a number of factors: international organisations requiring local companies to adhere to environmental conservation policies, evidence from within South Africa that efforts are being made to reduce environmental pollution in line with other countries and keeping abreast of the latest technologies that have been incorporated into vehicles to reduce emissions.

In light of these problems associated with emissions, a study was initiated by the Department of Transport and the School of Bioresources Engineering and Environmental Hydrology at the University of Natal to investigate and develop a method of predicting emissions from a diesel engine. The main objective of this research was to incorporate this model into SimTrans in order to estimate emissions generated from a vehicle while it is travelling along specific routes in South Africa. SimTrans is a mechanistically based model, developed at the School, that simulates a vehicle travelling along a route, requiring input for the road profile and vehicle and engine specifications.

After a preliminary investigation it was decided to use a neural network to predict emissions, as it provides accurate results and is more suitable for a quantitative analysis which is what was required for this study. The emissions that were predicted were NOx (Nitric oxide-NO and Nitric dioxide-NO_2), CO (carbon monoxide), HC (unburnt hydrocarbons) and particulates. The neural network was trained on emissions data obtained from an ADE 447Ti engine. These neural networks were then integrated into the existing SimTrans. Apart from the neural network, an algorithm to consider the effect of ambient conditions on the output of the engine was also included in the model. A sensitivity analysis was carried out using the model to prioritise the factors affecting emissions. Finally using the data for the ADE 447Ti engine, a trip with a Mercedes Benz 2644S-24 was simulated using different scenarios over the routes from Durban to Johannesburg and Cape Town to Johannesburg in South Africa to quantify the emissions that were generated.

I wish to certify that the work reported in this dissertation is my own unaided work except where specific acknowledgement is made. In addition I wish to declare that this dissertation has not been submitted for a degree in any other university.

Signed : 

P. GOVINDASAMY

Acknowledgements

The author wishes to record his sincere appreciation for the assistance given by the following:

Professor P.W.L. Lyne, Head of the School of Bioresources Engineering and Environmental Hydrology, University of Natal, for the supervision of this project.

Doctor A.C. Hansen, Department of Agricultural Engineering, University of Illinois at Urbana-Champaign, for assistance, support, invaluable advice and co-supervising this project.

Doctor C.E. Goering, Department of Agricultural Engineering, University of Illinois at Urbana-Champaign, for his assistance, advice and sharing his expertise.

Dr. A.B. Taylor, Head of the Centre for Automotive Engineering, University of Stellenbosch, for his advice and the use of the CAE diesel engine testing facility.

Mr. A.J. Bell, Centre for Automotive Engineering, University of Stellenbosch, for his assistance and advice.

Mr A. Stone, Centre for Automotive Engineering, University of Stellenboscch, for his assistance in performing the engine and emissions testing at CAE.

Mr. D.J. Clark, School of Bioresources Engineering and Environmental Hydrology, University of Natal, for his assistance in Delphi programming.

Mr. A. Hill, School of Bioresources Engineering and Environmental Hydrology, University of Natal, for his assistance and advice.

The Eastern Centre of Transport Development (ECOTD) for funding this project.

My family and friends for their encouragement and moral support during my studies.

TABLE OF CONTENTS

LIST OF TABLES

LIST OF FIGURES

1. INTRODUCTION

South Africa is coming under increasing pressure to conform to the rest of the world in terms of emissions regulations. The pressure is caused by a number of factors: international organisations requiring local companies to adhere to environmental conservation policies, evidence from within South Africa that efforts are being made to reduce environmental pollution in line with other countries and keeping abreast of the latest technologies that have been incorporated into vehicles to reduce emissions.

In the light of these problems associated with emissions a study was initiated by the Department of Transport and the School of Bioresources Engineering and Environmental Hydrology at the University of Natal with the objective of investigating and developing a method for predicting emissions from diesel vehicles generated over specific routes in South Africa. This tool has been incorporated into SimTrans (vehicle simulator) and may be used to assess the problem of diesel emissions in South Africa. At present there is no legislation for emissions regulations in South Africa, and this model can be used to determine the need for them.

The emissions that are regulated internationally are NOx (Nitric oxide - NO and nitrogen dioxide-NO_2), carbon monoxide (CO), particulates, and unburnt hydrocarbons (HC). The most serious of these emissions are NOx and particulates, and most research has been aimed at reducing these emissions simultaneously, as there exists a trade-off between them. There is a need for a quantitative analysis of these emissions and the proposed model will have many applications for fleet operators as well as environmentalists.

There are different ways of predicting emissions, the most common being combustion-emissions models and regression models. Combustion-emissions models are very complicated and are mostly restricted to a qualitative analysis. Regression models are common, not necessarily for emissions modelling, but for modelling in general. After reviewing the different modelling approaches, a new method of modelling using neural networks was selected.

A back propagation neural network was used for each of the four emissions. Training the neural networks was an important part of the modelling procedure. This involved a trial and error analysis to obtain the best model. SimTrans needed to be modified to accommodate the neural network, however before this could be done the model had to be verified by testing the neural network on a separate set of data. Emissions data was obtained for an ADE 447Ti engine.

It was also decided to modify SimTrans to adapt to ambient conditions. These conditions included ambient temperature and pressure. Ambient pressure is important, as it is very dependent on altitude, which varies substantially across the country. Temperature was estimated using a temperature profile that was derived empirically. The torque available from the engine was then adjusted using an ambient condition correction factor obtained from the literature.

Once the neural network and the ambient correction factor was incorporated into SimTrans, the sensitivity of the model to the different operating conditions had to be made. Finally the model was used on a Mercedes Benz 2644S-24 to predict emissions on routes from Durban to Johannesburg and from Cape Town to Johannesburg.

2. DIESEL ENGINES AND EMISSIONS

The diesel engine has been arguably one of the most significant inventions of the 20th century. The high efficiency associated with diesel engines coupled with its durability and reliability guarantees Dr. Rodolf Diesel's invention as the best liquid fuel burning prime mover ever derived (Lilly, 1984). However the major disadvantage of diesel engines lies in its emissions.

Growing concerns over the effects of emissions from diesel engines have prompted legislation to regulate these emissions. Most countries world-wide have thus imposed strict regulations on the emissions of NOx, particulates, unburnt hydrocarbons (HC) and carbon monoxide (CO). South Africa is now coming under increasing pressure to conform to the rest of the world in terms of these regulations.

NOx and particulates, in particular, are of major concern and usually receive the most attention. Most efforts to reduce one of these emissions usually result in an increase in the other. Diesel particulate emissions are the focal point of most health investigations, as it is believed to contain known carcinogens and mutagens. NOx on the other hand is the cause of photochemical smog and also contributes to acid rain when it reacts with atmospheric ozone (Mullins, 1991).

Exhaust emissions from a diesel engine are highly dependent on the combustion process, which is greatly influenced by the design of the combustion chamber and the fuel injection parameters. However, due to the complex interactions that occur between these two processes, the formation of emissions is still not fully understood (Gardner, 1992).

The emissions problem combined with the growing concern with the depleting crude-oil reserves has generated investigations into the use of alternative fuels. The production of alternative fuels has associated with it, a high cost, but will be justified if it can be competitive as a renewable source of environmentally friendly fuel. Synthetic fuels have been shown to reduce all regulated emissions. Apart from synthetic fuels, research has also been done on alcohol and biodiesel blended fuels.

Ambient conditions, especially pressure, which is dependent on altitude, have a major influence on emissions. South Africa is especially vulnerable as the variation of altitude, over which diesel powered vehicles operate, ranges from sea-level up to approximately 1800m (Hansen *et al.*, 1990). Ambient temperature and humidity have also been shown to affect emissions.

Before trying to understand how diesel emissions are formed an understanding of diesel combustion is required. Diesel combustion is based on compression ignition and differs from spark ignition as is explained in the following section.

2.1 Compression-Ignition (CI) Engines

Compression ignition engines do not depend on a spark for ignition. What distinguishes them from spark ignition engines is that they depend entirely on the fuel to ignite spontaneously when conditions within the combustion chamber (cylinder) are conducive. Compression ignition engines operate on high compression ratios typically between 16:1 and 23:1 which accounts for their high efficiency.

In the CI engine, air is inducted into the cylinder at atmospheric pressure until the piston passes bottom-dead centre (BDC), upon which time the inlet valve closes and compression commences (Figure 1). Fuel (diesel) is then injected into the cylinder near the end of the compression stroke, i.e., near top-dead centre (TDC) when the temperature and pressure are high enough for the fuel to autoignite. The combustion of fuel causes a rapid increase in pressure which forces the piston downward (power stroke). The cycle is then ended by an exhaust stroke when the burnt gases are forced through an open exhaust valve.

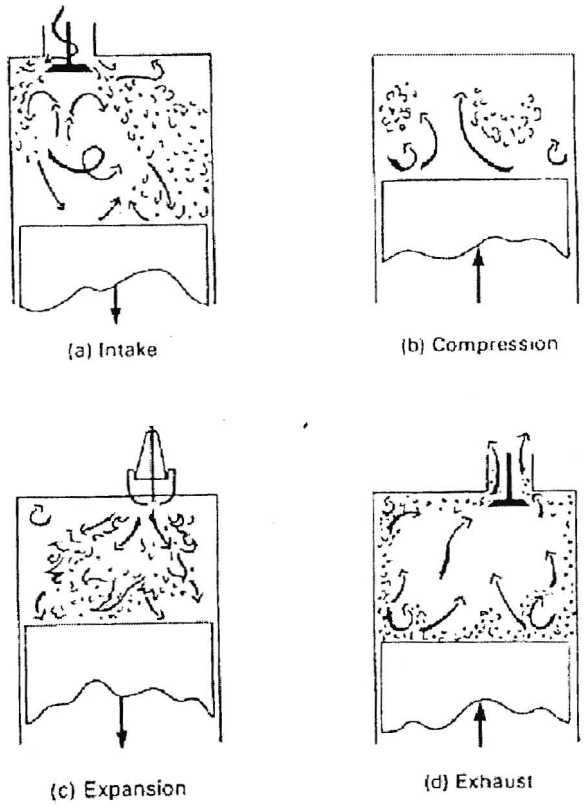

Figure 1 Flow structure in a compression ignition engine, (after Reynolds, 1978)

Combustion does not start instantaneously upon injection. This time lapse is referred to as the ignition delay (Figure 2). The initial spontaneous combustion which causes a rapid increase in pressure and temperature in the cylinder is called the premixed combustion phase which is followed by a slow, rate dependent combustion phase known as the diffusion combustion phase (mixing-controlled combustion phase).

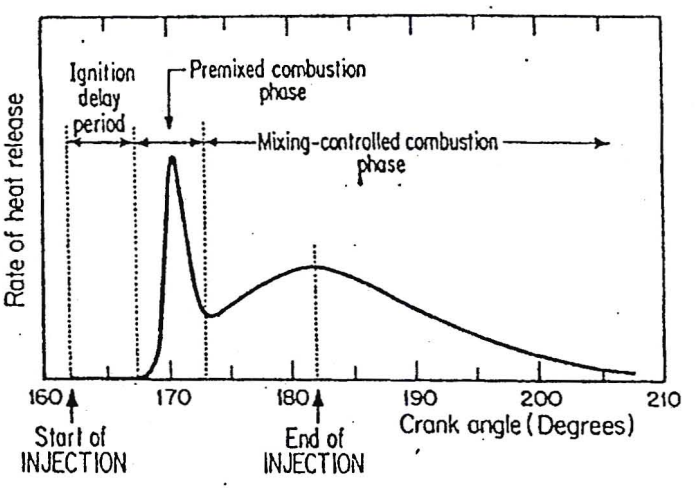

Figure 2 Typical heat release rate for diesel combustion, (Balles and Heywood, 1988)

2.1.1 Ignition-delay period

The ignition-delay period can be further classified into a physical delay period and a chemical delay period known collectively as preparation (Taylor, 1987). The physical delay is responsible for processes including break-up, atomisation, evaporation, and mixing of the fuel molecules (Kamimoto and Kobayashi, 1991). The chemical delay is the time required for the reactions between the fuel and air to occur which are necessary for the mixture to ignite under the necessary conditions (Taylor, 1987).

2.1.2 Premixed combustion

Once the fuel and air have mixed to within combustible limits, the cylinder pressure increases rapidly as combustion occurs. Since the fuel-air mixture is heterogeneous, combustion will only occur in those regions where the mixture is fully prepared. As there is no progressive flame front, all the premixed fuel burns almost simultaneously (Taylor, 1979). Premixed combustion will continue rapidly until all the prepared fuel is consumed. It is thus evident that with extended ignition delay extremely high rates of heat release can occur during premixed combustion. The duration of premixed combustion is short and this form of combustion yields minimal luminosity, radiation

and offensive emissions (Taylor, 1987). The mass of premixed burning increases with factors that increase mixing rate like high air swirl, high rates of fuel injection and the use of multi-hole injectors (Kamimoto and Kobayashi, 1991).

2.1.3 Diffusive combustion

In premixed combustion preparation processes occur at successive stages in time. In diffusion combustion, however, the successive processes occur in separate physical zones. The diffusion flame completely surrounds the fuel droplets and pre-combustion reactions of the evaporated fuel occur in a zone between the droplet and flame (Taylor, 1987).

In contrast to premixed combustion, the pre-combustion reactions of diffusion combustion occur prior to the mixing of fuel and air. Heat released during premixed combustion causes pressures and temperatures involved in diffusion combustion to be far higher than those involved in premixed combustion. The result of this combined with radicals already released is that the ignition delay for diffusion combustion is only a fraction of that for premixed combustion (Edwards, 1977). Diffusive combustion is controlled by the rate of mixing of air and fuel (Balles and Heywood, 1988). Rate of mixing is influenced by charge motion and turbulent mixing (Balles and Heywood, 1988; Kamimoto and Kobayashi, 1991). Diffusive combustion continues until all the fuel has been burnt and is followed by the exhaust stroke when all the burnt products are evacuated from the cylinder.

2.2 Diesel Emissions

The emissions that are of particular concern are NOx, particulates, unburnt hydrocarbons (HC) and to a lesser extent carbon monoxide (CO). These emissions are hence regulated in most countries throughout the world.

2.2.1 NOx emissions

While nitric oxide (NO) and nitrogen dioxide (NO_2) are usually grouped together as NOx emissions, nitric oxide is the predominant oxide of nitrogen produced inside the engine cylinder. NO_2 contributes between 10-30% of the total exhaust oxides of nitrogen emissions (Heywood, 1988). According to Lilly (1984) the Zeldovich mechanism can be taken as controlling the emission of nitric oxide from diesel engines. Heywood (1988) suggests that the formation of NO from molecular nitrogen based on the extended Zeldovich mechanism is defined by the following reactions:

$$O + N_2 \overset{k_1^{+/-}}{\longleftrightarrow} NO + N$$

$$N + O_2 \overset{k_2^{+/-}}{\longleftrightarrow} NO + O$$

$$N + OH \overset{k_3^{+/-}}{\longleftrightarrow} NO + H$$

The forward and reverse rate constants (k_1+/-) for these reactions have been measured in numerous experimental studies. Heywood (1988) provides a table of values determined from a critical review of published data. This mechanism is highly dependent on temperature and hence NOx is predominantly formed in the early stages of combustion (premixed combustion) where peak temperatures and pressures are reached (Lilly, 1984). Figure 3 shows how the ratio of the average cylinder NO concentration to exhaust NO concentration varies during the combustion process. NO concentrations reach a maximum shortly after the time of peak pressure. Heywood (1988) also reports that results from similar cylinder dumping experiments where injection timing and load were varied also showed that almost all of the NO forms within the 20 degrees following the start of combustion.

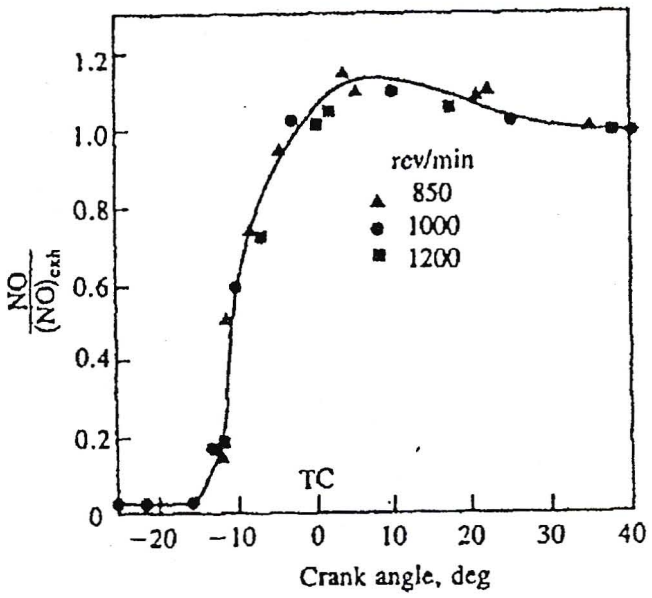

Figure 3 Ratio of cylinder-average NO concentration at given crank angle to exhaust NO concentration, (Heywood, 1988)

2.2.2 Particulates

Diesel particulates consist principally of combustion generated carbonaceous material (soot) on which some organic compounds have become absorbed. It is a mixture of carbon and heavy hydrocarbons, arising from incomplete combustion of the fuel, together with traces of sulphuric acid arising from the sulphur from the fuel. Apart from soot, particulates also consist of a soluble organic fraction (SOF). The soluble organic fraction is extracted during the dilution process and includes compounds that may cause health and environment hazards. Diesel exhaust smoke is related to the amount of light attenuated by particles present in the raw or undiluted exhaust and is perceived by the eye in 'blackness'. According to Heywood (1988) the processes illustrated in Figure 4 define the formation of diesel particulates. Initially carbon particles are produced which are called nuclei. Surface growth of these nuclei then takes place, this occurs when unburnt hydrocarbons and sulphates become absorbed on the nuclei to form spherules. Agglomeration of the spherules takes place to form larger particles. Finally adsorbtion and condensation occurs in the atmosphere and this is simulated in a dilution tunnel. Oxidation occurs throughout the formation of particulates and is responsible initially for oxidising about 90% of the soot formed.

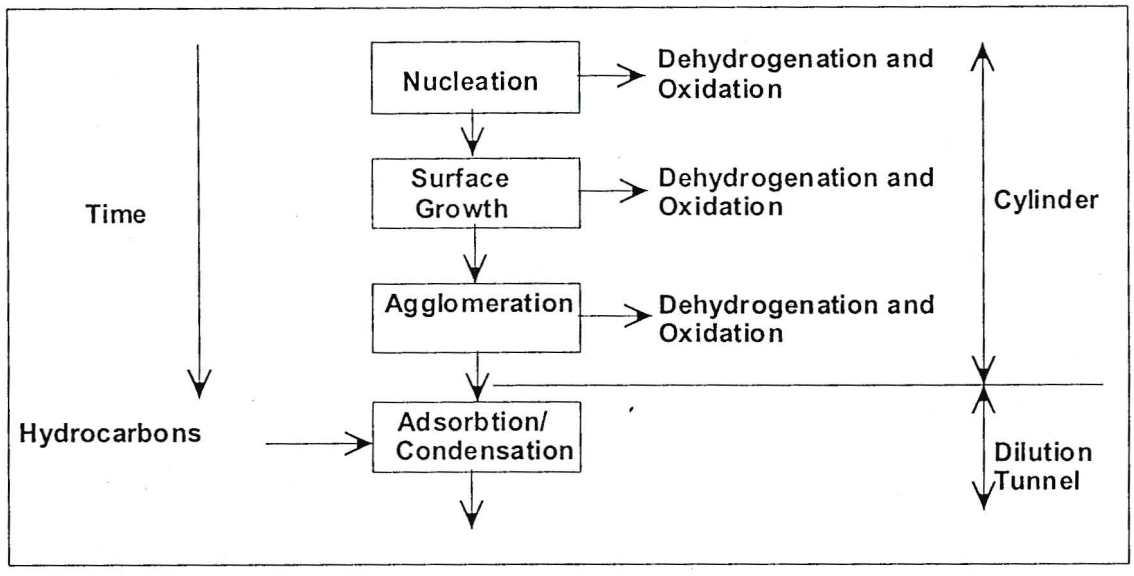

Figure 4 Processes leading to net production of diesel particulates, (after Heywood, 1988)

Diesel particulates are of special concern in possible health outcomes; they are small enough to be readily respirable (90% are less than 1μm by diameter), and they have many chemicals adsorbed to their surfaces, including known or suspected mutagens and carcinogens (Mundt *et al.*, 1999).

Studies have investigated the association between exposure to diesel particulates and adverse health effects, including cancer. Investigations performed on rats exposed to diesel exhaust emissions have resulted in tumours, and the risk to humans has been questioned. An elevation in lung cancer rates among occupationally exposed individuals has been shown to be 20-50% higher than those that weren't (Nauss, 1995). However, questions have been raised by the Health Effects Institute (HEI) as to whether the human data can be used for quantitative risk assessment. Studies in this field are continually being pursued and there is rising concern over the effects of particulates from diesel engines, therefore these emissions will receive attention from health institutions, governments and engine manufacturers.

2.2.3 Unburnt hydrocarbons (HC)

Diesel fuel contains hydrocarbon compounds with higher molecular weights and hence higher boiling points than gasoline. Since substantial pyrolysis of fuel compounds occurs within the fuel sprays, the composition of the unburnt and partially oxidised hydrocarbons in the diesel exhaust is very complex. There are two major causes of HC emissions in diesel engines under normal operating conditions (Heywood, 1988):

1) fuel mixed to leaner than the lean combustion limit during the ignition delay period;
2) under-mixing of fuel which results in the fuel-air mixture being too rich to ignite or support a flame.

Over-mixing (over-leaning) is an important source of HC, especially under light load operation. As injection commences the amount of fuel that is mixed leaner than the lean combustion limit, increases. This mixture will be too lean to autoignite and combustion will be incomplete. These hydrocarbons will thus escape from the cylinder unburned. The magnitude of the unburned HC from these over-lean regions will depend on the amount of fuel injected during the ignition delay period, the mixing rate with air during this period and the extent to which prevailing cylinder conditions are conducive to autoignition (Heywood, 1988).

Lilly (1984) suggests that over-fuelling (under-mixing) occurs as a result of secondary injections and high nozzle sac volumes. Secondary injections occur when fuel is injected late in the expansion stroke due to wave effects in the fuel line. This fuel mixes slowly and as a result will leave the cylinder unburnt. Fuel that also escapes the primary combustion phase is that volume of fuel that is trapped in the injector sac volume (Heywood, 1988). Figure 5 shows the relationship between exhaust HC and nozzle sac volume. The extrapolation to zero indicates that the fuel that is trapped in the nozzle holes also contributes to unburnt hydrocarbons.

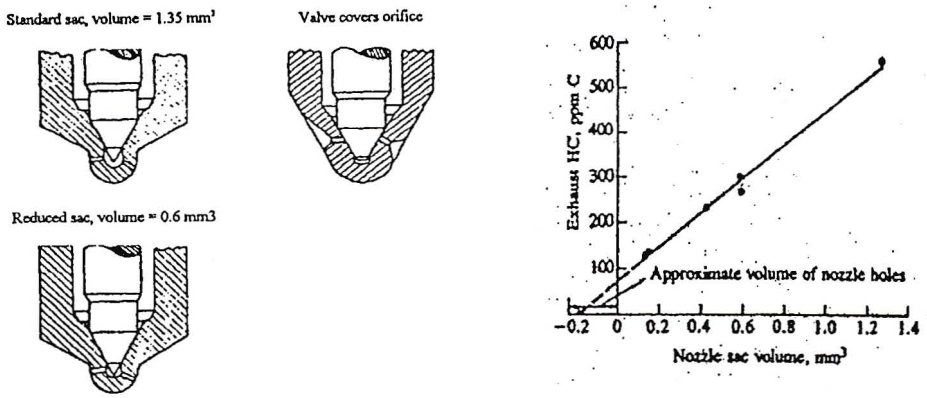

Figure 5 Effect of nozzle sac volume on exhaust HC concentration, (after Heywood, 1988)

2.2.4 Carbon monoxide (CO)

CO emissions result from incomplete combustion of the fuel. Diesel engines always operate on excess air and as a result CO emissions are lower than their gasoline counterpart. Diesel engines therefore have little difficulty in meeting legislated levels (Lilly, 1984).

2.2.5 Unregulated emissions

The emissions, NOx, particulates, HC and CO are all regulated emissions (i.e. they are covered by legislation in most countries excluding South Africa), however, due to constituents other than hydrogen and carbon in the fuel, and the different chemical species in the atmosphere, there are other emissions that are unregulated. These include sulphur oxides, aldehydes, ammonia, benzene, polycyclic aromatic hydrocarbons (PAH) and nitropolycyclic aromatic hydrocarbons (Lilly, 1984). Sulphur oxides comprise sulphur dioxide (SO_2) and sulphur trioxide (SO_3). They arise from the sulphur content in the fuel. These emissions can react with water vapour in the atmosphere to form acid rain. Aldehydes are formed by incomplete combustion. They are considered to be odorous and irritants. Some PAH emissions are known to be carcinogenic. All of these

emissions can become absorbed on carbon atoms to form particulates, otherwise in their normal state they are not of particular concern (Heywood, 1988).

2.3 Factors Affecting Emissions

Diesel emissions are affected by various factors. The most important being the fuel injection system, type of fuel and ambient conditions. Understanding these parameters and how they affect emissions is imperative to the process of predicting emissions.

2.3.1 Fuel injection system

Exhaust emissions from a diesel engine are highly dependent on the combustion process which is greatly influenced by the fuel injection system (Gardner, 1992). Injection pressure, timing and duration of injection pulses, number of injectors, swirl ratio, number of holes in injector nozzle, and the diameter of the holes are parameters associated with the fuel injection system, and have to be optimized to improve air-fuel mixing which is necessary for the reduction of exhaust emissions (Uchida *et al.,* 1992).

Often changes in fuel injection parameters, which result in the improvement of one emission characteristic, may result in the deterioration of another. For example, high injection pressures, small spray hole diameters and high swirl will achieve good fuel atomisation and lower particulates, but will usually result in higher NOx emissions (Gardner, 1992). In much the same way retarding the start of injection will reduce NOx emissions and advancing will reduce particulates, but only with a corresponding increase in the other pollutants (Montgomery and Reitz, 1996). Due to this trade-off that exists, an optimum solution needs to be achieved between all the parameters in order to reduce all the emissions.

Researchers have opted for a multi-injector system to eradicate the trade-off characteristics of particulates and NOx. Montgomery and Reitz (1996) used a common rail injector system capable of four independent injection pulses per combustion event. The NOx -particulate trade-off curves were shifted closer to the origin by increasing the number of injections. Han *et al.* (1996) used a similar system to Montgomery and Reitz

(1996), and obtained comparable results. Figure 6 shows trade-off curves for a single and double injection with 75% of the fuel injected during the first pulse followed by the rest of the fuel injected in the second pulse after an 8 degree crank angle delay. Takeda and Niimura (1995) also studied a multi-injector system but used a three injector system, one mounted vertically on the centre of the cylinder head and the other two diagonally from the side. This configuration was used to control the spatial and temporal variation of fuel into the combustion chamber. They also achieved similar results.

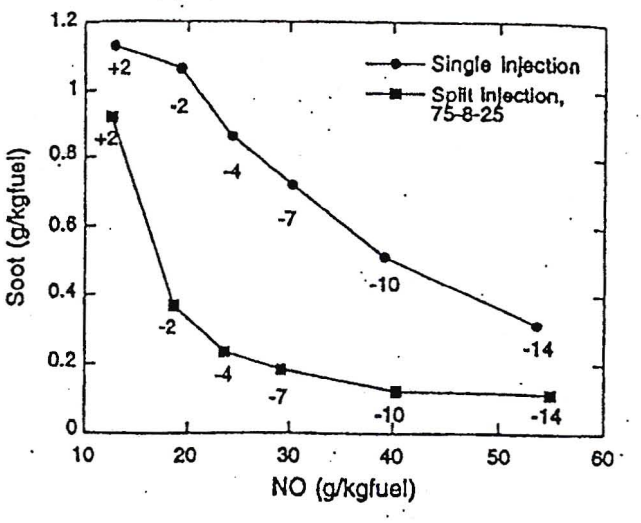

Figure 6 Soot-NO trade-off showing emission reduction using split injections, (Han et al., 1996)

The number of injector holes and the diameter influences the air-fuel mixing rate and this has a significant influence on emissions. Lipkea *et al.* (1987) showed an unlikely decrease in NOx ratio (ratio of NOx produced and the baseline results) with an increase in the number of holes, however, investigations performed by Gardner (1992) showed an increase in NOx emissions and a corresponding decrease in particulates as one would expect.

Air swirl has the most directly observable influence on the combustion process and the resulting emissions through its effect on fuel-air mixing. Increased air swirl generally reduces particulates, hydrocarbons and smoke, but often results in higher NOx (Gardner, 1992). Swirl is induced during the intake stroke and air is forced to flow in a circular motion due to the geometry of the inlet port which in most cases takes the form

of a directed port or a helical port. The valve stem acts as an axis for the swirl motion. The swirl level is influenced by the angle of the port to the cylinder head (Hansen, 1989).

2.3.2 Supercharging

The purpose of supercharging is to increase the mass of air trapped in the cylinder of the engine by raising its density. This allows more fuel to be burnt, increasing the power output of the engine for a given swept volume of the cylinders (Lilly, 1984).

Air density is raised by means of a compressor. There are two ways a compressor can be driven: one is when it derives power directly from the crankshaft (supercharging), and the other method is when it is driven by a turbine that receives energy from the exhaust stream (turbocharging).

Supercharging reduces the ignition delay during the combustion process, which reduces the peak value of heat release rate during the premixed combustion phase and a growth in the early part of the diffusion combustion phase occurs. This is because more of the fuel burns in the diffusion combustion phase due to the increased amount of charge (Uchida *et al.*, 1992). Uchida *et al.* (1992) also noted that supercharging reduces all emissions except NOx, which is not surprising as supercharging, apart from raising the air density also aims to improve the air-fuel mixing process. However, as NOx is temperature driven, cooling the air from the turbocharger before it enters the cylinder (intercooling) can be used to reduce it.

2.3.3 Fuel type

The emissions problem combined with the growing concern with the depleting crude-oil reserves has initiated investigations into the use of alternative fuels. Some of these fuels have advantages over conventional diesel in terms of emissions and coupled with the fact that they will do much to relieve the strain on existing crude-oil resources, makes them invaluable in future diesel engine development.

2.3.3.1 Biodiesel blended fuels

Biodiesel is an alternative renewable source of fuel that may help in reducing the net production of CO_2 and dependence on crude oil. The methyl esters of vegetable oils, which are produced by combining methanol with the vegetable oil are of particular interest. These fuels tend to burn cleaner, perform comparably to conventional diesel fuel, and combust similarly as well. The monoester of vegetable oils is produced by combining a vegetable oil with an alcohol, in particular, the more popular methyl ester of soybean oil, also commonly known as biodiesel, is made by combining soybean oil with methanol (Scholl and Sorenson, 1993, cited by Choi and Reitz, 1999).

Choi and Reitz (1999) performed studies to investigate the effects of increasing biodiesel concentrations on emissions. They used a 20% and 40% blend of biodiesel and diesel and an unblended diesel. Due to the increased fuel viscosity, shorter fuel injection duration for the biodiesel-blended fuels was required. The results showed a decrease in soot concentration (particulates) but no significant change in NOx. Clark *et al.* (1999) performed similar investigations, and their results showed the expected trade-off characteristic between particulates and NOx.

2.3.3.2 Alcohol blended fuels

The alcohols that are used in alcohol-diesel blends are typically ethanol and methanol. Since the ignition performance of alcohol blended fuels are inferior to the conventional diesel fuel, they are more difficult to use in diesel engines as compared to gasoline engines (Weidman and Menrad, 1984).

Ethanol and methanol have poor cetane ratings and lack lubricity to preserve the life of a high pressure injection system and therefore cannot be used directly in an unmodified diesel engine (Clark *et al.*, 1999). Studies performed on diesel engines run on alcohol blended fuel showed reductions in NOx and particulates, but increases in CO and HC (Weidmann and Menrad, 1984; Clark *et al.*, 1999).

2.3.3.3 Synthetic fuels

Synthetic diesel fuel can be made from a variety of feedstock, including coal, natural gas and biomass. Synthetic diesel fuels can have very low sulphur and aromatic content and excellent autoignition characteristics (Norton *et al.*, 1999). Sasol diesel fuel is a synthetic diesel and is processed using the Sasol Slurry Phase Distillate process in South Africa. In this process coal derived synthesis gas is reformed to produce carbon monoxide and hydrogen, which is then converted into heavy hydrocarbons by means of a Fischer-Tropsch process employing metal catalysts (Clark *et al.*, 1999).

Generally synthetic diesel fuels have favourable characteristics for use in compression-ignition engines. They can be used in an unmodified diesel engine, are liquids at ambient conditions, have low sulphur and aromatics content, have energy densities comparable to conventional diesel and good autoignition characteristics (Norton *et al.*, 1999).

Table 1 and Table 2 summarise the results obtained by Clark *et al.* (1999) from investigations performed on an engine run on diesel A and B with different cetane ratings, biodiesel (BD) with different percentages of biodiesel blends, Fischer-Tropsch derived synthetic fuel from Malaysia (F-T), Mossgas (MG) derived synthetic fuel using Fischer-Tropsch methods, and a California diesel (CA Diesel). Table 2 illustrates the significance of the synthetic fuels in reducing all emissions including both particulates and NOx, over the conventional diesel fuels.

Table 1 Properties of fuels used by Clark *et al.*, (1999)

Fuel Designation	**Fuel Type**	**Density kg/l**	**Total Sulphur weight %**	**Cetane No.**	**Aromatics weight %**	**Oxygen weight %**
Diesel A	Off-road diesel	0.8520	0.04	48.80	29.30	~0
BD 20	80% diesel A and 20% BD	0.8580	0.03	49.40	23.44	2.20
BD 50	50% diesel A and 50% BD	0.8680	0.02	50.30	14.65	5.50
BD 100	Nopec Biodiesel (BD)	0.8840	0.00	51.8	0.0	11.0
Diesel B	49-states diesel	0.8500	0.35	44	<30	~0
F-T	Malaysian F-T	0.7905	<0.05	73.7	0.1	~0
CA Diesel	California diesel	0.8329	0.01	53.7	18.1	~0
Diesel B	49-states diesel	0.8500	0.35	44	<30	~0
MG	Natural gas derived F-T	0.8007	<0.001	51.4	10.1	0
MG90/IB10	90%MG and 10%Isobutanol	0.8016	<0.001	~46	9.0	2.20
MG50	50% MG and 50% diesel	0.8254	0.18	47.7	~20	~0

Table 2 Results of emissions tests performed on alternative fuels, (Clark *et al.*, 1999)

Fuel Type	Test No.	HC (g/bhp-hr)	CO (g/bhp-hr)	CO_2 (g/bhp-hr)	NO_x (g/bhp-hr)	PM (g/bhp-hr)
Diesel A	Test 1	0.298	1.732	634.2	5.471	0.128
	Test 2	0.290	1.704	626.9	5.501	0.121
	Test 3	0.310	1.762	619.9	5.685	0.112
	Average	0.299	1.733	627.0	5.552	0.120
BD 20	Test 1	0.280	1.159	625.4	5.592	0.053
	Test 2	0.299	1.173	625.9	5.678	0.048
	Test 3	0.278	1.090	619.2	5.666	0.046
	Average	0.286	1.141	623.5	5.645	0.049
BD 50	Test 1	0.207	1.089	621.6	5.502	0.092
	Test 2	0.215	1.045	620.2	5.559	0.079
	Test 3	0.209	1.040	616.6	5.579	0.076
	Average	0.210	1.058	619.5	5.547	0.082
BD 100	Test 1	0.132	0.967	627.2	5.709	0.077
	Test 2	0.112	0.840	625.4	5.812	0.067
	Test 3	0.103	0.851	624.0	5.860	0.063
	Average	0.116	0.886	625.5	5.794	0.069
Diesel B	Test 1	0.316	1.573	647.5	5.475	0.119
	Test 2	0.352	1.578	641.9	5.367	0.121
	Test 3	0.370	1.602	641.9	5.277	0.121
	Average	0.346	1.584	643.745	5.373	0.120
F-T	Test 1	0.211	0.991	610.9	4.722	0.108
	Test 2	0.209	0.954	613.0	4.653	0.102
	Test 3	0.174	0.959	610.6	4.445	0.101
	Average	0.198	0.968	611.489	4.607	0.104
CA Diesel	Test 1	0.229	1.025	613.9	4.716	0.119
	Test 2	0.299	1.110	618.6	4.915	0.102
	Test 3	0.293	1.136	615.1	5.049	0.106
	Average	0.274	1.090	615.849	4.893	0.109
Diesel B	Test 1	0.427	1.492	623.6	5.381	0.124
	Test 2	0.435	1.490	626.5	5.495	0.122
	Test 3	0.475	1.446	628.0	5.504	0.120
	Average	0.446	1.476	626.0	5.460	0.122
MG	Test 1	0.407	1.359	624.6	5.178	0.109
	Test 2	0.427	1.243	623.6	5.087	0.103
	Test 3	0.388	1.254	622.6	5.049	0.098
	Average	0.407	1.284	623.6	5.105	0.103
MG90/IB10	Test 1	0.544	1.380	590.1	5.035	0.085
	Test 2	0.551	1.454	587.9	5.103	0.099
	Test 3	0.518	1.492	580.6	5.094	0.098
	Average	0.538	1.442	586.2	5.077	0.094
MG 50	Test 1	0.401	1.314	616.0	5.065	0.112
	Test 2	0.399	1.408	609.2	5.213	0.110
	Test 3	0.394	1.444	615.6	5.205	0.109
	Average	0.398	1.389	613.6	5.161	0.110

The results presented in Table 2 were obtained from three hot start transient cycles employing the Federal Heavy Duty Engine Transient Test Procedure. The Malaysian synthetic fuel (F-T) shows superior results to the other fuels. A 90% blend of Mossgas derived synthetic fuel and isobutanol depicted better results for NOx and particulates but deteriorated results for HC, CO and carbon dioxide (CO_2) over the 100% Mossgas synthetic fuel (MG). The opposite of these results occurs for the 50% blend. The low results for the California diesel over the other two diesels (Diesel A and B) can be attributed to the higher cetane value, lower aromatics and sulphur content. An average of the three tests was taken due to the variability in the transient analysis.

2.3.4 Ambient Conditions

Diesel engines fitted to trucks operate at different atmospheric conditions, which effect its performance and emissions. The most important conditions are altitude and temperature.

2.3.4.1 Altitude (Pressure)

The altitude at which diesel engines fitted to transport vehicles operate in South Africa varies from sea level up to approximately 1800m. An increase in altitude results in a reduction of pressure, temperature and the amount of oxygen in the atmosphere producing less efficient combustion (Hansen *et al.*, 1990). Figure 7 shows the effect of altitude on peak pressure of an engine. This effect is manifested at high engine loads where the greatest demand for oxygen is generated (Hansen *et al.*, 1990).

Hansen *et al.* (1990) also showed that with an increase in altitude the smoke output increased at high loads. These variations could be expected, as with a decrease in efficiency, the smoke output usually increased due to the less efficient combustion.

Chaffin and Ullman (1994) investigated the effects of high altitude on heavy-duty diesel engines using a High Altitude Constant Volume Sampler (HA CVS) system. The system provides reduced pressure to both the intake and exhaust of the test engine, thereby simulating high altitudes.

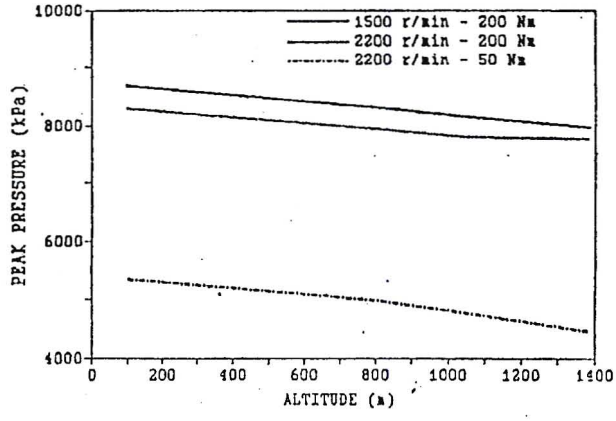

Figure 7 Peak pressure versus altitude for three load settings, (Hansen *et al.*, 1990)

The barometer pressures used to simulate the increase in altitude were 98.9, 82.6 and 77.9 kPa. Figure 8 shows the variation of NOx and particulates with increased altitude. Particulate matter showed a strong correlation to barometric pressure, and increased significantly with an increase in simulated altitude. The results were obtained for a transient test and show a poor correlation of NOx to altitude with no significant changes through the variation of pressures.

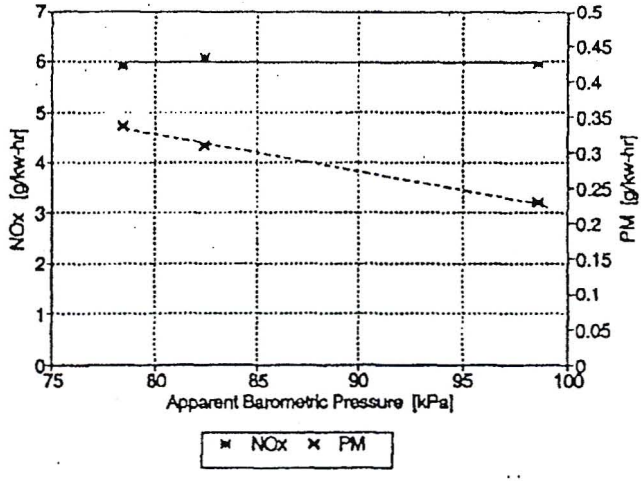

Figure 8 Effect of altitude on NOx and particulate matter (PM) using the HA CVS system, (Chaffin and Ullman., 1994)

2.3.4.2 Temperature

Rakopoulos (1991) investigated the effect of ambient temperatures on emissions. His conclusions are summarised in Figure 9. The graphs show the variation of temperature over a one year period in Athens, Greece and the effect of these on efficiency (0_e), brake mean effective pressure (P_e (bar)) (which is an indication of power), NO and smoke density (SD (g/m^3)). The analysis also included humidity (w (%)). Rakopoulos (1991) noticed from his investigation that ambient humidity only caused a mild change in NO and smoke and the results can be assumed to 'depend on temperature alone. Small increases in ambient temperature (θ_a) showed substantial increases in both emitted NO and smoke. It should also be noted that there is a corresponding decrease in specific power output during the warmer months which is not surprising as there should be a decrease in density of the air and hence less efficient combustion.

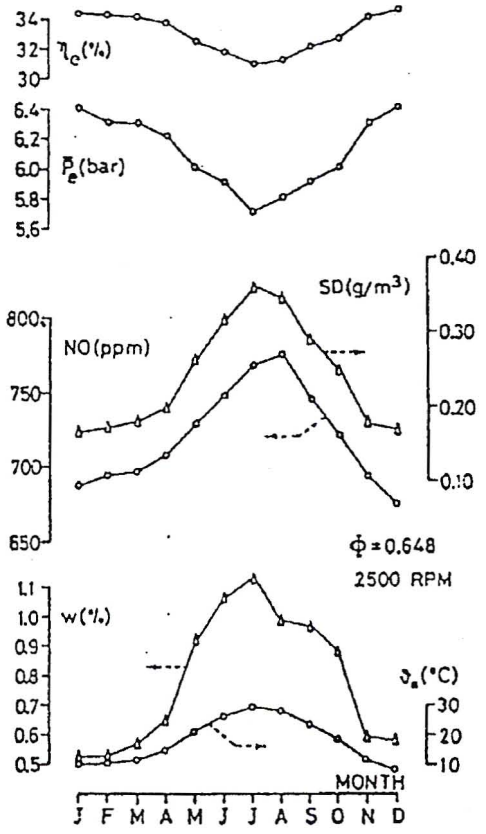

Figure 9 Variation of NO, smoke, efficiency and power with ambient temperature and humidity for a typical year in Athens, (Rakopoulos, 1991)

2.3.4.3 Correcting power for atmospheric conditions

SAE Standard J1995 (1992) provides a method for correcting engine power to standard conditions. The theory is based on the fact that increased ambient air temperature reduces the air density and thus reduces the mass of air that is present in the cylinder. However, the engine is at a higher temperature than the ambient air and transfers heat to it as the air enters the engine thus increasing the temperature of the air. This implies that the higher the temperature of the incoming air, the less heat is transferred to it. These two phenomena are the basis for the inclusion of the variables m and n, whose values are chosen based on investigations of the relative interaction between them.

The correction for diesel engines is shown below:

$$T_{bs} = f_a^{fm} T_{bo} \qquad (1)$$

where : T_{bs} = brake power at standard conditions (kW)

T_{bo} = brake power at observed conditions (kW)

f_a = $(101.325/BP_o)^m * (T_o/298)^n$

BP_o = barometric pressure at observed conditions (kPa)

T_o = temperature at observed conditions (K)

for naturally-aspirated and supercharged diesel engines, m=1.1 and n=1.2

for turbocharged or turbocharged and intercooled diesel engines, m=n=0.6

Also,

$$f_m = \begin{cases} 0.3 & q/r < 40 \\ 0.036\, q/r - 1.14 & 40 < q/r < 65 \\ 1.2 & q/r > 65 \end{cases}$$

where : q = 60 000*F*X/(D*N)

F = fuel consumption rate (g/s)

D = engine displacement (L)

N = engine speed (rpm)

X = revs/cycle = 1 for two-cycle engines or 2 for four cycle engines

r = $(BP_o$ + turbo boost)/BP_o

for naturally aspirated engines turbo boost = 0 and r = 1.

The observed pressure may be estimated by ignoring climatic effects and calculating the change in hydrostatic air pressure between sea level and the altitude of interest. Sears *et al.* (1987) gives the derivation of equation 2, which calculates the observed atmospheric pressure at a specified altitude above sea level using the ideal gas laws and hydrostatics. The standard atmospheric pressure at sea level is assumed to be 101.325 kPa.

$$BP_o = BP_s e^{-Mgy/RT} \quad (2)$$

where : BP_s = barometric pressure at standard conditions (kPa)

M = average molecular mass of air = 28.8 x 10^{-3} (kg/mol)

g = acceleration due to gravity = 9.8 (m/s^2)

y = altitude above sea level (m)

R = ideal gas constant = 8.314(J/mol/K)

T = air temperature (K)

2.4 Methods of Predicting Emissions

There are various methods of predicting emissions and the choice depends on the application. Combustion-emissions modelling is the approach used by researchers and is mostly restricted to a qualitative analysis. Methods for quantifying emissions have been accomplished by means of a regression or neural network analysis.

2.4.1 Combustion-emissions modelling

Combustion modelling is classified into 3 categories (Heywood, 1978) :

- zero-dimensional,
- quasi-dimensional, and
- multidimensional.

Zero-dimensional models are based on the first law of thermodynamics. These models are used to determine heat release and do not consider the space and time resolutions required for emissions modelling. In quasi-dimensional models the rate of burning is derived from a physical sub-model of the combustion process, as opposed to the empirically derived rate of burning of zero-dimensional models. Multidimensional modelling, which is the most detailed modelling approach, resolves the flow field spatially and temporally and is aimed at solution of the partial differential equations (sub-models) for the physical processes of mass, momentum, energy and the complex kinetic mechanisms that control species emission rates (Hou and Abraham, 1995). For emissions modelling two approaches have been adopted. One approach is to use phenomenological modelling and the other is to use multidimensional modelling.

2.4.1.1 Phenomenological modelling

Phenomenological or quasi-dimensional modelling concentrates only on those components that directly influence the phenomenon or in this case pollutant species of interest (Newhall, 1978). Since these models provide interactions of fluid dynamics and chemical processes and they are successful in providing time resolved in-cylinder pressure and work, they have demonstrated their potential to be used as a framework for soot and nitric oxide predictions (Lipkea and DeJoode, 1994).

Phenomenological models are usually multi-zone. This means that the fuel spray during injection is broken up into discrete zones. Each zone has its own properties for example, volume, mass, temperature and composition. The pressure in each zone can be calculated but in most cases is assumed uniform throughout the cylinder. The first law of thermodynamics is applied to each zone. The pressure inside the cylinder can then be determined from a differential equation by summing the volumes of all the zones since

the volume of the cylinder is known. The temperature of each zone is then calculated by integrating the first law of thermodynamics.

Bazari (1992) developed a model to predict combustion and emissions from a direct injection (DI) engine. The model takes into account details of fuel spray formation, droplet evaporation, air-fuel mixing, spray wall interaction, swirl, heat transfer, self-ignition and rate of reaction. The emissions model uses the chemical equilibrium and kinetics of fuel, NO, CO and soot reactions to calculate the pollutant concentrations within each zone. Figure 10 shows the division of the spray segment into zones. The spray is symmetric about the spray centre line and ranges from the centre line to the spray edge on both sides. The model was sensitive to fuel injection, intake swirl, turbocharging and engine operating conditions and predicted the known trends correctly. The results for NO prediction were correlated well with the measured values, and the predicted smoke correlated well with the measured values at low to medium speeds but at high speeds was over-estimated. HC, CO predictions were reasonable when the complexity of the model was taken into account.

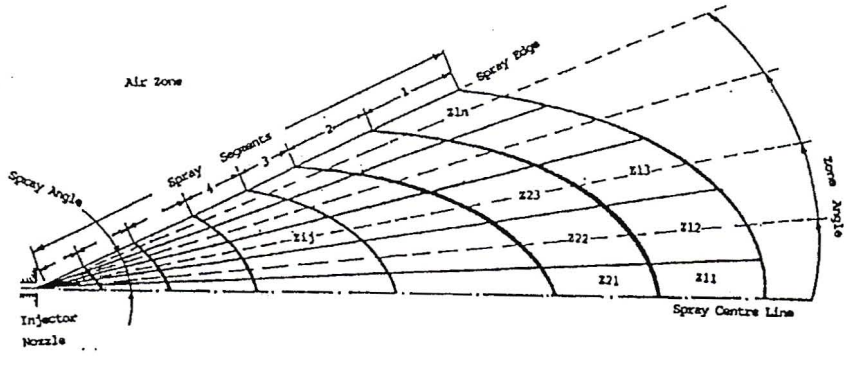

Figure 10 Visualisation of the multi-zone spray segments for a fixed point in time, (Bazari, 1994)

Bazari (1994) also describes a model developed to predict emissions under transient operating conditions again adopting the quasi-dimensional multi-zone combustion-emissions model.

Other phenomenological models include the model developed by Kouremenos *et al.*, (1997), which divides the spray axially and radially into zones. The proposed model takes into consideration the engine cylinder, fuel injection system and the inlet and exhaust manifolds. The engine cylinder simulation makes use of a heat transfer model, blowby model, combustion model and a gas exchange model. The model showed good correlation for cylinder pressure at all loads.

The NO and soot prediction was more accurate compared to the model proposed by Bazari, (1992). The model was an important achievement as it predicted both engine performance and emissions. The success of the model was probably due to the emphasis placed on the physical processes occurring in the combustion chamber and the modelling of the engine subsystems.

The model also omits unnecessary empirical relations and pays particular attention to the effect of operating conditions on engine behaviour. The model is useful in that it provides information regarding the combustion mechanism by producing a temperature distribution within the fuel jet as well as the distribution of NO and soot. Finally the model describes the structure of the jet and the history of the zones after wall impingement.

2.4.1.2 Multidimensional modelling

Multidimensional models are based on the Navier-Stokes equations, which are essentially equations that determine fluid flow in 3-dimensions. These models provide the strongest relationship between fluid flow and chemical processes at the microscale level. However, the complexity and computational cost of these models restricts their use. It was only until recently, huge advances in computing technologies have facilitated the use of these models, and with the trend now set, the accuracy of emissions modelling can only improve.

Multidimensional modelling has been improved with the development of the KIVA code (multidimensional chemically reacting flows), which was initially developed at the Los Alamos National Lab (Amsden *et al.*, 1989; cited by Xin *et al.*, 1997). The model developed by Xin *et al.*, (1997) included sub-models for the spray, ignition, combustion and emissions.

The extended Zeldovich mechanism was used to model the NO formation as was the case for the previous models considered. The soot model included differential equations for the rate of formation and oxidation of soot and the net soot is the difference between the two as shown in the following equation:

$$dm_{soot}/dt = dm_{form}/dt - dm_{oxid}/dt \quad (3)$$

Results for cylinder pressure obtained by Xin et al., (1997) were found to have excellent agreement with the measured results. The results for NOx were in good agreement with the experimental results at all loads and soot results were well predicted at medium and high loads, however the analysis at light loads deteriorated due to the fact that the SOF contribution to the model was omitted.

Combustion-emissions modelling are complicated as they have to account for all the physical processes within the combustion chamber, and many assumptions have to be made. It is for this reason that this type of modelling is mostly restricted to a qualitative analysis. In this regard combustion and combustion-emissions modelling helped researchers better understand diesel combustion, and to a great extent reduce the amount of experimental work involved in combustion research.

Apart from combustion-emissions modelling there are other methods of predicting emissions. These include regression models and the use of neural networks.

2.4.2 Regression models

Regression analysis is usually used for a quantitative analysis, as it is based on mathematical relationships between the output and the input variables. Fomunung *et al.*, (1999) developed a statistical model for the prediction of NOx from gasoline powered cars. The model can, however, be very easily extended to a diesel-powered vehicle. Fomunung *et al.*, (1999) used data obtained from 19 different driving cycles to develop

their model as well as using the driving cycles as variables. The model also included variables for acceleration, deceleration, power, drag, cruise and idle and demonstrated a reasonable model fit with an overall R^2 value of 0.623.

2.4.3 Neural networks

A fairly new approach to emissions modelling is the use of neural networks. Like a regression model a neural network analysis also involves many experimental data. A neural network is a computing system made up of a number of simple, highly interconnected processing elements, which processes information by its dynamic state response to external inputs. A typical neural network consists of three layers: an input layer, a hidden layer and an output layer (figure 11). The input layer consists of the same number of processing elements as there are number of inputs. The hidden layer can be any number allowed by the specific network. Each processing element receives input from every element in the intermediate layer. A single processing element is also referred to as a neuron.

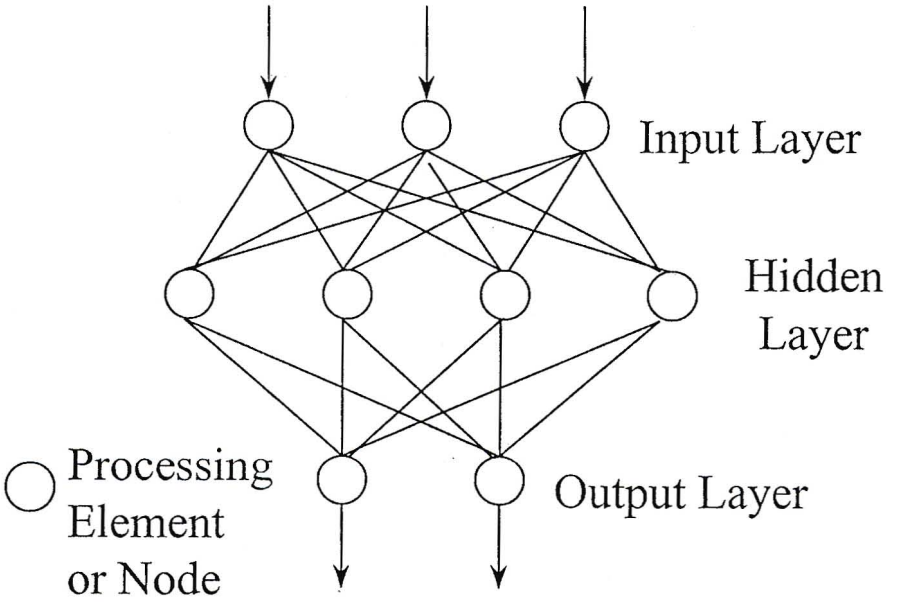

Figure 11 Typical example of a neural network structure

The neuron is characterised by a set of inputs, weights, and a non-linear mapping function called a transfer function (figure 12). A set of processing elements connected

to a neuron each contain a signal level called an activation value. These activation values are weighted and summed at the input to a neuron. The transfer function is a function of the sum of the products of the activation values and the weights.

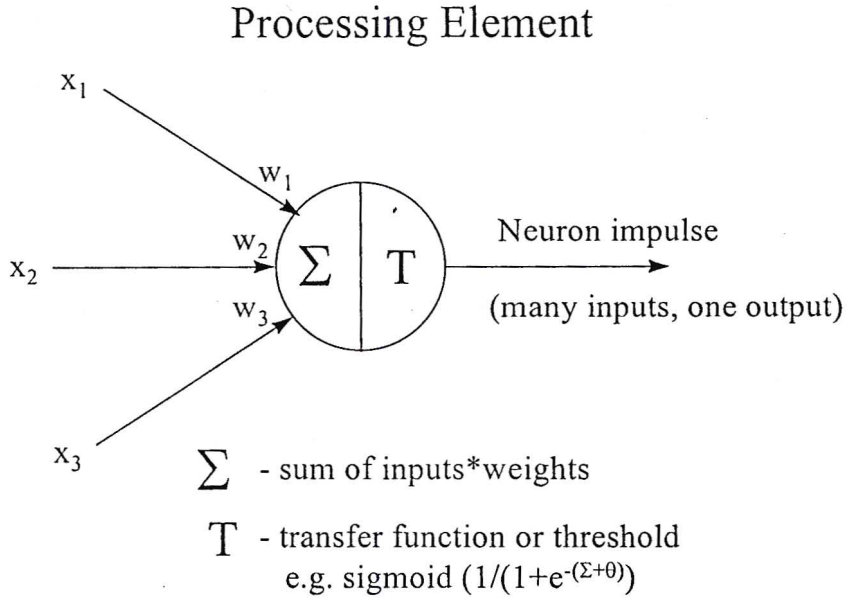

Figure 12 Schematic of a single neuron.

Atkinson *et al.*, (1998) developed a neural network to predict engine performance, fuel efficiency and emissions for both spark and compression ignition engines. The neural network was able to predict these parameters in real time. The system was trained in real time by the signals from sensors that were directly connected to the engine while it was running. The neural network was able to predict emissions to within 5-10% of the measured results when it was trained from 30 minutes of data that were collected from the engine.

The inputs to the neural network were:

- intake manifold air temperature,
- intake manifold boost pressure,
- fuel rack position,
- engine coolant temperature,
- engine speed, and
- fuel rail temperature and pressure.

The output parameters that were predicted were:

- instantaneous engine torque or power output,
- fuel consumption,
- carbon dioxide emissions,
- exhaust gas temperature, and
- engine exhaust emissions (CO, HC, NOx and smoke).

This method of predicting emissions proved very accurate (Atkinson *et al.*, 1998) and the results of their investigation will probably raise many questions on the ability of neural networks to be able to predict emissions so accurately. However, neural networks will most definitely receive much more attention in diesel engine research and modelling.

2.5 Discussion

Diesel combustion, which is associated with compression ignition engines, is a very complex process and is highly dependent on the design of the combustion chamber and fuel injection parameters such as pressure, timing and number of pulses. The accuracy of a combustion-emissions model to predict emissions will thus be very sensitive to these parameters. Combustion-emissions modelling will therefore also be complex and is mostly restricted to a qualitative analysis, and is therefore not practical for present quantitative applications.

The emissions problem has prompted the investigation into the use of alternative fuels to reduce emissions. The type of fuel has a notable effect on emissions from a diesel

engine and this is especially significant in South Africa where use is made of synthetic and crude-oil derived diesel.

Altitude also has a major influence on emissions. Particulate emissions are closely correlated to pressure drop, which implies that with an increase in altitude there is an increase in particulate emissions. NOx on the other hand is not as sensitive to altitude increases and there is a very small correlation with pressure. Because of its high variability, the effect of altitude is highly significant in South Africa, and therefore it must be taken into account for emissions prediction under South African conditions.

Ambient temperature is another factor that influences emissions. Small increases in ambient temperature results in considerable increases in NOx and smoke emissions, and therefore will also have to be accounted for in the model. The final model to be integrated into SimTrans will have to include the above parameters if a reasonable prediction of emissions is to be expected. The model will be in the form of a neural network. Regression models are more practical but lack the accuracy associated with neural networks.

3. EXPERIMENTAL PROCEDURE

The emissions testing was performed by the Centre for Automotive Engineering (CAE) at their diesel engine testing facility in Atlantis, Cape Town. Engine parameters and emissions were recorded at various speed and load settings. The data obtained from these tests were then used to train a neural network. This chapter will focus on these two procedures.

3.1 Engine Testing and Determination of Emissions

An ADE 447Ti engine was used. Specifications for the engine are shown in table 3. The engine was coupled to a 450 kW Schenck dynamometer. Engine speed and torque were measured using the dynamometer, and the data saved using a data acquisition system. Emissions were observed using gas analysers and logged by the computer using a Siemens data logger.

Table 3 Engine specifications

Make and model	ADE 447Ti
Layout and Type	In-line Intercooled Turbo
No. of cylinders	6
Cylinder bore (mm)	128
Piston stroke (mm)	155
Displacement (cm^3)	11 967
Rated power (kW) @ rpm	276 @ 2100
Max Torque (Nm) @ rpm	1635 @ 1400

NOx, CO and HC were measured using gas analysers. Particulates were measured with a partial flow dilution system that was developed at CAE. Figure 13 shows a layout of the engine test cell. NOx, CO and HC were measured at a point just after the exhaust manifold. Particulates were measured at a different point further down the exhaust. CO_2 was measured with a gas analyser at the point where NOx, CO and HC were measured

as well as after the dilution system. This was used to calculate the dilution ratio of the system.

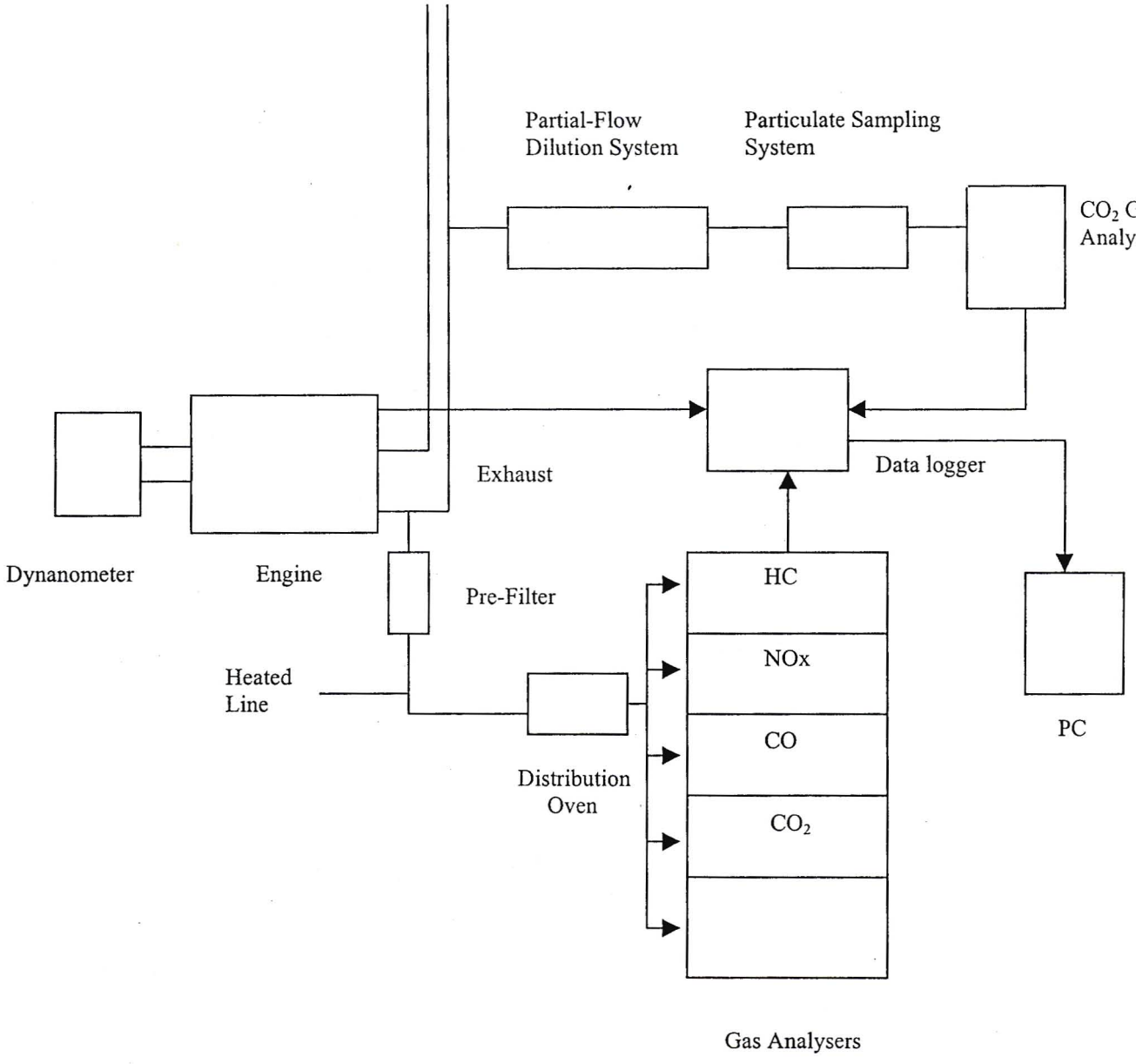

Figure 13 Block diagram showing experimental layout

The first pre-filter was used to remove all the heavy particles from the exhaust gas including smoke and particulates. The gas was then carried to the distribution oven via a heated sample line. The test required that NOx be maintained at a temperature of 95 – 200^{0}C. HC needed to be controlled to a temperature of 180 – 200^{0}C. The temperature of the heated sample line was kept at a constant temperature of 192^{0}C. CO_2 and CO were transported to the gas analysers using the heated sample line, however they were not sensitive to the actual temperature, as this would not affect the results. The distribution oven was used to filter the gas for impurities that may have escaped the pre-filter as well as distributing the gas to the appropriate analysers and at the same time maintaining the desired temperature (SAE, 1990)

The measurements of carbon monoxide, carbon dioxide at steady-state conditions were based on continuous sampling and analysis by non-dispersive infrared (NDIR) methods. Measurement of NO was determined using a chemiluminescense nitrogen oxide analyser.

3.1.1 Measurement of CO and CO_2

The NDIR method is based on the fact that individual exhaust-gas components absorb infrared light at various specific rates, according to their characteristic wavelengths. Thus if a beam of infrared radiation is passed through carbon monoxide the intensity of the beam is attenuated. The degree of attenuation depends on the amount of carbon monoxide present in the path of the beam; the more carbon monoxide the greater the attenuation. A schematic diagram is shown in figure 14. As can be seen, the analyser consists of four elements, a source of infrared radiation, a reference cell, a sample cell and a detector with its associated electronics. Infrared radiation is transmitted from an emitter which has been heated to approximately 700^{0}C. The radiation is divided, part of it passing through the reference cell and the other part passing through the sample cell. However, before the radiation reaches the cells it has to pass through a filter. This can either be a thin film interference filter or a cell filled with an appropriate non-absorbing gas, typically pure carbon dioxide. The reference cell is filled with a zero gas used for calibrating the analyser, in this case, zero air. The sample cell contains the sample gas (SAE, 1990).

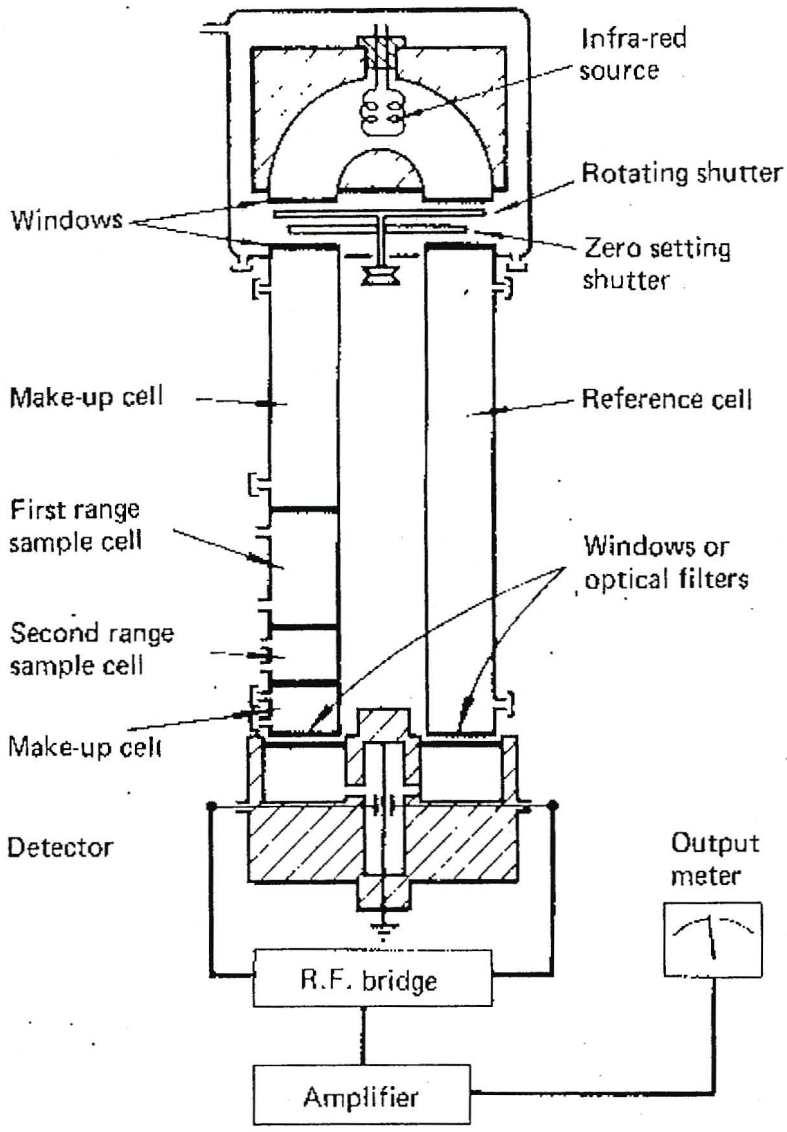

Figure 14 Schematic of non-dispersive infra-red analyser for measuring CO and CO_2, (Lilly, 1984)

The beam passes through the reference cell before entering the detector. When the CO-content is to be measured, the detector which is split in two by a thin membrane contains in one half, gas with a defined CO content, which absorbs a portion of the CO-specific radiation. This absorption is accompanied by an increase in the temperature of the gas, producing a gas current, which flows through the membrane. A rotating shutter

induces a rhythmic interruption in the beam, producing an alternating flow pattern between the two volumes of gas separated by the membrane (Lilly, 1984).

The flow sensor converts this motion into an alternating electric signal. When a test gas with a variable CO content flows through the reference cell, it absorbs radiant energy in a quantity proportional to its CO content; the energy is then no longer available in the detector. The result is a reduction of the base flow in the detector. The deviation from the alternating base signal provides an index of the CO content in the test gas.

CO_2 is measured in exactly the same way except that the reference cell is filled with carbon dioxide free dry air.

3.1.2 Measurement of NOx

NOx was measured using the method of chemiluminescence. This has the advantage over the NDIR method in that it can be used to detect nitric oxide as well as nitrogen dioxide. A schematic arrangement of a chemiluminescence analyser is shown in figure 15. To measure nitric oxide the exhaust gas is passed into a reaction chamber where it reacts with ozone generated within the instrument using O_2. This produces nitrogen dioxide in an electronically excited state. When these molecules return to their ground state they emit photons of radiation. These are detected and amplified by a filter and photomultiplier tube housed within the reaction chamber.

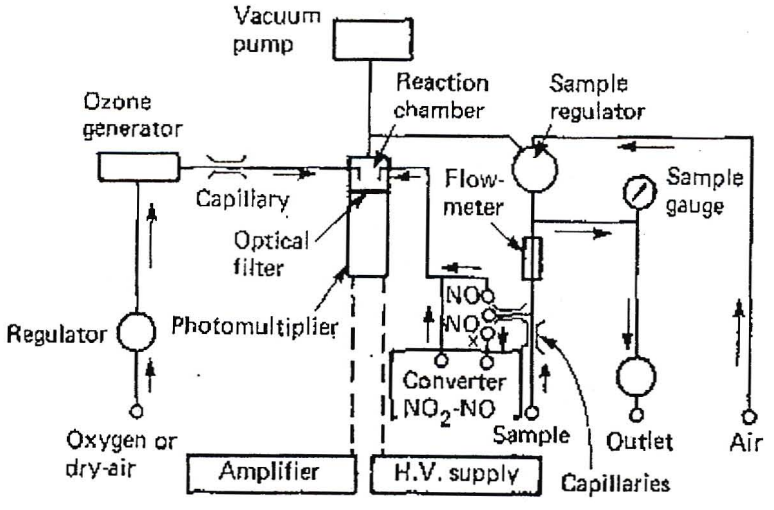

Figure 15 Schematic of chemiluminescence NOx analyser, (Lilly, 1984)

The output of the photomultiplier is proportional to the nitric oxide concentration. This method however only gives an indication of nitric oxide. To determine total nitrogen oxides the exhaust gas sample is diverted through a chemiluminescence converter instead of being passed directly into the chamber where it reacts with ozone. The converter thermally or catalytically reduces nitrogen dioxide to nitric oxide. The reduced gas is then passed through the ozone reaction chamber where the total nitric oxide content is measured (SAE, 1990).

3.1.3 Measurement of HC

Hydrocarbons in diesel exhaust gases are universally measured using a heated flame ionisation detector (HFID). This comprises a flame ionisation detector cell, together with the necessary electronic signal processing and readout equipment (figure 16). For diesel exhaust gas measurement where the hydrocarbons are of fairly high molecular weight and consequently of higher boiling points, it is essential to avoid losses due to condensation on any surfaces in contact with the gas sample. This is achieved by maintaining all sample lines and all parts within the analyser, which come into contact with the sample at 191^{0}C. This temperature has been selected as that which gives the maximum detector response for hydrocarbons. When a hydrocarbon is burnt in a flame, ions are produced.

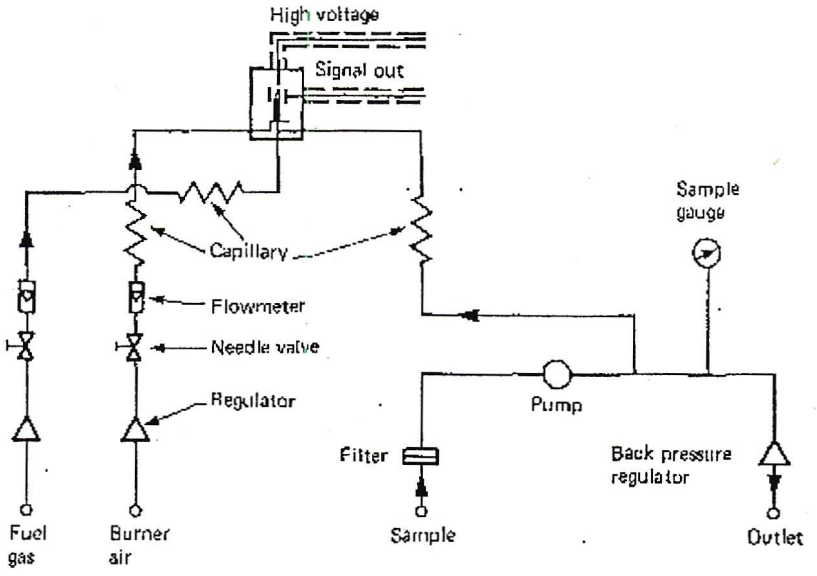

Figure 16 Schematic of heated flame ionisation detector (HFID) for measuring unburnt hydrocarbons, (Lilly, 1984)

In the flame ionisation detector the exhaust gas sample is passed through a capillary to control the flow rate, and into a flame obtained by burning either hydrogen or a mixture of hydrogen and helium or hydrogen and nitrogen in air. A potential difference is applied across the flame and as the hydrocarbons burn the ions produced move towards one of the electrodes applying the field. This produces an electric current which is amplified and measured, the magnitude of the current being proportional to the number of carbon atoms passing into the flame. The analyser has to be calibrated with a known hydrocarbon gas, in this case propane. The results are specified as parts per million (ppm) carbon which gives a true measure of the amount of hydrocarbon present without the need to specify the individual hydrocarbons (SAE, 1990).

3.1.4 Measurement of particulates

The determination of particulates required a partial-flow dilution system capable of maintaining the temperature of the diluted exhaust gas at or below 325 K (52^0C) and preventing water condensation. Figure 17 shows a schematic drawing of this system. A particulate sampling system in conjunction with specified particulate sampling filters and a microgram balance, which were placed in an air-conditioned weighing chamber was used for the sampling of particulates. Two filters were used for the measurement of particulates. This comprises of a primary filter and a back up filter that are located in series in a filter housing. The filters were weighed before sampling and were returned to the weighing chamber and conditioned for at least two hours, but not more than 36 hours, and then weighed. This time period was essential for an accurate measurement.

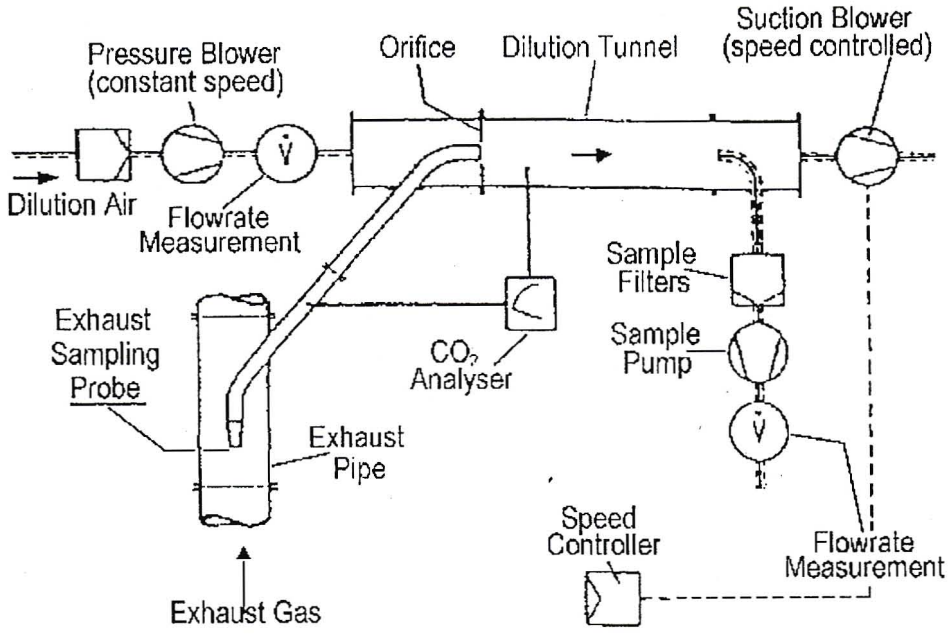

Figure 17 Schematic of partial-flow dilution system used for the sampling of particulates

The mass of particulates was the difference between the sum of the mass of the primary and the back up filters after sampling and the mass of the filters before sampling.

3.2 Testing Procedure

Before emissions testing could be performed, calibration of the analysers was essential, this calibration required a zero gas and a span gas. The analysers had a measuring range compatible with the accuracy required to measure the concentrations of the exhaust gas sample pollutants. Table 4 shows the zero gas and the span gas used for the analysers. The accuracy of the analysers was ± 2.5% of full-scale or better.

Table 4 Zero and span gases used for calibration of analysers

Analyser	Zero Gas	Span Gas
NOx	O_2	1384 ppm NO
HC	O_2	250 ppm propane (C_3H_8) + N_2-balance
CO	O_2	909 ppm CO + N_2-balance
CO_2	O_2	9.1 % CO_2 + N_2-balance

The analysers were left on for a minimum of two hours before the test, so as to stabilise at the required operating temperature. The engine was started and warmed up under load until all temperatures and pressures reached equilibrium. The engine was then ready for testing. Data was accumulated at different speed and load points as described in table 5. For NO, HC, CO and CO_2 the engine was operated for at least 10 minutes in each test point, allowing at least 5 minutes for emissions measurements.

Table 5 Data points on Speed-Torque curve for emissions testing

Speed (rpm)	Load (%)
600	100, 75, 50, 25
800	100, 80, 60, 40, 20
1000	100, 80, 60, 40, 20
1200	100, 80, 60, 40, 20
1400	100, 80, 60, 40, 20
1400-1600	Full throttle curve – 4 points
1600	100, 80, 60, 40, 20
1800	100, 80, 60, 40, 20
2000-2100-rated	Governed region- 4 points on full throttle curve

The zero and span gas had to be checked after each test point and if either changed more than 2% of full scale, the test point had to be repeated. For particulates sampling ± 6-8 minutes was allowed at high load and ± 10-12 minutes at low load points. The above was repeated until all test points were complete. A complete set of data can be found in Appendix A.

3.3 Neural Network Procedure

The data obtained from the emissions testing was used to formulate a neural network based prediction algorithm to be used in SimTrans. A separate network was used for each emission. The data had to first be prepared before being used in the neural network. Obtaining the 'best' neural network involved a trial and error analysis.

3.3.1 Preparing training and test data

The raw data that was obtained from the engine testing was used as the training data set and one data point for each mode was used as the test set. The data was then normalised by dividing each value by the maximum value of that parameter. Anomalies and outliers had to be manually discarded from the training set. Other neural network packages have the option of removing the outliers, however this was not available in the software used for this study. The outliers were easily recognised in the data set and could be attributed to the equipment used. This typically occurs in emissions testing due to the sensitivity of the of the gas analysers. The data was then ready for analysis in the neural network.

3.3.2 Neural network topology and architecture

It was initially decided to use the default settings of the Thinks^{TM} (1994) software. This included the back propagation network (BPN) learning rule. The BPN learning rule is probably the most widely recognised and most commonly used supervised learning algorithm. It was one of the first algorithms to be used effectively with neural networks, and its success is due to a robust ability to achieve generalisation, and it remains a useful standard by which others are compared. Associated with the BPN learning rule are the following parameters:

- Initial weights value,
- Weights decay,
- Learning rate (α) and
- Momentum rate (β).

The initial weights parameter was set to the system default value of 1. The weights decay and momentum parameters were set to 0. The learning rate parameter (α) was the only parameter that was altered. The default value was set at 0.01, however increasing this value resulted in improved network performance.

The architecture type determines how weights are interconnected and which learning rules may be used. The multilayer normal feed forward architecture type, which is the most commonly used architecture, was adopted for all the networks. The network error type determines how error is computed. Since the goal of the network training was to minimise error, the choice of the type of network error effects the weight adjustments, which in turn determines the accuracy of the model. The mean square error type was used. The dot product input function and the sigmoid transfer function were used as the networks input and transfer functions respectively. The number of hidden layers as well as the number of nodes in each layer for the final neural networks is shown in table 6 as well as the other network information. These settings were chosen on a trial and error basis and were perceived to yield the best models.

Table 6 Architecture and Topology for Neural Network

Emission	No. of Hidden layers	No. of nodes in each layer	Architecture	Learning rule	Error type	α	No. of iterations
NOx	3	6-4-3	Normal Feed Forward	BPN	Mean Square	0.5	24000
PM	3	6-4-3	Normal Feed Forward	BPN	Mean Square	0.9	30000
HC	3	6-4-3	Normal Feed Forward	BPN	Mean Square	0.5	16000
CO	3	6-4-3	Normal Feed Forward	BPN	Mean Square	0.5	9000

The no. of iterations gives an indication of the ability of the neural network to successfully predict emissions. For particulates an α value of 0.9 was used as well as a high number of iterations, as this is the most difficult emission to predict. Results of the neural network based on the architecture shown in table 6 are presented in chapter 5.

4. MODIFICATIONS TO SIMTRANS

In order to predict emissions from SimTrans, a few modifications were needed. Firstly, account had to be taken of the effect of ambient conditions. Secondly, the neural network needed to be integrated into the model. Before the modifications are discussed, a short description of the model is given.

4.1 Introduction to SimTrans

SimTrans is a windows based application, programmed in Delphi 3. Simulation of a vehicle is achieved by the interaction of the route profile, engine data, vehicle geometry and mass. Data for this is stored in files that are used as input to the model. The model consists of procedures and functions that control different aspects of the vehicle simulation. The main procedure controls the overall simulation of the vehicle and calls all the other functions and procedures when required.

4.1.1 Main procedure

Initially checks are made on the speed limit, payload and whether the vehicle is stationary. A more detailed description of specific procedures and functions, as well as the main procedure is given by Clark (1996). The motion resistance, which includes air, grade and rolling resistance, is then calculated.

Air resistance is dependent on the frontal area and coefficient of drag of the vehicle. Grade resistance is a function of road grade and the gross vehicle mass (GVM), and is the resistance to motion that the vehicle experiences due to its weight and the slope of the road. Rolling resistance may be defined as the difference between the energy supplied to a wheel axle, and the remaining energy available to accomplish useful work in acceleration and in overcoming air and grade resistance. Rolling resistance is the energy lost in the tyres due to tyre deformation, air rotational resistance, and at the tyre-travel surface interface due to friction and deformation of the travel surface (Clark, 1996).

Next a check is made on the gear mode that is currently in operation. The current governed speed and engine speed is then calculated from the ground speed and gear. The torque is calculated from the maximum torque available at the current governed speed and engine speed. This is read from the full throttle curve in the vehicle data file. The transmission losses are determined and the thrust calculated. The power left over is used to accelerate the vehicle to the desired speed. The fuel consumption is estimated using a regression equation with engine speed and torque as variables. The new route altitude and total distance travelled are also calculated. The above process is repeated till the simulated route has been completed.

The ambient correction algorithm that had to be included in SimTrans directly effects the GetMaxEngTorque procedure. This will be discussed next.

4.1.2 GetMaxEngTorque function

The engines of the simulated vehicles are assumed to operate with a mechanical governor. The governed range is set to a constant value of 200 r/min (figure 18). This function returns the maximum torque available from the engine for the current engine and governed speeds. This torque value is read from a look up table of speed and torque values representing the full throttle torque curve. If the current engine speed is greater than the governed speed, then the maximum torque is calculated by interpolating between the maximum torque at the governed speed and zero at 200 r/min greater than governed speed. On the other hand if the current engine speed is equal to the governed speed and is between the lowest speed in the look up table and rated speed, the maximum torque is estimated by searching through the look up table and locating two speed values on either side of the current engine speed, and interpolating between them. Finally, if the current engine speed is less than the lowest speed in the look up table, then the maximum torque is estimated by interpolating between the maximum torque at the lowest speed and 90% of this value.

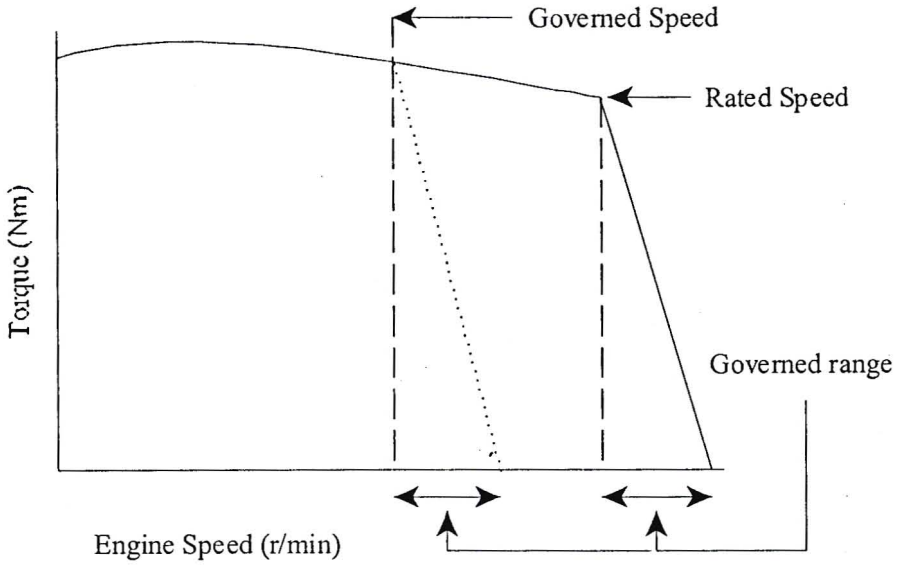

Figure 18 Full throttle torque curve showing governed range, after Clark (1996)

4.2 Ambient Conditions Simulation

In order to correct the torque for ambient conditions, the atmospheric pressure and ambient temperature at the geographical location of the vehicle, had to be accounted for.

4.2.1 Atmospheric pressure

The atmospheric pressure was estimated using Equation 2 (page 24). The altitude was obtained from the route data file and the air temperature was the ambient temperature and will be discussed next.

4.2.2 Ambient temperature

The ambient temperature was estimated using a model that predicts temperature during the day based on maximum and minimum values, which were obtained from Schulze (1997). The temperatures were given on a monthly and provincial basis.

4.2.2.1 Derivations of mean maximum and minimum temperatures

Schulze (1997) used a stepwise multiple regression, based on observations from over 1300 stations, to estimate the temperature at grid points where no measurements were made.

The factors that Schulze (1997) used for this estimation were:

- Latitude: South Africa extends from 12 - 34^0 S. Temperatures decrease with an increase in latitude polewards.
- Altitude: Generally the higher the altitude the lower the temperature.
- Continentally: The distance from the ocean has a moderating effect on temperature. There are smaller variations in temperature near marine locations whereas in inland locations there are rapid increases in daytime temperatures and decreases in night-time temperatures.
- Temperature region: South Africa consists of a number of different regions where different factors will determine temperature regimes in different seasons of the year.
- Topographic Index: Occurring during cooler months, night-time cold air drainage into valley bottoms, caused by radiative cooling of uplands and valley slopes under clear sky conditions, assumes importance in hilly inland areas.
- Longitude: This factor is region dependent and is important mainly in those areas with an east-west alignment.

A comprehensive temperature profile was thus obtained for the whole country. Using statistical methods the mean monthly minimum and maximum temperature were then estimated for the nine provinces.

4.2.2.2 Diurnal temperature prediction

The model to predict temperature during a day was based on the assumption that the minimum temperature occurs at 4am and the maximum temperature at 3pm (Haurwitz, 1944). A cubic function, that calculates temperature using time as the variable, was then derived for this relation (figure 19).

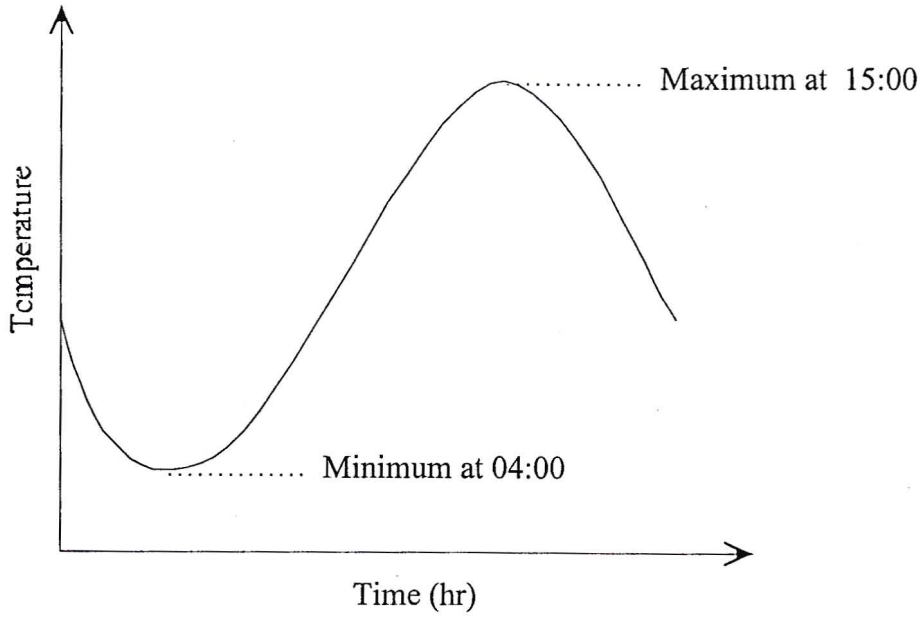

Figure 19 Hourly temperature distribution during a typical day

The mean monthly minimum and maximum temperatures are shown in table 7 and table 8 respectively. The temperatures are given for each South African province.

Table 7 Provincial mean monthly minimum temperatures for South Africa, (Schulze, 1997)

	Jan	Feb	Mar	Apr	May	Jun	Jul	Aug	Sep	Oct	Nov	Dec
NP	18.3	18.1	16.8	13.5	9.1	5.7	5.5	7.9	11.7	14.7	16.6	17.8
M	15.3	15	13.8	10.8	6.9	3.8	3.7	6	9.3	11.7	13.4	14.7
NW	17.4	17	14.7	10.3	5.1	1.2	0.9	3.7	8.3	12.4	14.8	16.5
NC	15.6	15.8	13.9	9.9	5.9	2.9	2.3	3.8	6.7	9.8	12.4	14.4
G	14.9	14.6	12.9	9.3	4.8	1.5	1.3	3.9	8.1	11.2	13	14.2
FS	14.4	14.1	12.2	8.1	3.6	0.5	0.1	2.4	6.3	9.6	11.7	13.4
KZ	16.4	16.4	15.2	12.4	9.1	6	6	7.9	10.6	12.4	14	15.5
EC	14.1	14.3	12.9	9.6	6.6	4	3.5	4.9	7.2	9.3	11.2	13
WC	14.1	14.6	13.1	10.2	7.6	5.3	4.5	5.3	6.9	9	11.3	13.1

NP = Northern Province, M = Mpumulanga, NW = North West Province, NC = Northern Cape, G = Gauteng, FS = Free State, KZ = KwaZulu Natal, EC = Eastern Cape,
WC = Western Cape.

Table 8 Provincial mean monthly maximum temperatures for South Africa, (Schulze, 1997)

	Jan	Feb	Mar	Apr	May	Jun	Jul	Aug	Sep	Oct	Nov	Dec
NP	30.3	29.7	28.6	27	24.9	22.2	22.2	24.6	27	28.5	29.3	29.7
M	26.8	26.5	25.6	23.6	21.7	19.1	19.4	21.7	24.1	25	25.3	26.4
NW	32	30.6	28.7	25.6	22.7	19.3	19.6	22.6	26.2	28.9	30.2	31.4
NC	32	31.3	29	25.2	21.7	18.1	18	20.2	23.4	26.6	29.1	31
G	27.5	27	25.8	23.4	21	18	18.3	21.1	24.3	25.9	26.2	27.2
FS	29.1	27.9	26	22.8	19.9	16.6	16.9	19.7	22.9	25.2	26.5	28.3
KZ	27.5	27.2	26.5	24.6	22.7	20.6	20.7	22.2	23.8	24.5	25.3	27
EC	27.8	27.4	25.7	23	20.5	17.6	17.7	19.6	21.4	23	24.7	26.9
WC	29.8	29.4	27.3	24	20.5	17.5	17.1	18.3	20.5	23.3	26.1	28.1

NP = Northern Province, M = Mpumulanga, NW = North West Province, NC = Northern Cape, G = Gauteng, FS = Free State, KZ = KwaZulu Natal, EC = Eastern Cape, WC = Western Cape.

The equation is of the form :

$$\text{Temperature} = A_1T^3 + A_2T^2 + A_3T + A_4 \quad (4)$$

where :

T = Time (0 - 23)

A_1 - A_4 = constants.

The constants A_1 - A_4 were derived by solving a set of simultaneous equations:

$$\text{MinTemp} = A_1(4)^3 + A_2(4)^2 + A_3(4) + A_4 \quad (5)$$

$$\text{MaxTemp} = A_1(15)^3 + A_2(15)^2 + A_3(15) + A_4 \quad (6)$$

Differentiating Equation 4 with respect to time yields the following equation:

$$\frac{\text{dTemperature}}{\text{dTime}} = 3A_1T^2 + 2A_2T + A_3 \quad (7)$$

At T = 4 and T = 15, $\frac{\text{dTemperature}}{\text{dTime}} = 0$

then,

$$0 = 3A_1(4)^2 + 2A_2(4) + A_3 \quad (8)$$

$$0 = 3A_1(15)^2 + 2A_2(15) + A_3 \quad (9)$$

Using Equations 5, 6, 8 and 9, the four constants (A_1 - A_4) could be solved. These constants were stored in the model. The equation does not accommodate the fact that the temperature at T = 0 (12 am) and T = 24 (T = 0 for following day) is the same. This was rectified by a straight-line approximation from T = 17 to T = 24. T = 17 was chosen as it provides for a smooth conjunction between the quadratic equation and the straight-line descent to T = 24.

Finally, in order to be able to estimate the temperature, a procedure to calculate the date and time of day was required. This was easily accomplished as the time taken to complete a route was simulated in the model. All that was then needed was a start time and date for the simulation.

4.3 Fuel Type

The type of fuel was the most difficult of all the parameters to account for in the model. The differences in fuel from a molecular level to the different additives present were not easy to include in the model empirically and therefore it was decided that the emissions data that the neural network was to be trained on would be fuel type independent. This means that for a different fuel type a new set of data would have to be generated.

4.4 Torque Correction Function

With the ambient temperature and pressure available, the new corrected torque was calculated using the SAE corrections for atmospheric conditions as given in Equation 1 (page 23). The boost pressure was calculated using a simple regression with variables of speed and torque (Appendix C). The new GetMaxEngTorque function was adjusted by multiplying the maximum torque by the ratio of the corrected torque to the original torque. Figure 20 shows a flow diagram of the algorithm.

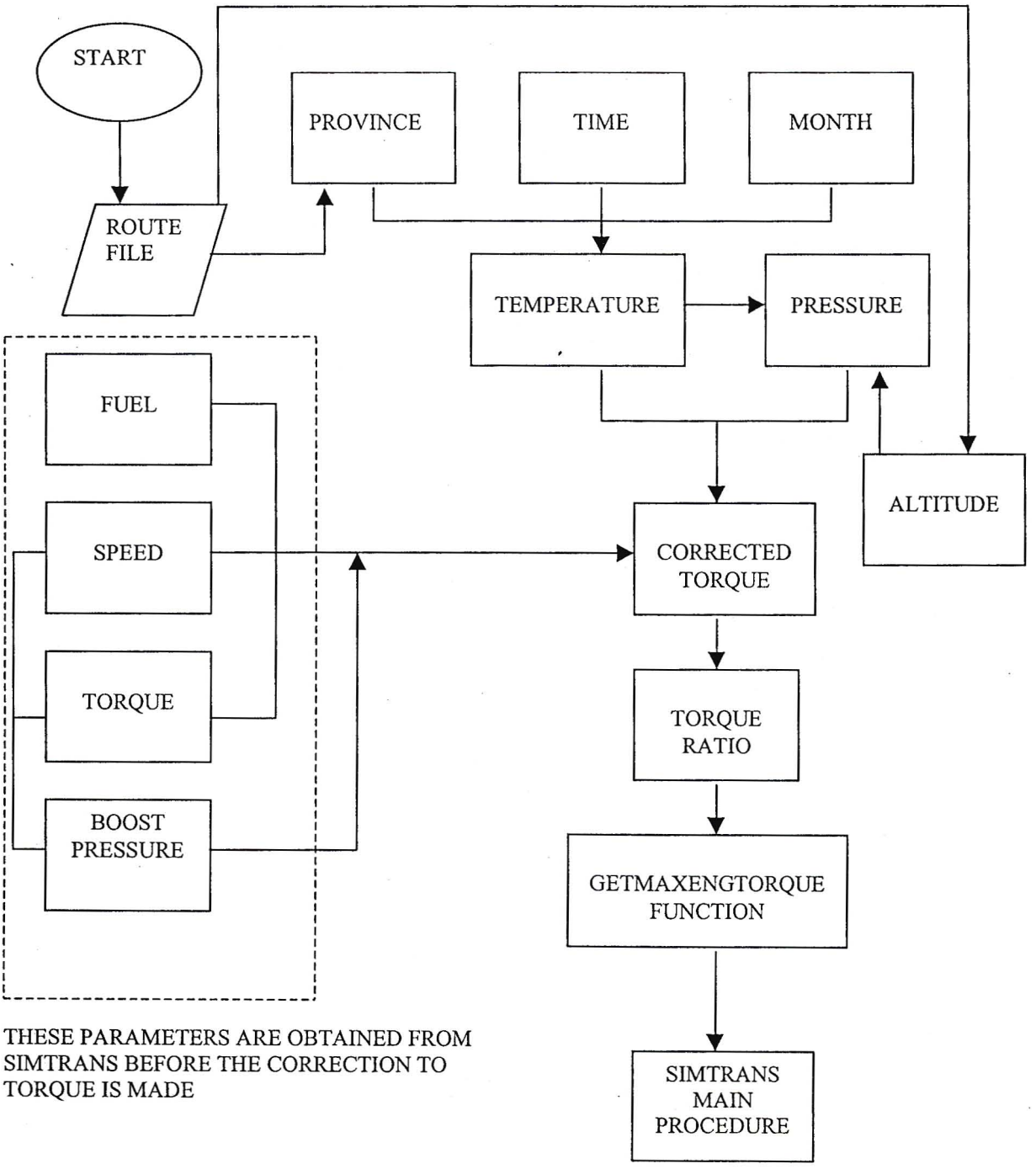

Figure 20 Flow diagram showing the corrected torque algorithm due to ambient conditions

By applying the torque correction to the GetMaxEngTorque function, the full throttle torque curve was adjusted according to the present ambient conditions. This limited the maximum torque that was available to the vehicle. The full throttle torque curve that was described in the vehicle file is assumed to be at standard conditions i.e. sea level (101.325 kPa) and 25 ^{0}C. So then for example if the vehicle is operating at an elevated altitude and higher ambient temperature, the full throttle torque curve will be lower than the curve at standard conditions (figure 21). The effect of ambient conditions on torque is thus directly responsible for the change in emissions, as the output of the neural network is based primarily on the inputs of engine speed and torque. This in turn will also adjust the fuel consumption as it is calculated from a regression equation with variables of engine speed and torque.

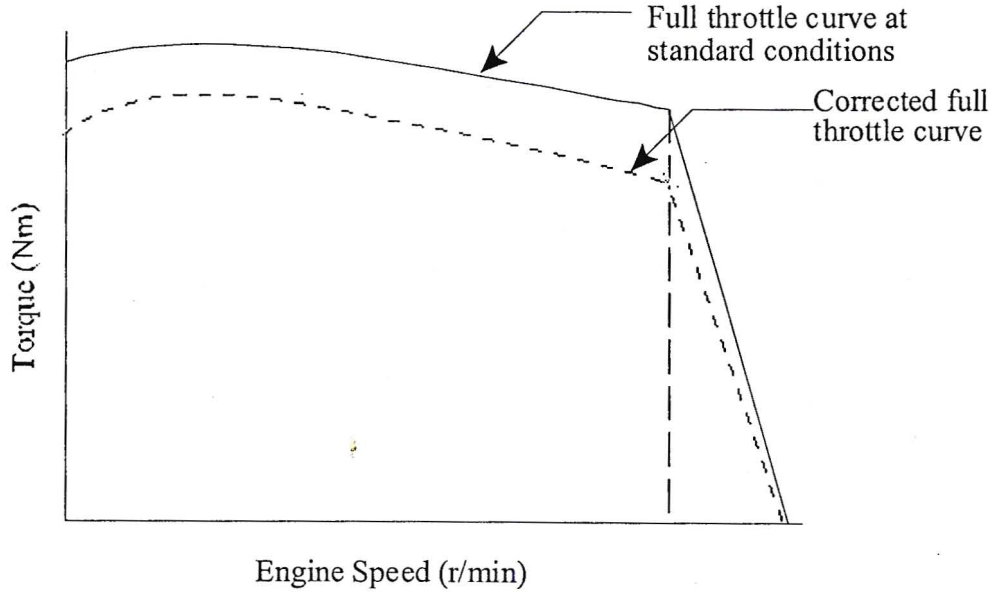

Figure 21 Engine map showing full throttle torque curve at standard conditions and corrected full throttle torque curve for ambient conditions.

4.5 Neural Network Analysis

Incorporating the neural network into SimTrans was easily implemented. Once training of a neural network was complete, the weights and other information were stored. Depending on the topology of the network that was chosen, different information was stored. A multilayer normal feed forward architecture was used for all the neural

network models. For this architecture, each processing element (PE) in each layer received an input vector, which was either the external input vector or the output vector of the prior layer. The activation of the multilayer normal feed forward network was obtained by feeding the external input to the first layer, using the corresponding input function to activate the PE's, and then applying the transfer function to the resulting activation. The vector output of this layer was then fed to the next layer, which was activated in the same way, and so on, until the output layer was activated, giving the network output vector. The dot product input function was used for all the networks. This function was just a weighted sum of the inputs plus a bias value. Given a vector of n values, $x_1, x_2, \ldots x_n$, and a set of $n + 1$ weights then,

$\mathbf{x} = (1, x_1, x_2, \ldots x_n)$ and, (10)

$\mathbf{w} = (w_0, w_1, w_2, \ldots w_n)$. (11)

The first element of **x** was a special constant input called a bias constant, and the first element of **w** was a special weight called a bias weight. A weighted sum was obtained by the dot product of **x** and **w**.

$f(\mathbf{x}, \mathbf{w}) = \mathbf{x}.\mathbf{w} = w_0 + x_1 w_1 + x_2 w_2 + \ldots + x_n w_n$.

The transfer function then acts on the value returned by the input function. It was the non-linearity of the transfer function that gives a neural network its advantage over traditional regression techniques. This function normalises the output of the PE (figure 22). The transfer function adopted for the present application was the sigmoid transfer function, which is denoted by the following:

$$T(f(x,w)) = \frac{1}{1+\exp(-f(x,w)}} \quad (12)$$

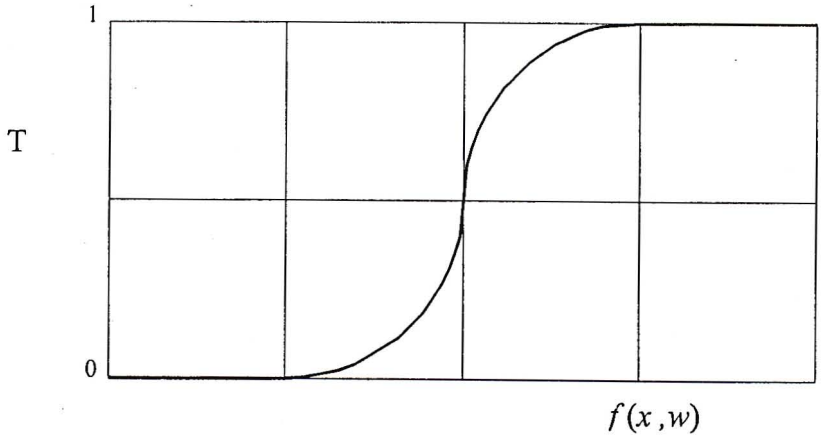

Figure 22 Sigmoid transfer function

The output for the structure shown in figure 23 can be calculated in the following way:

$$f_1 = wb_1 + x_1 w_1 + x_2 w_2 \quad (13)$$

where :

wb_1 = Bias weight

x_1, x_2 = Input value of speed and torque (normalised).

f_2 and f_3 are calculated similarly to f_1.

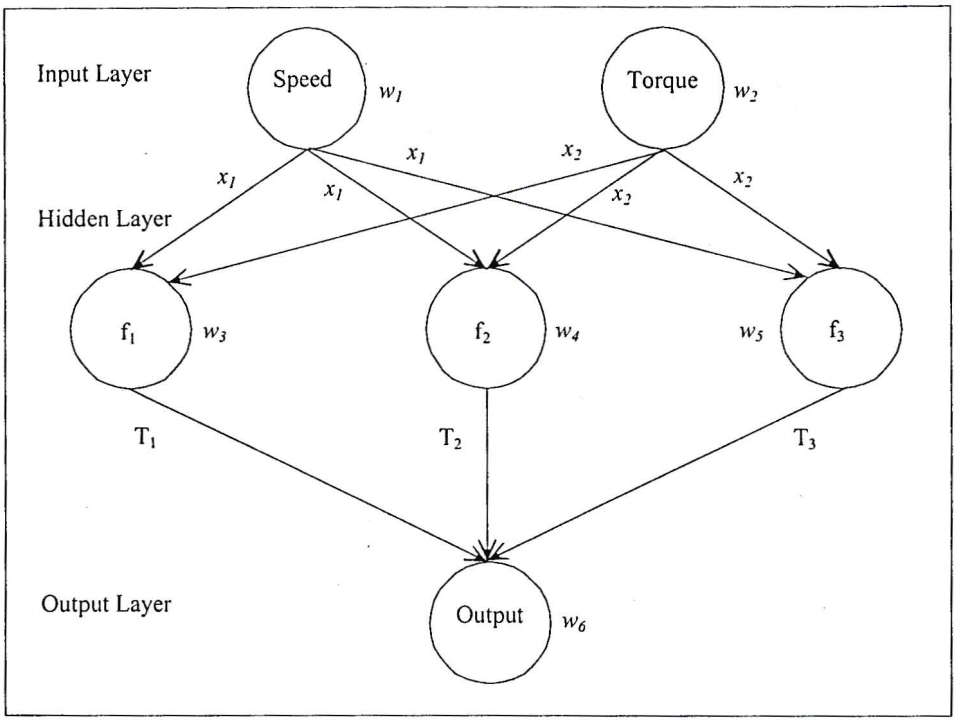

Figure 23 Schematic network showing input vectors, weights, input functions and transfer functions

$$T1 = \frac{1}{1 + \exp(-f1)} \tag{14}$$

T_2 and T_3 are calculated similarly to T_1.

Then,

$$f(\text{output}) = w_6(\text{output}) + w_3T_1 + w_4T_2 + w_5T_3 \tag{15}$$

$$T(\text{output}) = \frac{1}{1 + \exp(-f(\text{output})} \tag{16}$$

T(output) is the output from the network in a normalised form. Therefore all that is required to predict emissions within SimTrans are the weights that are set up by the neural network once training is complete. Thereafter it was a matter of solving the mathematical equations to calculate the required output, which in this case were emissions.

5. RESULTS AND DISCUSSION

Having introduced the ambient temperature and pressure into SimTrans it was necessary to analyse the effect of this modification to the engine torque. The model was altered in a way so as not to effect the speed. However the change in torque does effect the fuel consumption, because of the higher order variables of speed used in the regression for fuel consumption the overall effect was small. To assess the effect of temperature it was necessary to analyse a simulation at the two extremes i.e. hot and cold. Altitude was also varied between two extremes. The verification of the model to predict emissions was performed using the test data set in the neural network. This was sufficient, as the truck would always be operating within the engine map where the analysis was performed. The results from SimTrans could then be expected to have the same accuracy as that depicted from the testing of the neural network. These results will be presented here. It was also necessary to investigate the sensitivity of the emissions to the engine parameters and the ambient conditions. Finally two routes were investigated using a long distance transport vehicle that was powered by an ADE 447Ti engine (Mercedes Benz 2644S-24), i.e. the route from Durban to Johannesburg and the route from Johannesburg to Cape Town.

5.1 Investigating the Effect of Ambient Conditions on Torque

It was important to investigate the effect of ambient conditions on the performance of the engine before any emissions investigations were made. This would help in identifying the scale at which the torque was changed. This change would also show the effect that the corresponding increase or decrease would have on emissions.

5.1.1 Ambient temperature

To investigate the effect of ambient temperature on torque, a segment of the La Mercy to Mount Edgecombe route was used. Investigating the effect of low temperatures required a simulation at 4am in July for a hypothetical route in the Free State. The ambient temperature experienced by the engine at this time was 0.1^0C. For the maximum temperature analysis a simulation was performed at 3pm in January for the

same route. Temperature at this time was 29^{0}C. The results of this analysis are shown in figure 24 and figure 25.

Figure 24 indicates the comparison between the torque from the original SimTrans model and the corrected torque for the minimum temperature. Figure 25 indicates the same comparison for the maximum temperature.

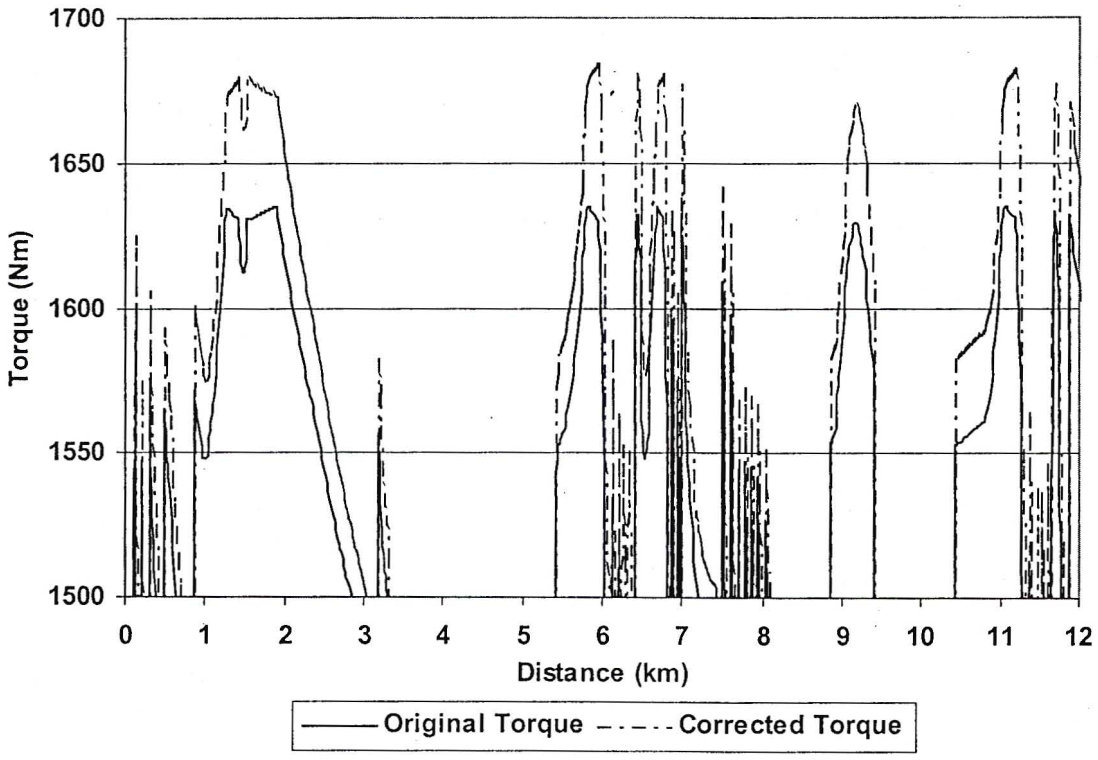

Figure 24 Comparison of original and corrected torque for minimum temperature simulation on the La Mercy to Mount Edgecombe route profile

Figure 24 indicates that there was an increase in torque due to lower ambient temperatures. The average difference in torque was 30.2Nm. The maximum difference was 55.1Nm, which corresponds to a percentage increase of 3.4 %. This increase in torque was due to the fact that the density of air increases with a decrease in temperature. This increase in density allows for a higher mass of air in the combustion chamber, which in turn results in improved combustion, and thus more torque.

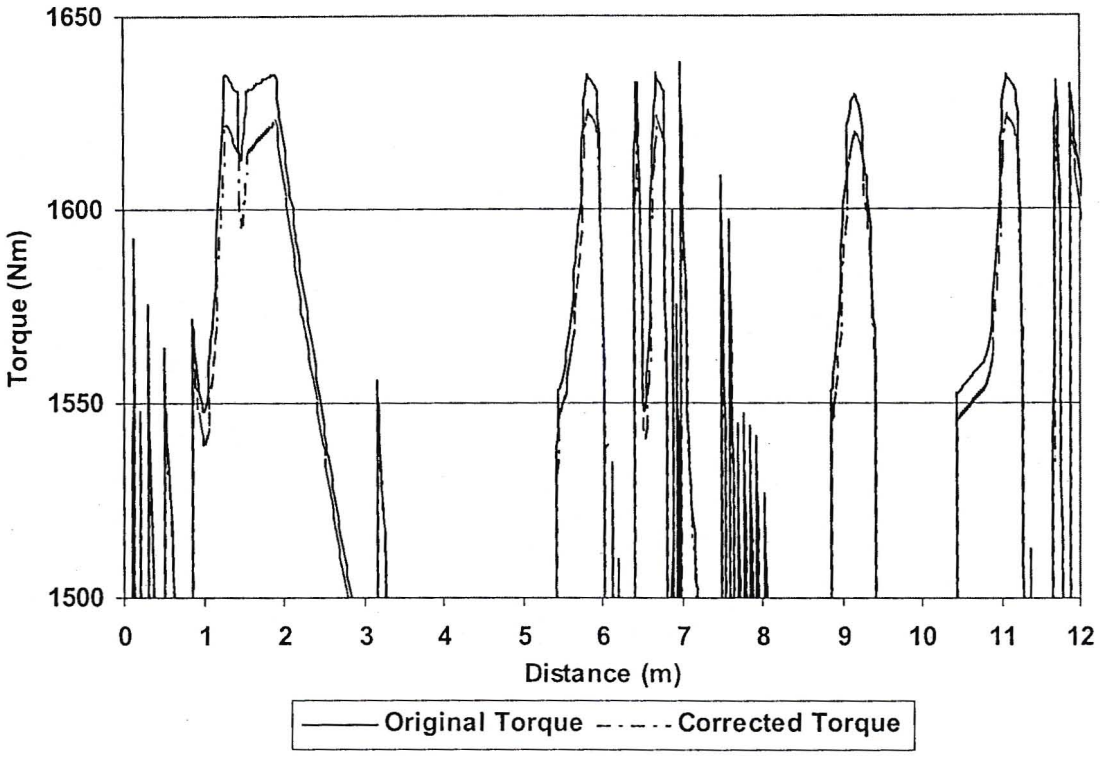

Figure 25 Comparison of original and corrected torque for maximum temperature simulation on the La Mercy to Mount Edgecombe route profile

From figure 25 it can be seen that there was a decrease in torque with an increase in temperature. This was due to the same phenomenon as described above. The average decrease in torque was 8.5Nm and the maximum difference was 16.5Nm, which corresponds to a 1 % decrease. The lower average difference in torque can be attributed to the fact that the engine data was accumulated at standard conditions, and the difference in temperature was larger at the minimum temperatures than at the larger temperatures.

5.1.2 Ambient pressure

To analyse the effect of ambient pressure on torque, a profile of the same route was chosen with a start altitude of 1600 m. This route was chosen because it had been used previously for actual performance tests and simulations.

This produced an average ambient pressure of 84.4 kPa through the route. Since the torque was corrected due to a compounded effect of temperature and pressure, the ambient temperature had to be chosen in such a way as to minimise its effect. This was achieved by choosing a temperature close to the ambient temperature observed during the engine testing, which was on average 22^0C. For this reason the April temperatures of the Free State were chosen. Figure 26 shows the comparison of torque for the original SimTrans model and the corrected torque due to a decrease in ambient pressure.

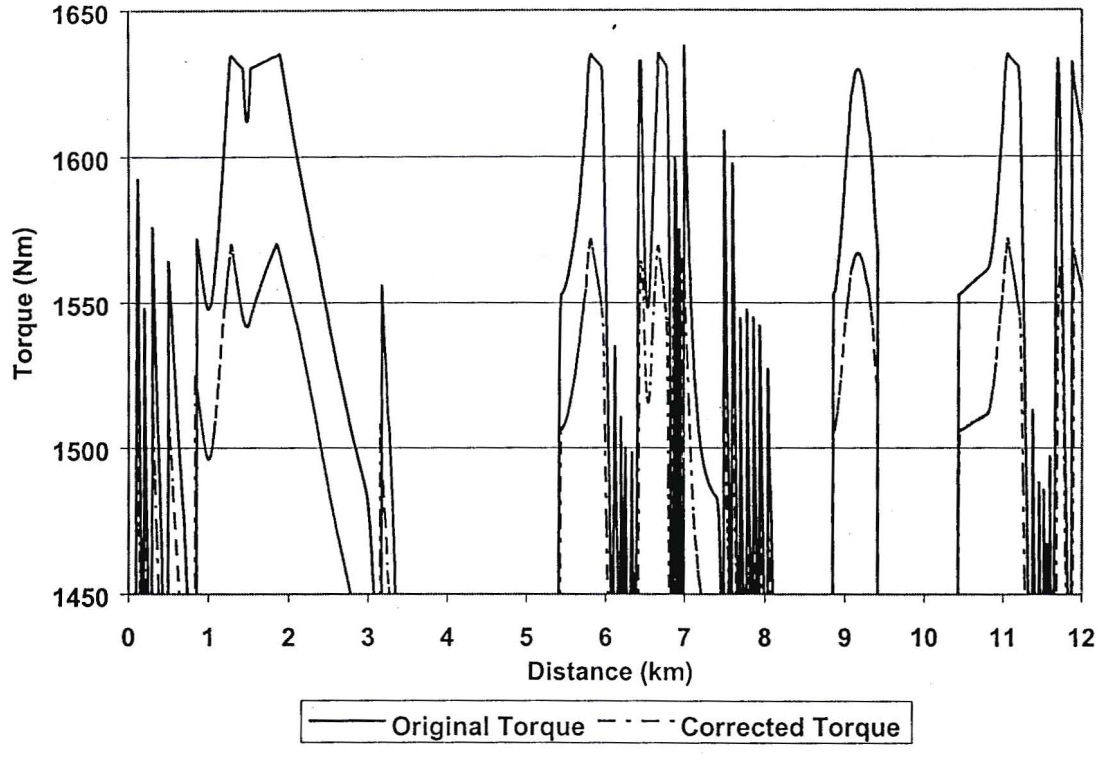

Figure 26 Comparison of original and corrected torque for altitude of 1600 m simulation on the La Mercy to Mount Edgecombe route profile

The average difference in the above torque was 56.3Nm with a maximum of 192.9Nm, which corresponds to a 12.3 % decrease. The reduced torque was due to the lower density of air that results from the lower pressure.

The above was quite significant as it indicated that vehicle operating parameters were very dependent on ambient conditions. This was clearly an important factor especially in South Africa as long distance hauliers experience vast changes in altitude and temperature whilst travelling across the country.

5.2 Results of Neural Network Analysis

The neural network training was a very time consuming task. It involved a trial and error analysis to obtain the best network. Table 9 shows the results of the training process. The basis for selecting the best network was the mean square error, with the network with the lowest value being selected. The percentage error was determined as the ratio of the mean square error to the actual measured test value. The network was also selected due to the 'flattening' or 'decreasing returns' effect. This occurs when the error does not decrease significantly any further and prolonged training does not produce improved results to justify the extra iterations.

Table 9 Results of neural network analysis

Emission	Mean Error (%)	Max Error (%)
Nox	0.9669	4.828
CO	0.5922	3.525
HC	0.5614	2.564
Particulates	0.7998	5.081

Apart from the mean square error, the maximum error was also very important. It gives a clear indication of the magnitude of the largest error. Even though the mean error may be small enough, the max error may still be high and this could account for a large part of the data. A low maximum error guarantees that all the data will be within that limit. This however did not ensure that the test set will be confined to these limits. Figure 27, figure 28, figure 29 and figure 30 show graphs of the measured and predicted results vs. the number of the test point, using the neural network for the test data.

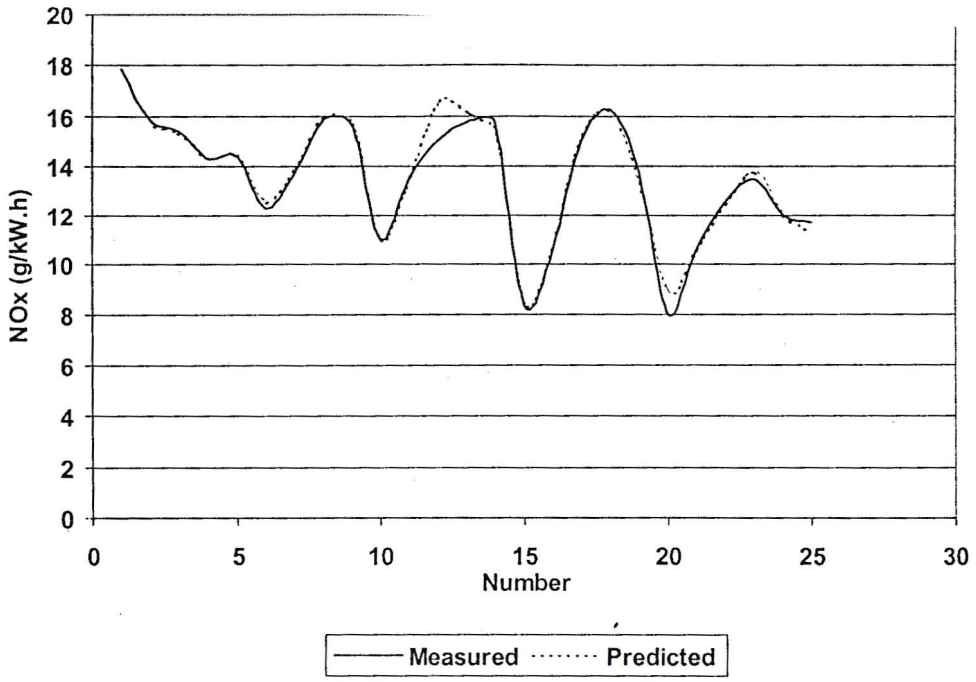

Figure 27 Comparison of measured and predicted results using neural network for NOx emissions

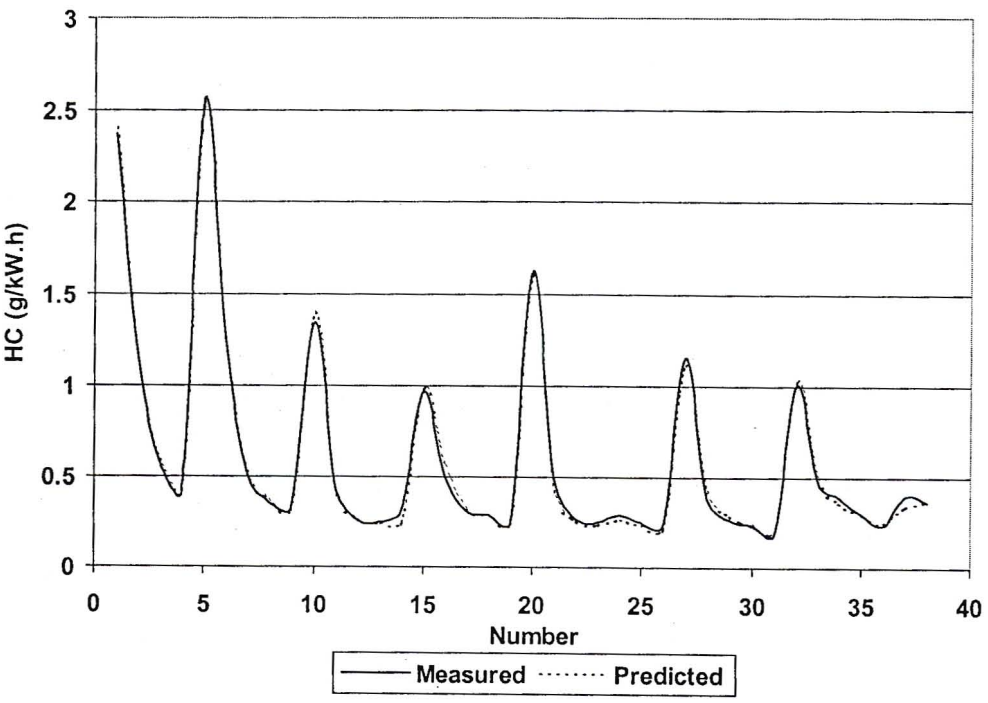

Figure 28 Comparison of measured and predicted results using neural network for HC emissions

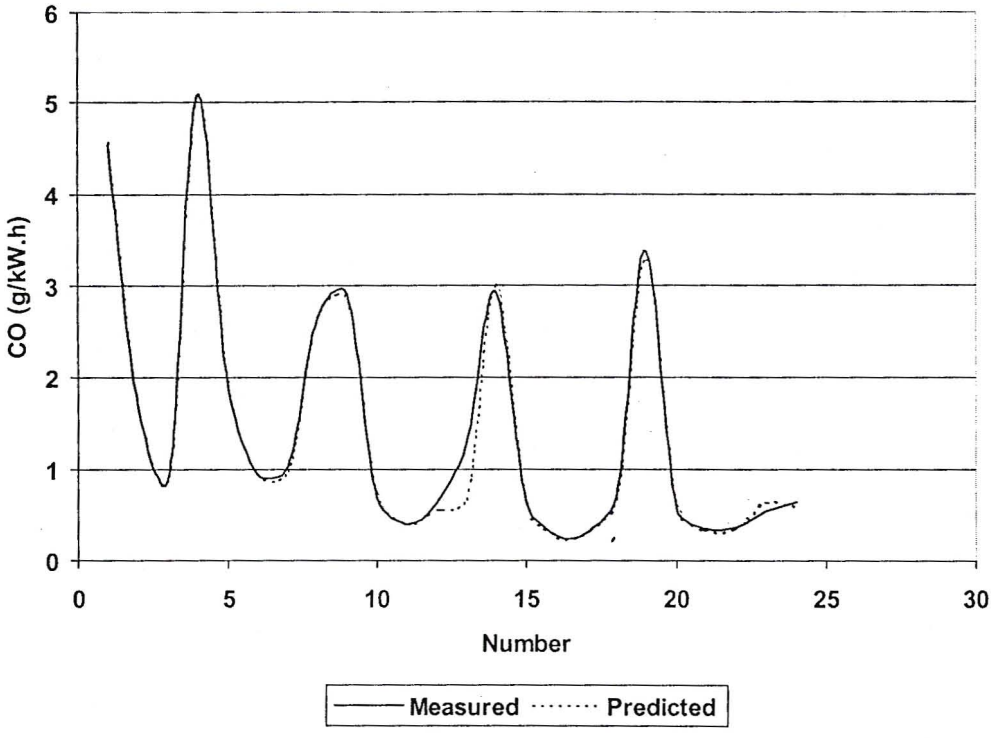

Figure 29 Comparison of measured and predicted results using neural network for CO emissions

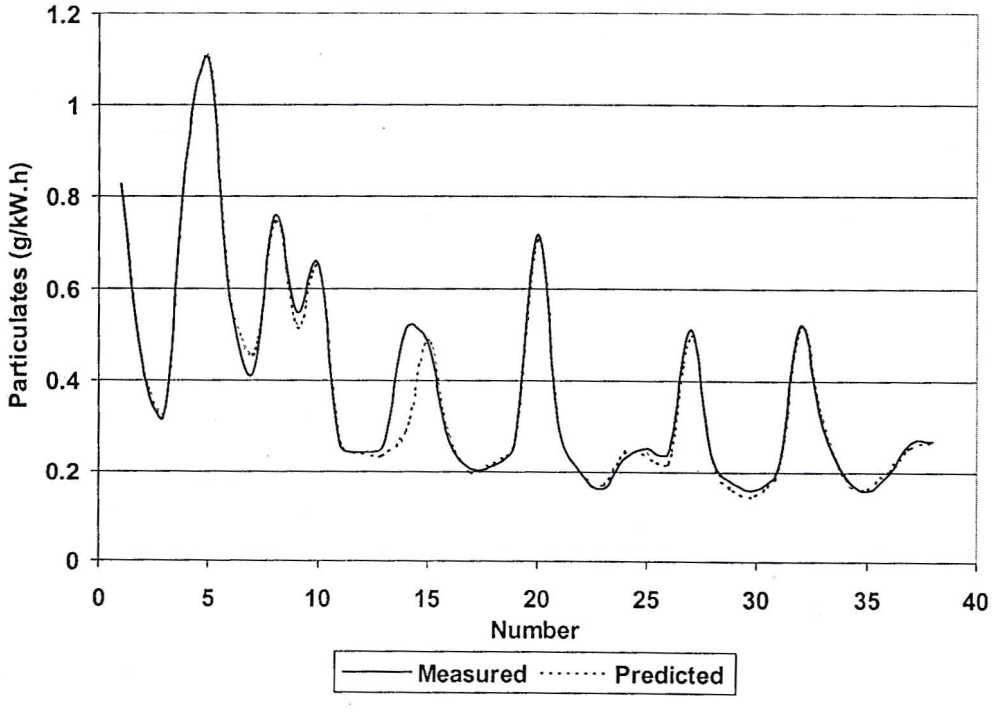

Figure 30 Comparison of measured and predicted results using neural network for particulate emissions

Table 10 provides a statistical analysis of the results. The mean square error was that given by the neural network for the test set and the R squared value was that determined for the measured and predicted results.

Table 10 Statistical results of neural network analysis.

Emission	Mean Square Error	R Squared
NOx	0.01994	0.974013
HC	0.01123	0.997318
CO	0.01993	0.991593
Particulates	0.02918	0.974115

The fit was further emphasised by the following graphs. Figure 31 shows plots of predicted vs. measured results for all emissions.

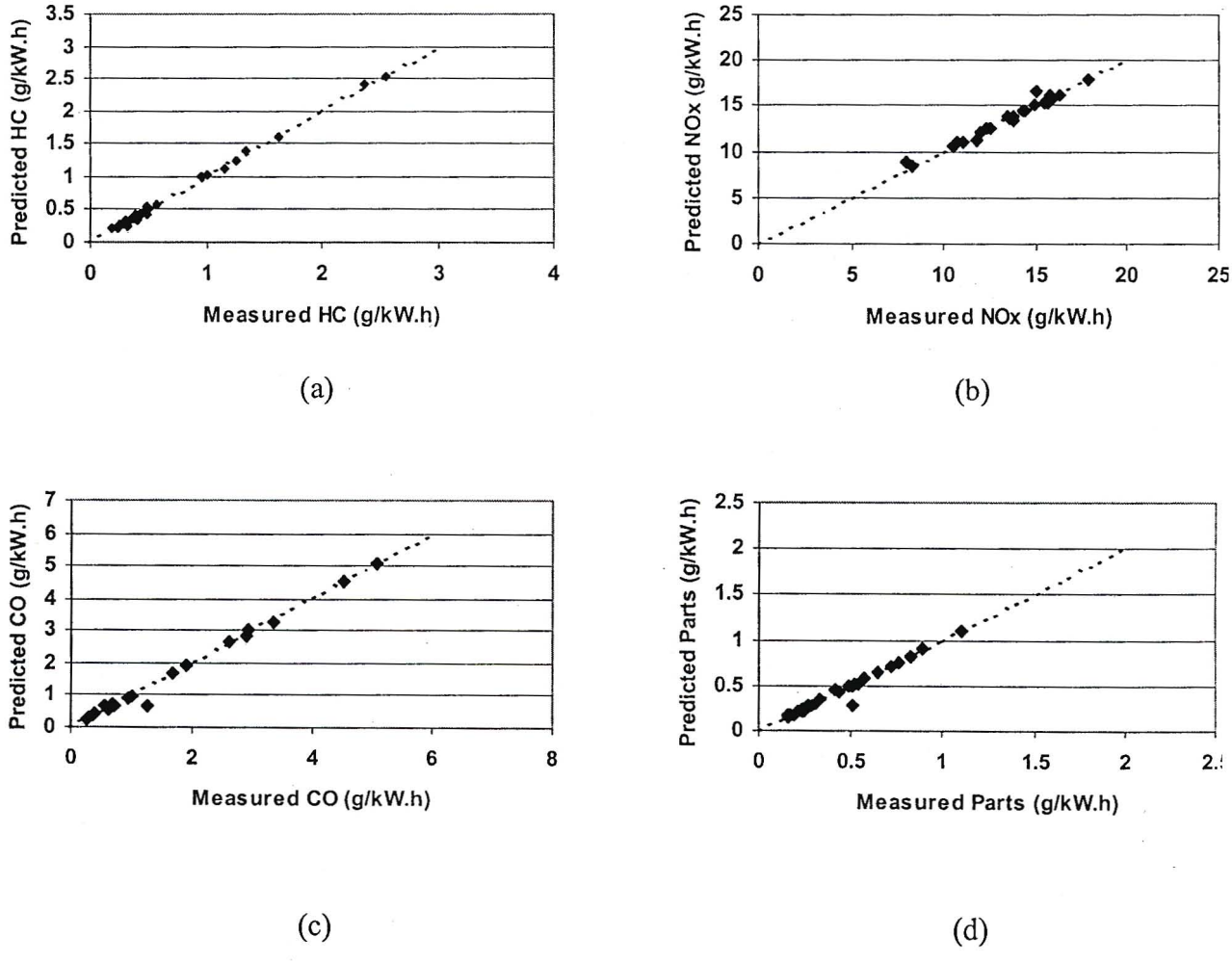

Figure 31 Predicted vs. measured results for emissions of (a) HC, (b) NOx, (c) CO and (d) particulate matter emissions

Figure 27, figure 28, figure 29 and figure 30 show good correlation between the measured and predicted results. The results for NOx and particulates were not as closely correlated as those for HC and CO, however they were still very promising as the R squared values of 0.974 suggests. HC displays the closest correlation between the measured and predicted results, which was also highlighted by its high R squared value of 0.997. CO analysis also shows a good fit with an R squared value of 0.991. Figure 31 gives a better view on the close correlation between the measured and predicted results. All the graphs show that majority of the data points were clustered along the linear trend line (dashed line) with only a few points visibly away from it. The linear trend line was a reflection of both axes. The closer the points were clustered along this line, the closer the correlation between the 2 parameters represented by the X and Y axes.

It was interesting at this stage to compare the above results to those obtained from the literature. Chapter 2 acknowledges work done in the same field by Atkinson *et al.* (1998). Figure 32, figure 33 and figure 34 are results for this study. Figure 32 shows a plot of predicted (virtual) vs. measured results for NOx emissions. Figure 33 shows a similar plot for HC emissions and figure 34 shows a plot of predicted vs. measured CO emissions.

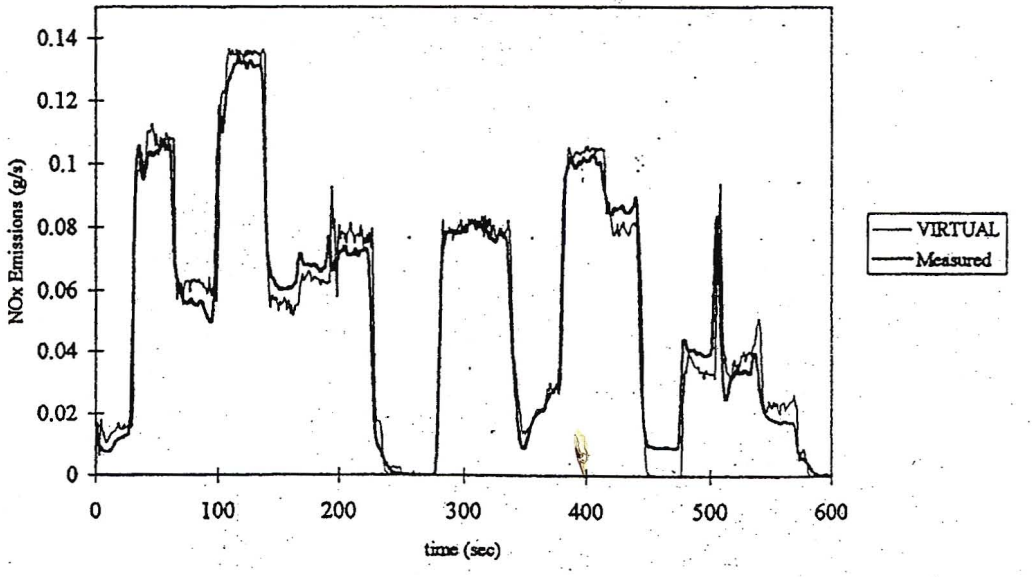

Figure 32 Comparison of measured and predicted results using neural network for NOx emissions, (Atkinson *et al.*, 1998)

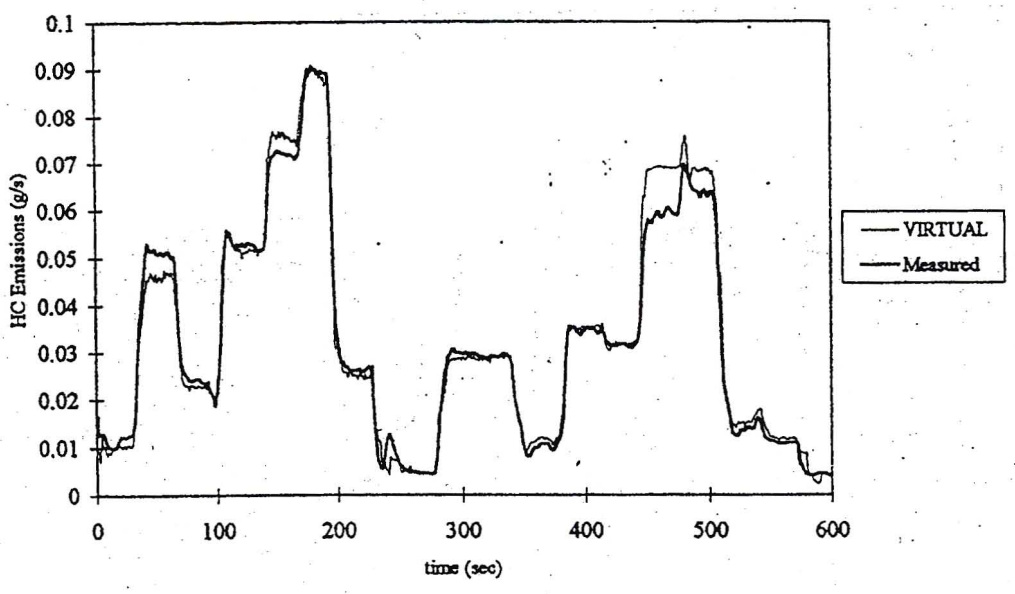

Figure 33 Comparison of measured and predicted results using neural network for HC emissions, (Atkinson *et al.*, 1998)

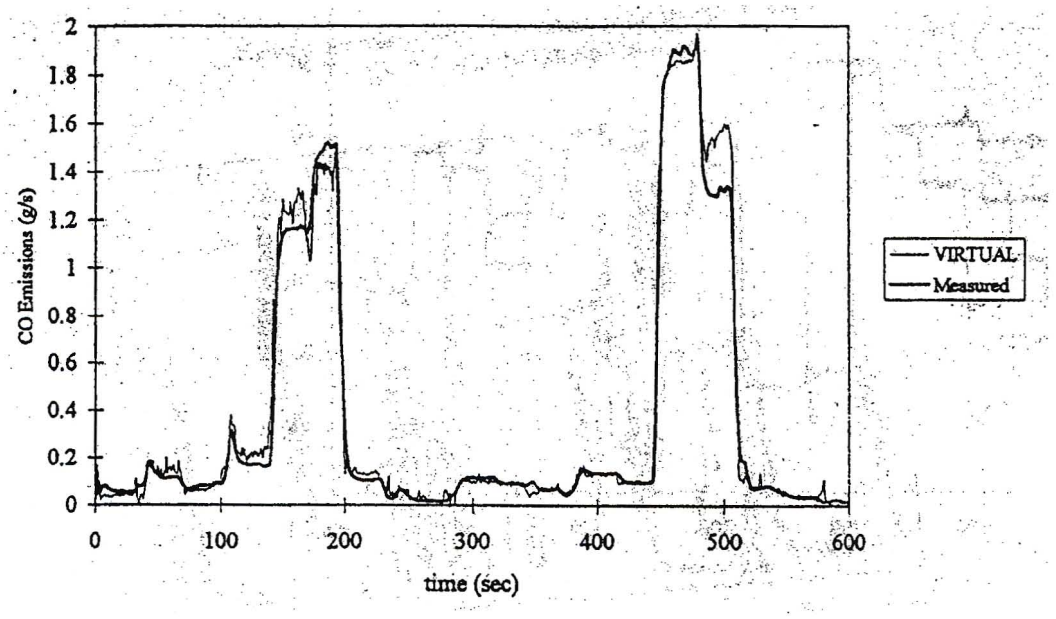

Figure 34 Comparison of measured and predicted results using neural network for CO emissions, (Atkinson *et al.*, 1998)

From a visual analysis the results obtained from this study were very comparable to those obtained by Atkinson *et al.* (1998). Unfortunately a particulate matter analysis was not done, however, the other emissions show close correlation between measured and predicted results, similar to that obtained in the present study. I believe these results can then be used with confidence, not only because of the close correlation obtained during testing but also due to their favourable showing in contrast to similar models.

5.3 Sensitivity Analysis

Another important step in developing a model was to perform a sensitivity analysis. In this case the response of the vehicle operating parameters to a change in ambient conditions will be assessed. In addition, the response of emissions with a change in ambient conditions as well as vehicle operating parameters was investigated.

5.3.1 Sensitivity of vehicle operating parameters to ambient conditions

For vehicle operating parameters only engine torque and fuel consumption were considered. Firstly the vehicle was modelled to operate at full throttle at 1400 rpm. At this speed, the engine was at the maximum torque of 1635Nm. This torque setting was chosen, as it was the area on the engine map in which SimTrans operates for majority of the time. The ambient temperature was kept at 25^0C. The torque and fuel consumption were recorded at different altitude intervals increasing from sea level. Figure 35 shows the response of torque to the change in altitude. The ambient pressure decreased linearly from 101.325 kPa at sea level to 90.405 kPa at 1000m above sea level.

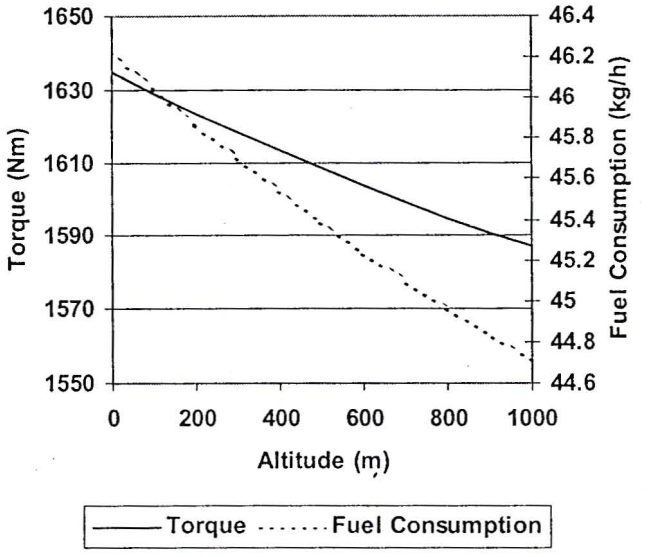

Figure 35 Response of torque and fuel consumption to changes in altitude

Figure 36 shows the sensitivity of torque to altitude. The figure gives the percentage decrease in torque due to changes in altitude from one level to the next (incremental) and the total change from sea level. With a 200m increase in altitude there was a 0.69% decrease in engine torque. However with a further 200m increase in altitude there was only a 0.65% decrease in engine torque. This shows that there was a non-linear relationship between engine torque and ambient pressure.

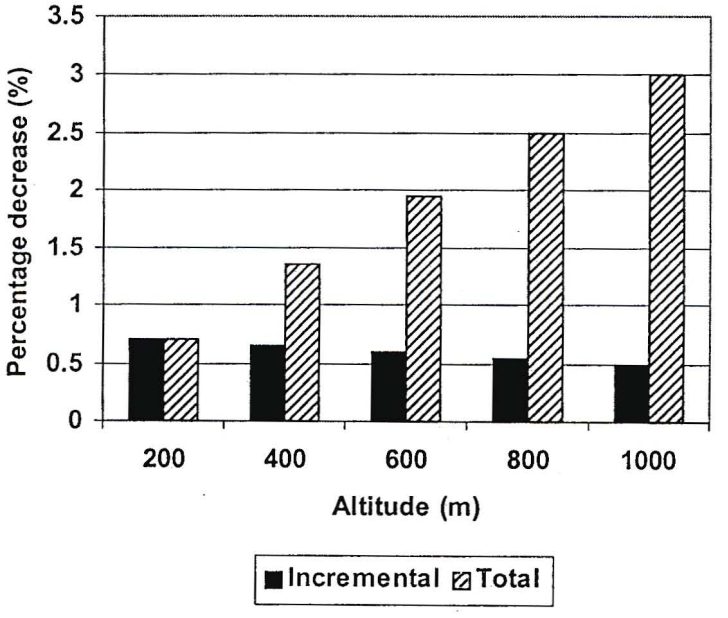

Figure 36 Percentage changes in engine torque expressed as incremental and total increase due to a change in altitude

The change in altitude from 800m to 1000m produces a 0.49% decrease in engine torque. The total decrease in torque resulting from the altitude of 1000m was 3% i.e. 1587Nm. Figure 37 was a similar analysis for fuel consumption. An increase in altitude of 200m from sea level produces a decrease in fuel consumption of 3.83%. The total decrease in fuel consumption for an increase in altitude from sea level to 1000m was 3.38% i.e. from 46.23 kg/h to 44.71kg/h. This decrease was due to the fact that at a higher altitude there was a decrease in density of air and hence less fuel will be required for combustion.

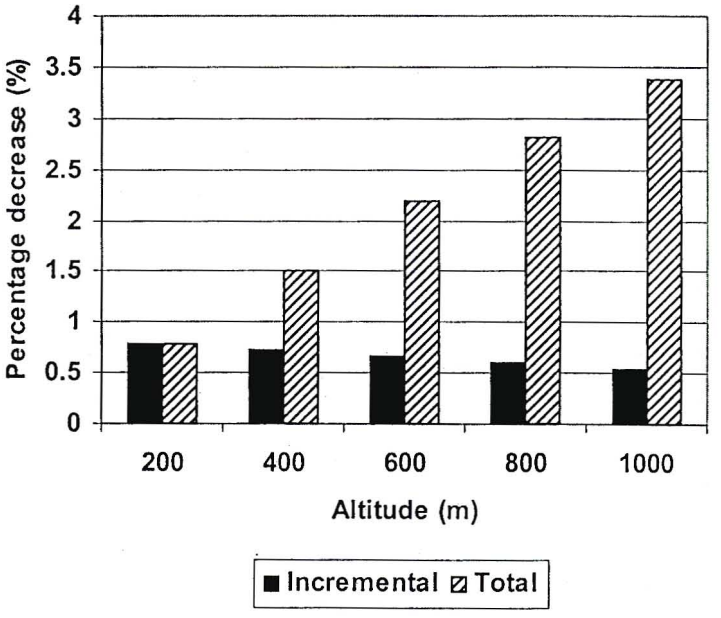

Figure 37 Percentage changes in fuel consumption expressed as incremental and total increase due to a change in altitude

To assess the sensitivity of the model to ambient pressure the vehicle was operated at the same mode on the engine map but the altitude was kept constant at sea level. The ambient temperature was then increased and decreased from 25^0C. Figure 38 illustrates the response of engine torque and fuel consumption to the change in ambient temperature. The response was almost linear.

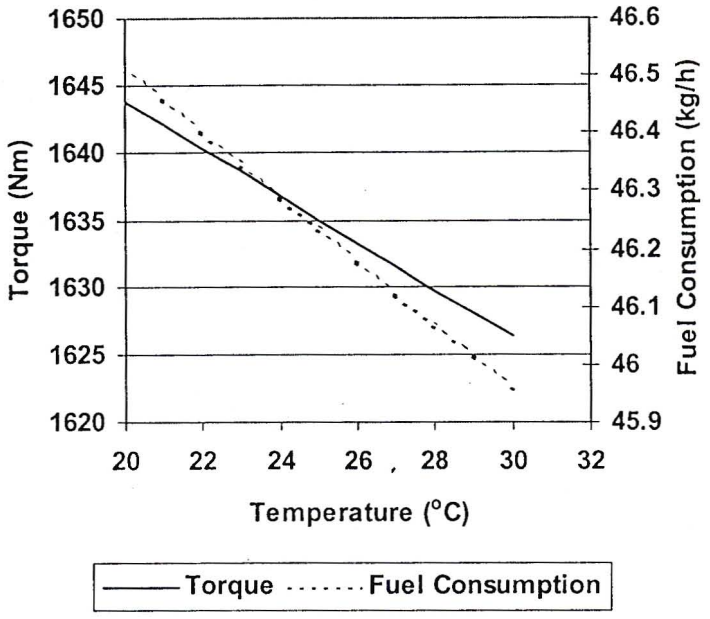

Figure 38 Response of torque and fuel consumption to changes in ambient temperature.

In figure 38 for temperatures greater than 25^0C there was a decrease in torque and fuel consumption and for temperatures less than 25^0C there was an increase. Even though the response of engine torque and fuel consumption to changes in ambient temperature appear to be linear as can be seen by figure 38 and figure 39, there was a slight discrepancy. For example there was a 0.43% increase in torque for a 4^0C decrease in temperature, and a 0.42% decrease in torque due to a 4^0C increase in temperature. This 0.01% discrepancy also exists for a 5^0C change in temperature. There was a 0.02% difference in fuel consumption for a 5^0C change in temperature. Although this value may be small it was important to note that the response was not linear.

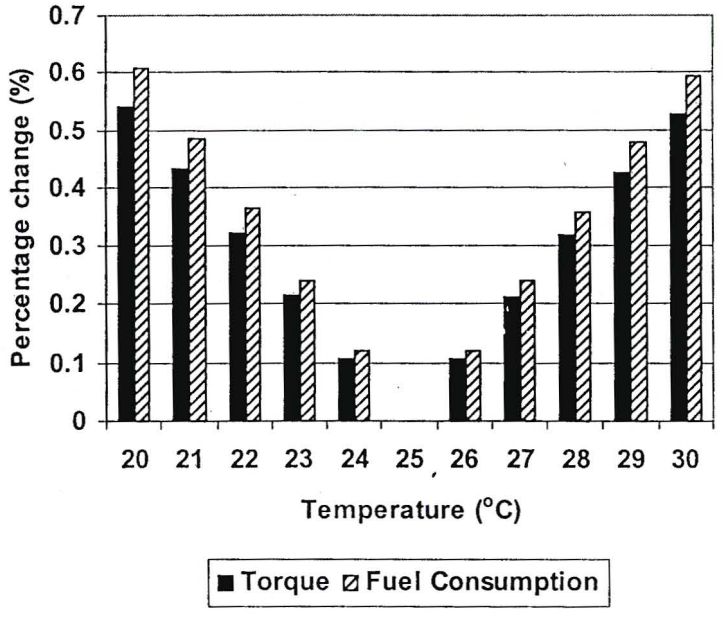

Figure 39 Percentage change in torque and fuel consumption due to changes in temperature

5.3.2 Sensitivity of emissions to ambient conditions and vehicle operating parameters

A more comprehensive analysis of emissions sensitivity was required. This was due to the different mechanisms working at different points on the engine map. For this reason 5 speed and torque settings were chosen (figure 40):

1) Low speed, low torque (800 rpm, 200Nm),
2) Low speed, high torque (800 rpm, 1054Nm),
3) High speed, low torque (2100 rpm, 200Nm),
4) High speed, high torque (2100 rpm, 1273Nm) and
5) Max torque (1400 rpm, 1635Nm).

For the sensitivity analysis of emissions to altitude the vehicle was operated at 25^0C, and the altitude was increased by 100m, 200m, 500m and 1000m from sea level. Figure 41, figure 42, figure 43, figure 44 and figure 45 illustrate the sensitivity of emissions to an increase in altitude for the above 5 speed and torque settings. The percentage values of these changes are given in table 11, negative values indicate decreases.

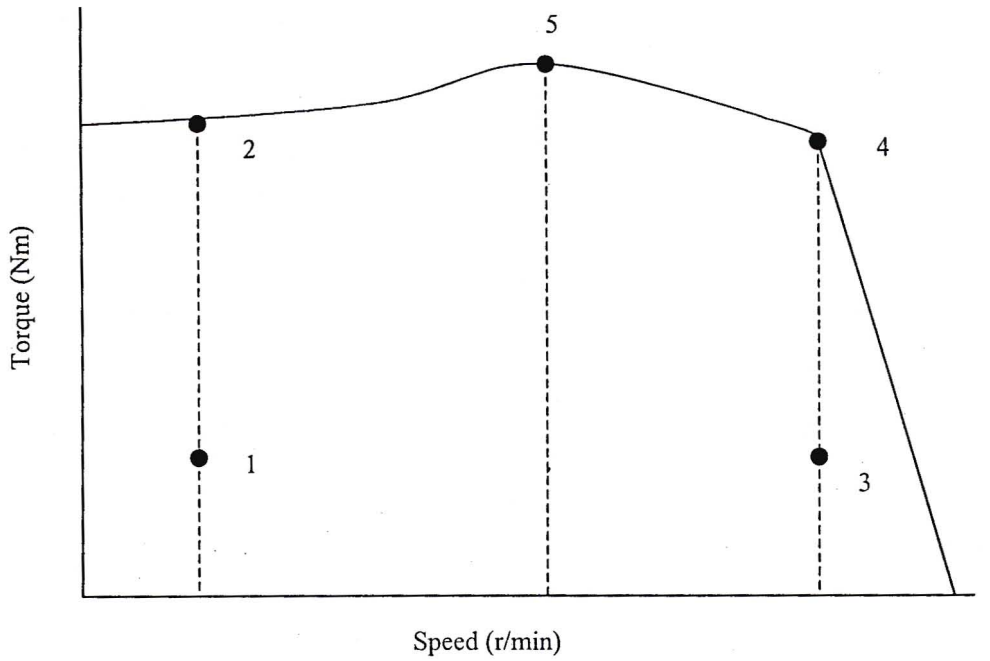

Figure 40 Engine map showing speed and torque settings used for sensitivity analysis

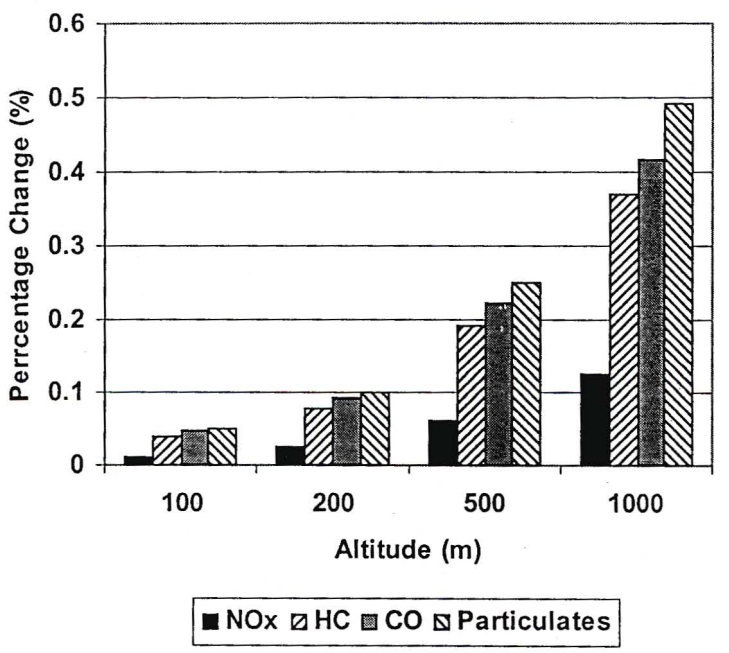

Figure 41 Percentage change in emissions due to increases in altitude from sea level for 800 rpm and 200Nm

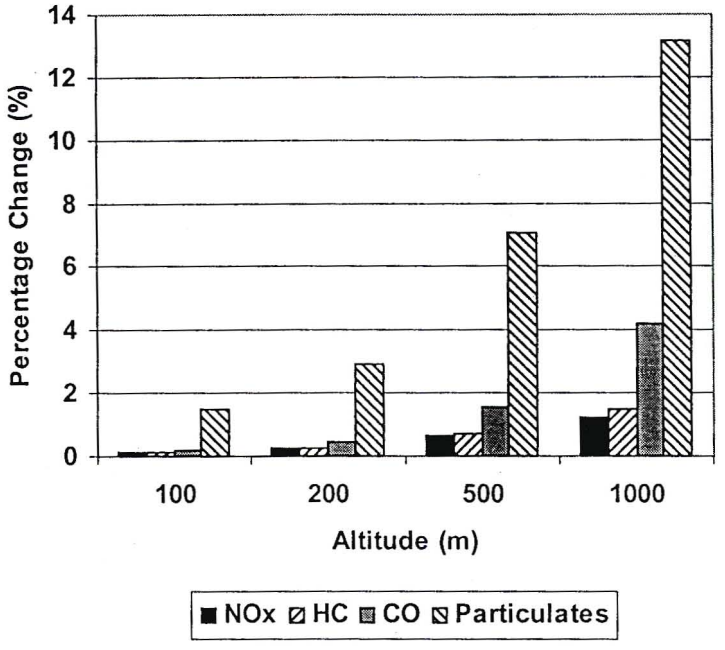

Figure 42 Percentage change in emissions due to increases in altitude from sea level for 800 rpm and 1054Nm

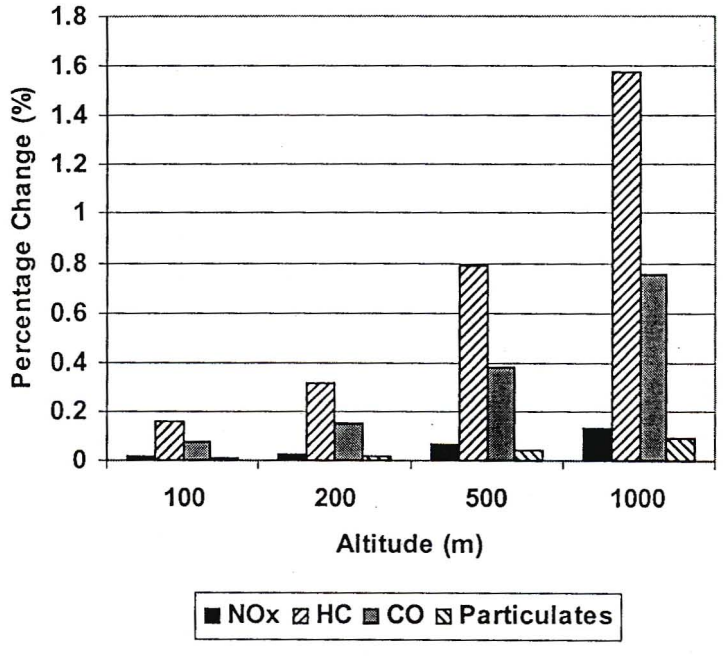

Figure 43 Percentage change in emissions due to increases in altitude from sea level for 2100 rpm and 200Nm

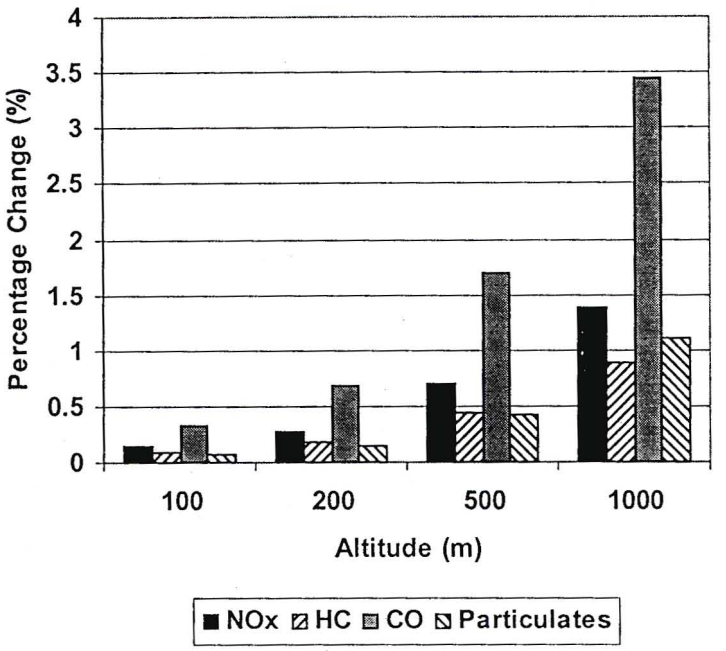

Figure 44 Percentage change in emissions due to increases in altitude from sea level for 2100 rpm and 1273Nm

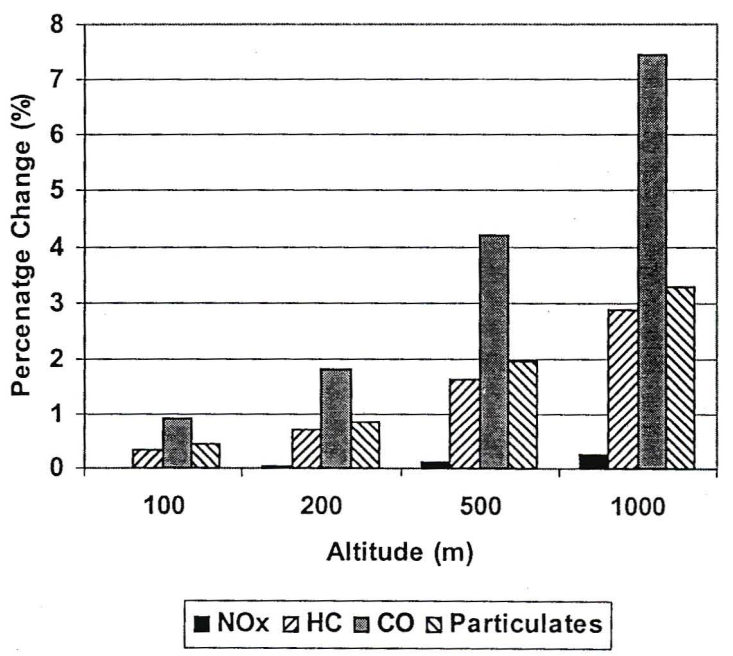

Figure 45 Percentage change in emissions due to increases in altitude from sea level for 1400 rpm and 1635Nm

Table 11 Percentage values for change in emissions due to increases in altitude

Altitude (m)	Speed (rpm)	Torque (Nm)	% Change NOx	% Change HC	% Change CO	% Change Particulates
100	800	200	-0.011752	0.038991	0.046865	0.050666
200	800	200	-0.023647	0.077517	0.09248	0.100973
500	800	200	-0.060173	0.190349	0.222131	0.249775
1000	800	200	-0.123757	0.369491	0.415991	0.49088
100	800	1054	0.142207	0.136662	-0.215598	1.479341
200	800	1054	0.279517	0.276929	-0.480255	2.923953
500	800	1054	0.662486	0.717329	-1.55888	7.043447
1000	800	1054	1.207621	1.503867	-4.223632	13.17924
100	2100	200	-0.013185	0.157822	0.075701	-0.008641
200	2100	200	-0.02634	0.315652	0.151397	-0.017318
500	2100	200	-0.065628	0.789163	0.378443	-0.043558
1000	2100	200	-0.130519	1.57833	0.756681	-0.087995
100	2100	1273	0.140901	0.089253	-0.336859	0.065969
200	2100	1273	0.281246	0.178442	-0.675557	0.141532
500	2100	1273	0.699356	0.445644	-1.702894	0.426355
1000	2100	1273	1.388662	0.889862	-3.453876	1.098815
100	1400	1635	0.012579	0.350197	0.927717	0.444281
200	1400	1635	0.029245	0.685964	1.811411	0.86287
500	1400	1635	0.100886	1.606667	4.210769	1.9608
1000	1400	1635	0.270876	2.858533	7.435307	3.2777

For the sensitivity analysis of emissions to ambient temperature the vehicle was operated at sea level, and the temperature was decreased by 1^0C, 2^0C, 5^0C and 10^0C from 25^0C. Figure 46, figure 47, figure 48, figure 49 and figure 50 illustrate the sensitivity of emissions to an decrease in ambient temperature for the same 5 speed and torque settings. The percentage values of these changes are given in table 12, negative values indicate decreases.

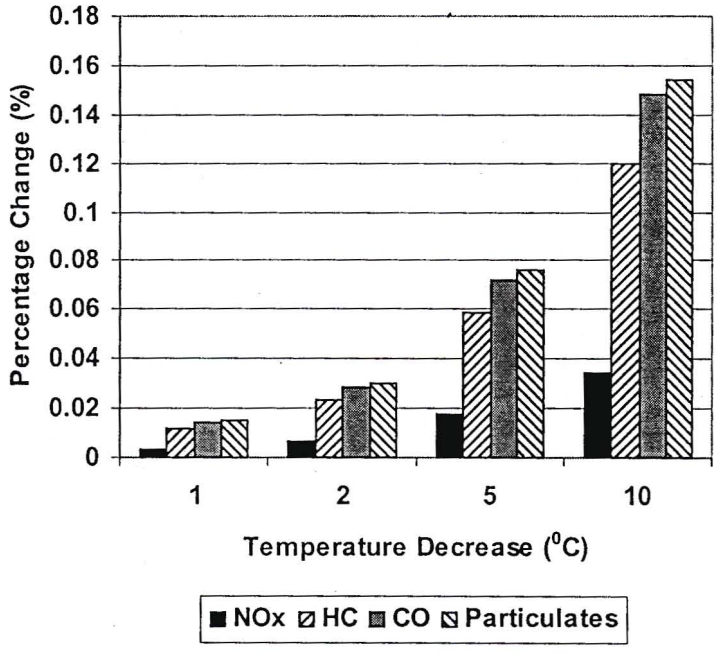

Figure 46 Percentage change in emissions due to increases in ambient temperature for 800 rpm and 200Nm

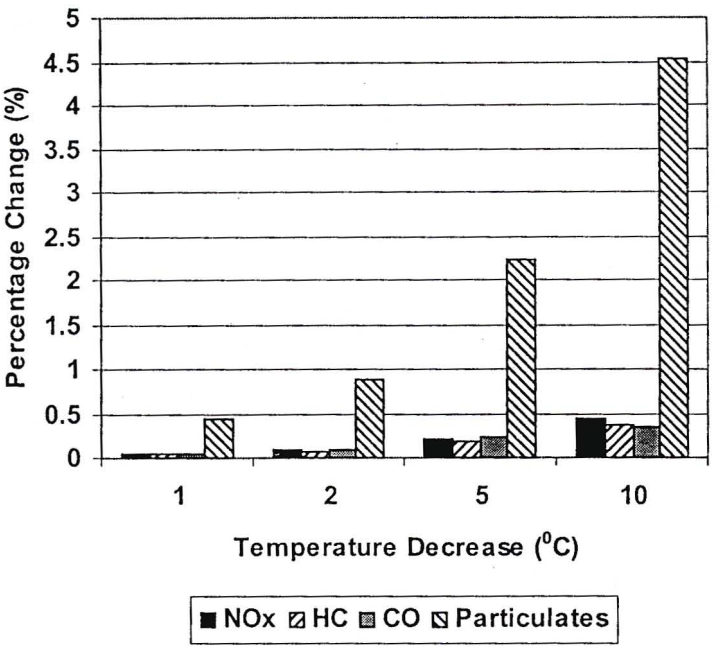

Figure 47 Percentage change in emissions due to increases in ambient temperature for 800 rpm and 1054Nm

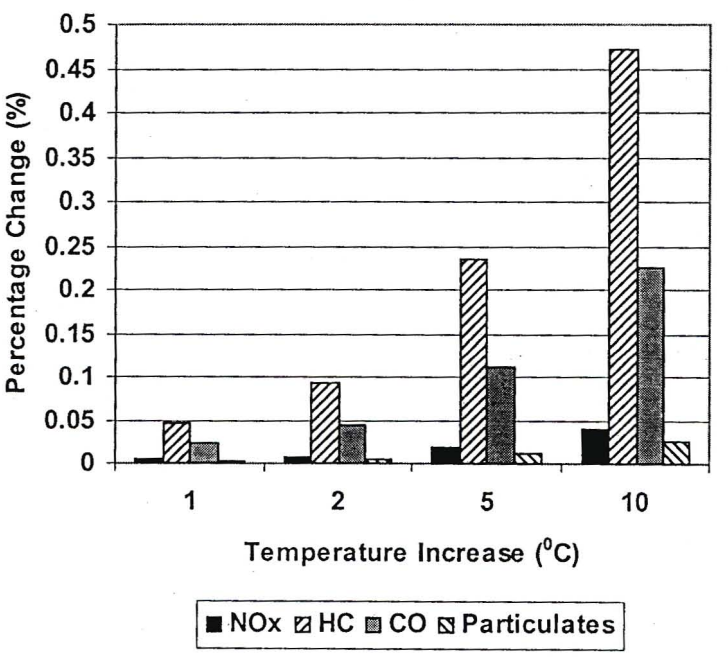

Figure 48 Percentage change in emissions due to increases in ambient temperature for 2100 rpm and 200Nm.

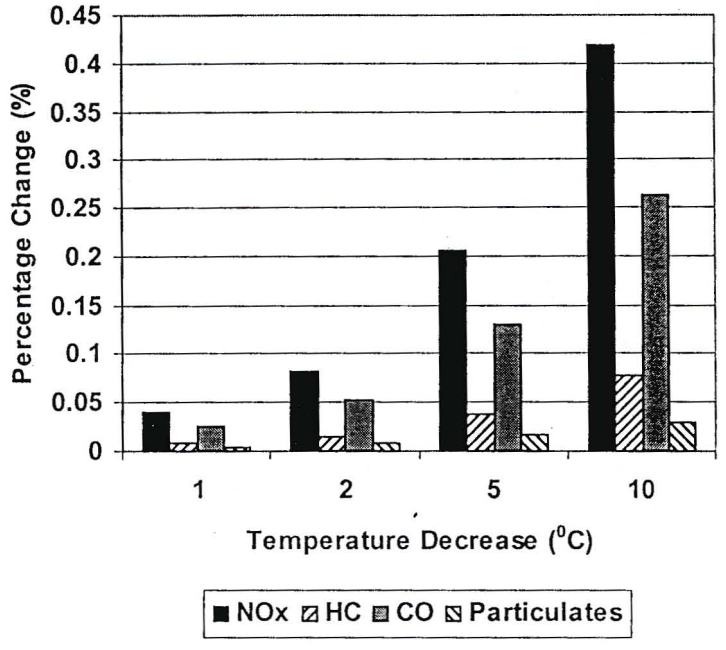

Figure 49 Percentage change in emissions due to increases in ambient temperature for 2100 rpm and 1273Nm

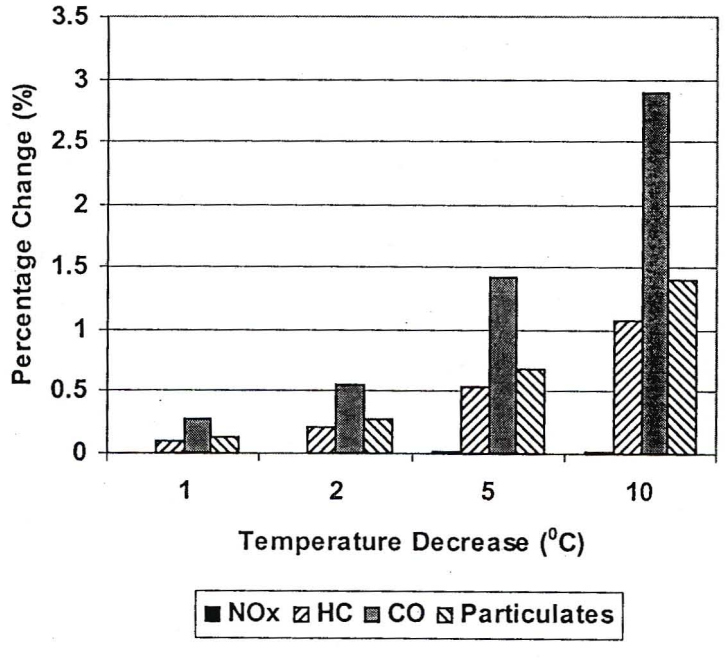

Figure 50 Percentage change in emissions due to increases in ambient temperature for 1400 rpm and 1635Nm

Table 12 Percentage values for change in emissions due to decreases in ambient temperature

Temperature (^{0}C)	Speed (rpm)	Torque (Nm)	% Change NOx	% Change HC	% Change CO	% Change Particulates
24	800	200	0.003436	-0.011582	-0.014057	-0.015003
23	800	200	0.006872	-0.023245	-0.028275	-0.030089
20	800	200	0.017171	-0.058721	-0.07191	-0.075846
15	800	200	0.034304	-0.119525	-0.148061	-0.153824
24	800	1054	-0.04277	-0.039487	0.053974	-0.441675
23	800	1054	-0.085939	-0.078615	0.103591	-0.885972
20	800	1054	-0.217858	-0.193817	0.226258	-2.234461
15	800	1054	-0.445857	-0.378384	0.343227	-4.532987
24	2100	200	0.003892	-0.046519	-0.022315	0.00254
23	2100	200	0.0078	-0.093195	-0.044706	0.005086
20	2100	200	0.01962	-0.234168	-0.112337	0.012757
15	2100	200	0.039644	-0.472341	-0.226617	0.025655
24	2100	1273	-0.040902	-0.007628	0.026137	-0.003805
23	2100	1273	-0.081994	-0.015283	0.052321	-0.007443
20	2100	1273	-0.206438	-0.038415	0.131152	-0.017342
15	2100	1273	-0.417905	-0.077537	0.263496	-0.030361
24	1400	1635	0.00288	0.105415	0.28058	0.135046
23	1400	1635	0.005367	0.211318	0.563115	0.271257
20	1400	1635	0.010515	0.531917	1.422662	0.686518
15	1400	1635	0.011631	1.075595	2.896371	1.398509

Next an investigation was performed on the sensitivity of emissions on torque and speed. For this analysis ambient temperature and temperature were kept at standard conditions. For the sensitivity of emissions on torque, speed was kept constant at 1400 rpm and the torque increased from 200Nm to 1000Nm. For speed sensitivity, torque was kept constant at 1400Nm and speed was increased from 1000 rpm to 2000 rpm. It was not possible to choose max load, as the torque would change as the speed increases. These speed and torque settings were chosen as it was within this area on the engine

map where the vehicle usually operates. Figure 51 illustrates the percentage change in emissions due to a change in torque. Figure 52 shows the effect of a change in speed on emissions.

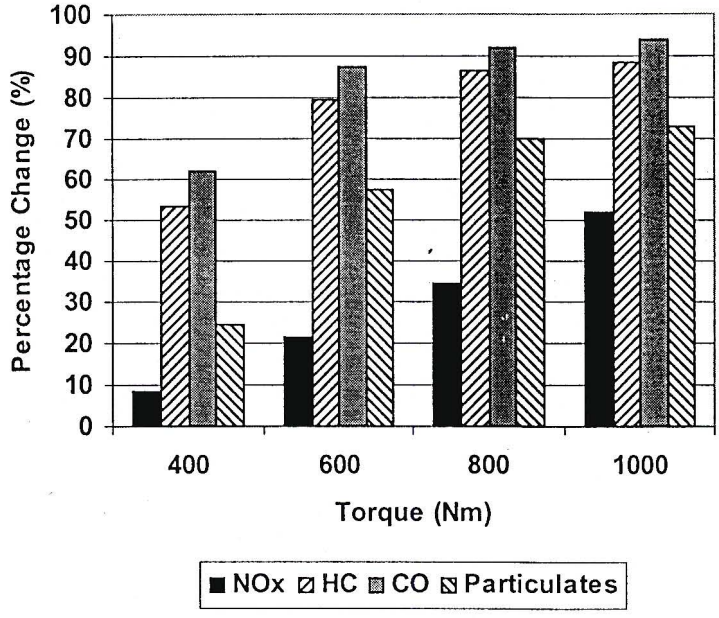

Figure 51 Percentage change in emissions due to changes in torque at a constant speed of 1400 rpm

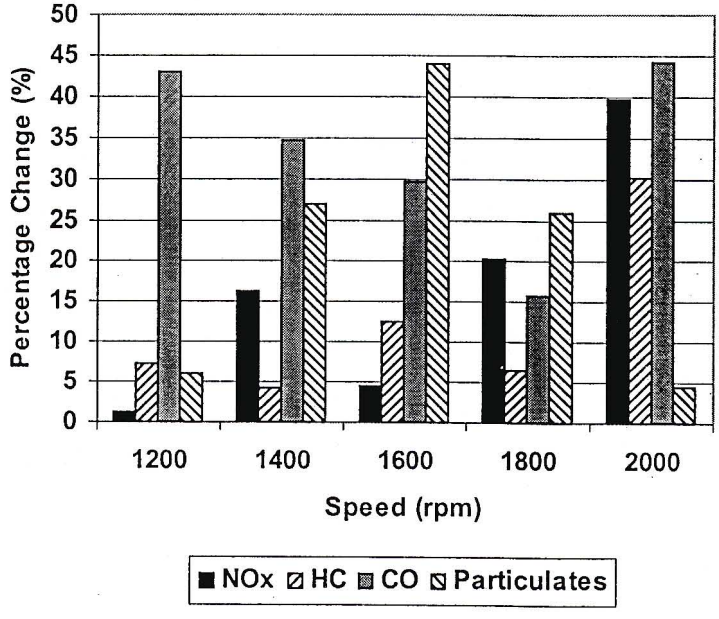

Figure 52 Percentage change in emissions due to changes in speed at a constant torque of 1400Nm

The analysis for the sensitivity of ambient conditions and vehicle operating parameters on emissions shows varying trends for the different speed and torque settings. The above figures and tables show the percentage changes in the emission. All the above results were analysed on a cumulative basis i.e. the change in emissions were calculated from the standard condition.

For the first speed and torque setting NOx decreased with an increase in altitude whereas the other emissions increased (figure 40). This was a low speed and load setting, and thus the reduction of load with the increase in altitude also reduced NOx, which usually predominates at higher loads. The decrease in CO was expected due to the limited air available for combustion at higher altitudes. HC and particulates also form more predominantly at low loads. This was due to over-leaning that occurs at low loads. The sensitivity of emissions to a 100m change in altitude at this setting was also small, with a 0.01% reduction in NOx and particulates increasing by 0.05% (table 11). The corresponding increase due to a 1000m increase in altitude was 0.1% and 0.5% respectively.

The opposite trends occur for the temperature analysis at the same speed and torque setting. This was because with a decrease in temperature there was an increase in density of air and hence an increase in torque. This explains the increase in NOx and the decrease in the other emissions. There was an even smaller sensitivity to a decrease in temperature, with the smallest change being NOx with a 0.003% increase and the highest change of 0.015% in particulates for a 1^0C change in temperature. A 10^0C decrease causes an increase in the response by 10 fold.

For the second speed and torque setting (800 rpm, 1054 Nm), CO decreases whereas the other emissions increase. This decrease in CO indicates that the engine was not operating very efficiently and the reduced air density increases the efficiency and hence the lower CO. This same explanation can be adopted for the other emissions. Most of the intake air may not be used in combustion and thus with the lower air density caused by the higher altitudes, the engine becomes more efficient and utilises the available air. These emissions were also more sensitive to a change in altitude than at the lower torque for the same speed. NOx increases by 0.14% with an increase in altitude of 100m and particulates increased by 1.5 %.

Once again the trends were opposite for decreases in temperature. Emissions were also more sensitive to temperature at this setting. For a 1^0C decrease in temperature there was a 0.04% and 0.44% decrease in NOx and particulates respectively. This was significantly larger than the changes that occurred at low torque. A 10^0C change in temperature produced a 0.45% and a 1.43% change in these emissions. This sensitivity can be based on the assumption that emissions that predominate at higher loads will be more sensitive to a change in temperature at those loads.

For the next setting, NOx and particulates decreased whilst HC and CO increased with an increase in altitude. This setting can be seen as high idle. Thus HC would have increased due to the over leaning effect. CO increased due to the reduced air density as explained earlier. NOx and particulates decreased due to the lower load caused by an increase in altitude. The sensitivity of particulates decreased at this setting compared to the first speed and torque setting. The sensitivity of NOx, CO and HC also increased with HC being most sensitive to a 100m increase in altitude with a 0.16% increase.

Even though the trends were opposite to that for altitude, HC was also most sensitive to a decrease in temperature with a 0.05% change for a 1^0C change in temperature. NOx was also more sensitive, but not as significant as CO. Particulates only changed by 0.002% as compared to the 0.01% that occurred at the first setting. CO was more sensitive at this sensitive as it was a high speed yet low load condition. This meant that combustion was not very efficient, and because there was more air being inducted into the cylinder per unit time, the CO formation would have depended on the volume of the air, in this case being effected by the density which was influenced by the decrease in temperature.

For the high speed and high torque setting all the emissions except CO, increase with an increase in altitude. This was similar to that for the second setting. In this case CO was most sensitive to an increase in altitude of 100m with a 0.34% change. NOx displays a very similar sensitivity as the second setting. Particulates were again less sensitive than that at the second setting with a 0.07% change, however not as low as the previous one. Particulates do however produce a higher sensitivity to a 1000m change in altitude. As expected NOx showed a high sensitivity due to the high load condition. Any change in the parameters that effect combustion will be sensitive to NOx formation at this setting.

In this case it was altitude, but it was also sensitive to temperature, as will be shown next. CO emissions were less at high load settings due to improved efficiencies. Particulates were also less dominant at high loads due to better mixing and improved combustion.

Particulates again show a small sensitivity to temperature. NOx has the highest sensitivity to a 1^0C decrease in temperature with a 0.04% change, as compared to the 0.004% change of particulates. Even for a 10^0C change in temperature particulates only changes by 0.03%. The above explanation was suitable for the sensitivity of emissions in this case as well.

When the speed was kept constant and the torque increased, the emissions displayed a large sensitivity. CO increased by 62% for a 200Nm increase in torque. NOx increased the least with 8%. For a 800Nm increase in torque, the four emissions of NOx, HC, CO and particulates increased by 52%, 89%, 94% and 73% respectively.

This was explained by considering that increasing load at a constant speed requires increasing the fuel delivery with no increase in air induction. The reduced air supply coupled with an increase in fuel describes the high sensitivity of CO. CO increases with a decrease in air supply due to incomplete combustion. NOx was not as sensitive as one would expect because it depends on atmospheric nitrogen for formation, which did not increase due to the constant engine speed.

For the speed analysis, the emissions behaved a little differently. Keeping the torque constant and increasing the speed, caused NOx to increase, decrease, increase and then decrease over the last two speed settings. Similar patterns were observed for the other emissions as well. For a 200 rpm increase in speed CO showed the largest sensitivity with a 43% change and NOx, HC and particulates changing by 1%, 7% and 6% respectively. For a 1000rpm increase in speed, NOx decreased by 40%, HC increased by 30%, CO increased by 44% and particulates decreased by 4%. These results were an indication of the increase in the air inducted as the speed was increased. The erratic change in emissions due to a changes made to engine speed can be attributed to the fact that the engine was running at part load, where it was not very stable. The initial

decrease in CO was due to the increase in air induction associated with the rise in engine speed.

5.4 Analysis of Different Routes in South Africa

To illustrate the usefulness of the model, simulations were performed on two test routes:

1) Durban to Johannesburg and
2) Cape Town to Johannesburg.

To illustrate the variations these routes were analysed for 3 different scenarios i.e.

1) January (Summer temperatures),
2) July (Winter temperatures) and
3) No payload.

The vehicle is loaded to maximum in its normal configuration in SimTrans, as it is most economical to do so. Therefore the other extreme was to operate the vehicle with no payload. Although overloading of vehicles occurs frequently it is not good practice and illegal and therefore not considered in this study. This investigation assessed the effect of payload on emissions, and thus a fully laden vehicle vs. an empty one was adequate for this. Based on the following results one can intuitively extrapolate the emissions that may be generated in relation to the degree of overloading, but this is beyond the scope of this project and not presently considered. The model is however capable of investigating the effect of an overloaded vehicle on emissions, as the payload can be edited in the vehicle input file.

5.4.1 Durban to Johannesburg

Vehicles travelling from Durban to Johannesburg use the N3 national highway. This route was approximately 556 km's. The difference in altitude between these 2 cities was over 1500 m. Figure 53 illustrates the varying altitude and ambient pressure across this route. The inverse trend that exists between these 2 parameters can easily be seen in this figure.

A vehicle travelling from Durban to Johannesburg using the N3 passes through 3 provinces, Kwazulu-Natal, Free State and Gauteng. Each of these provinces has a different temperature profile.

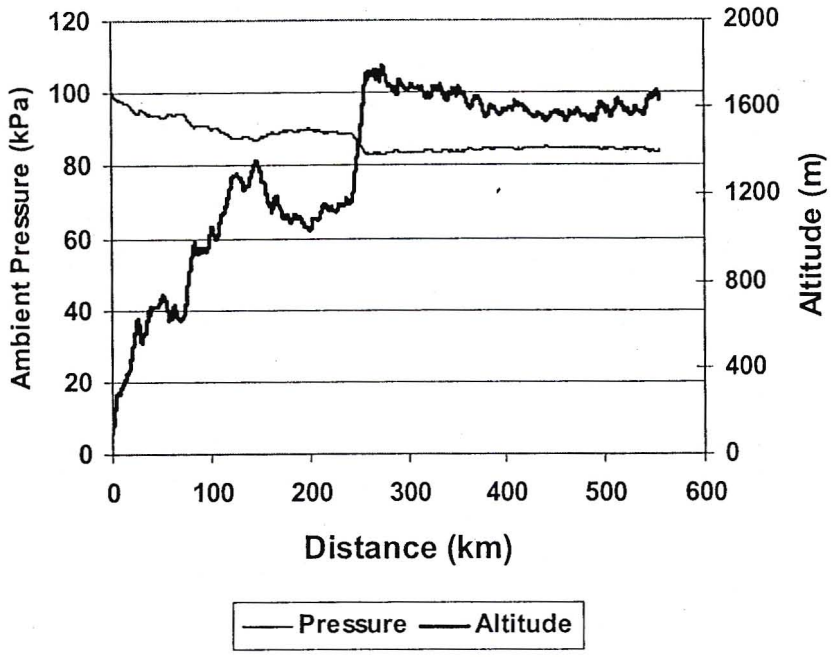

Figure 53 Altitude and ambient pressure across route from Durban to Johannesburg

Due to the different temperature profiles of the nine provinces, the temperature simulated during a route 'jumps' when the vehicle crosses a provincial boundary. This was attributed to the averaging of the temperatures for the whole province. For the present study, the temperature variation across a route was assumed to depend on time and province only. This aspect of the model can be improved at a later stage if the need arises and a more comprehensive temperature database is readily available. During the simulation of a test route a data file was created of the operating parameters during the run. It was therefore possible to observe changes in values such as engine torque or ground speed along the route and these can be summarised. Figure 54 shows histograms of data for speed and torque based on the percentage of maximum. It can be seen from these plots that the engine operates between 80% and 100% of maximum speed and torque for most of the time. This was due to SimTrans attempting to drive the vehicle at the speed limit at all times.

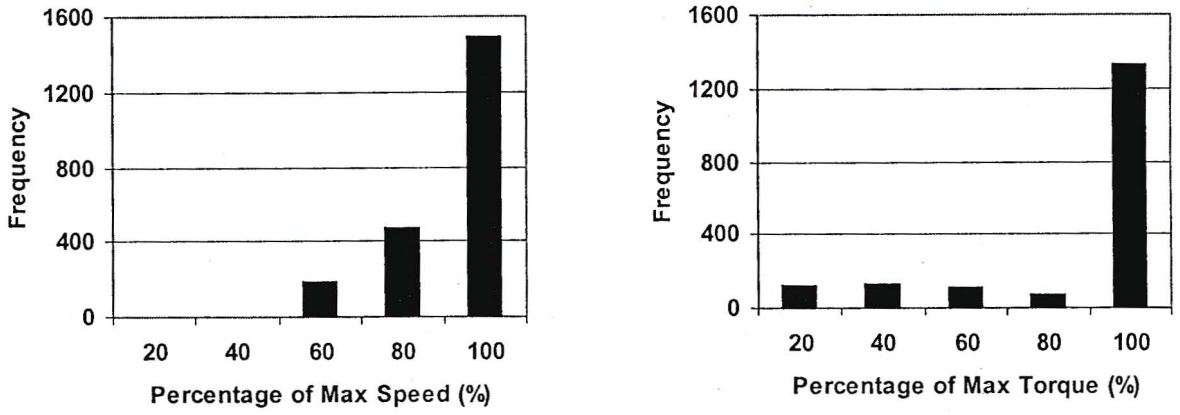

(a) (b)

Figure 54 Histogram showing frequency of data points from SimTrans for (a) speed and (b) torque

Figure 55, figure 56, figure 57 and figure 58 show the rate of emissions in g/s for NOx, HC, particulates and CO respectively. It can be seen that the higher concentration of points occurs at higher power. This was the area where the high torque and speed values occur. It should be noted that the high concentration of emissions at high power was because the engine was operating at these points for long periods of time.

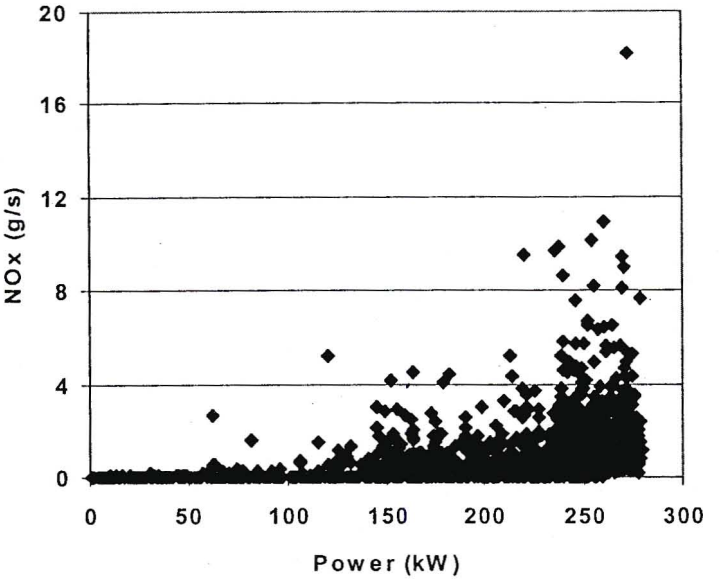

Figure 55 Rate of NOx formation for route from Durban to Johannesburg

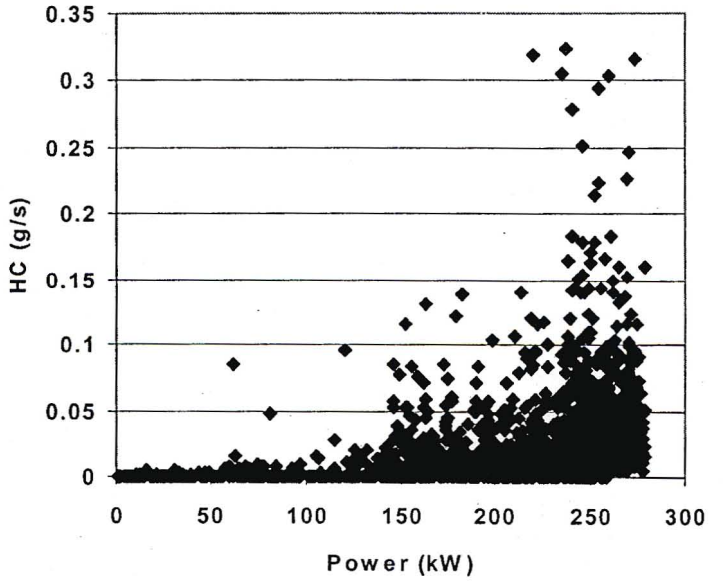

Figure 56 Rate of HC formation for route from Durban to Johannesburg

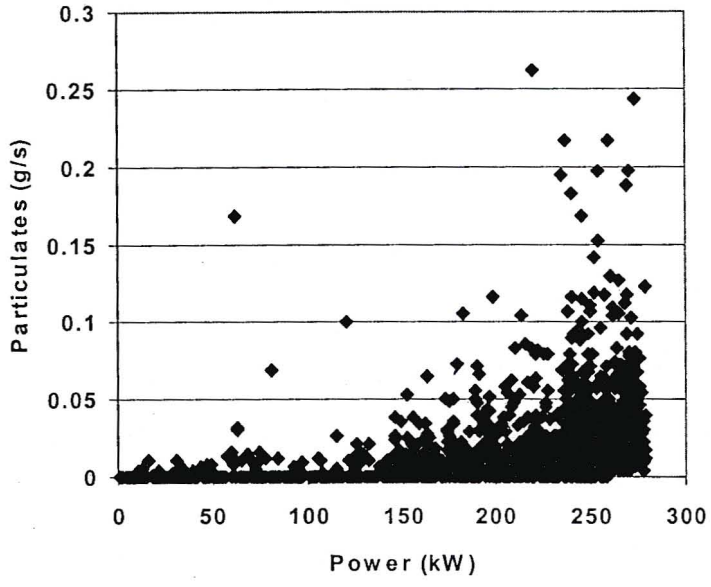

Figure 57 Rate of particulates formation for route from Durban to Johannesburg

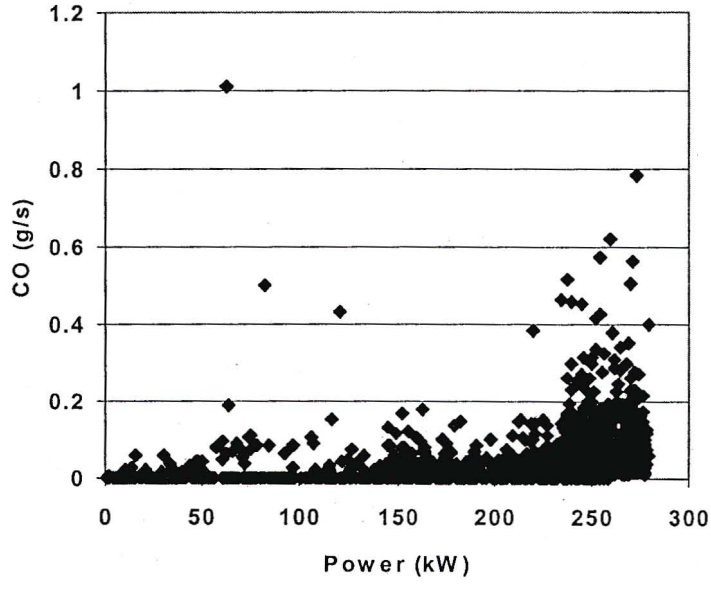

Figure 58 Rate of CO formation for route from Durban to Johannesburg

Table 13 gives a summary of the results for the 3 different scenarios. The unloaded simulation was performed for a gross vehicle mass (GVM) of 14 tonnes. The GVM of the loaded truck was 40 tonnes, which includes a payload of 26 tonnes. The unloaded simulation was performed in January. From table 13 it can be seen that the total emission over the route were approximately 8 times more with the loaded vehicle. This was expected as the load on the engine was directly influenced by the vehicle's payload. The comparison between simulations in January and July for total emissions shows a 1% difference for NOx, 3% for HC, 9% for particulates and 7% for CO.

Table 13 Summary of emissions results for Durban to Johannesburg route

		January	July	Unloaded-Jan
NOx	Total (g)	16974	16802	2201
	Average (g/s)	0.46	0.46	0.11
	Average (g/km)	34.06	33.71	5.34
	Average (g/l)	32.13	31.44	7.60
HC	Total (g)	476	492	59
	Average (g/s)	0.01	0.01	0.003
	Average (g/km)	0.95	0.99	0.14
	Average (g/l)	0.91	0.92	0.20
Particulates	Total (g)	337	368	41
	Average (g/s)	0.01	0.01	0.002
	Average (g/km)	0.68	0.74	0.10
	Average (g/l)	0.66	0.71	0.15
CO	Total (g)	859	917	115
	Average (g/s)	0.02	0.03	0.006
	Average (g/km)	1.70	1.82	0.28
	Average (g/l)	1.83	1.90	0.48

Particulates and CO depict greater differences with respect to km traversed and fuel consumption. The average particulates emitted per kilometre were 9% higher in July than January and 8% higher per litre of fuel. CO emitted per kilometre was 7% higher in July and 4% higher per litre of fuel. These differences were entirely due to the different temperatures experienced during the simulations in July and January.

5.4.2 Cape Town to Johannesburg

The N1 national highway was used as the route along which the vehicle was simulated to travel from Cape Town to Johannesburg. The altitude and pressure profile for this route is shown in figure 59. The vehicle passes through 4 provinces i.e. Western Cape, Northern Cape, Free State and Gauteng covering 1374 kilometres along the way.

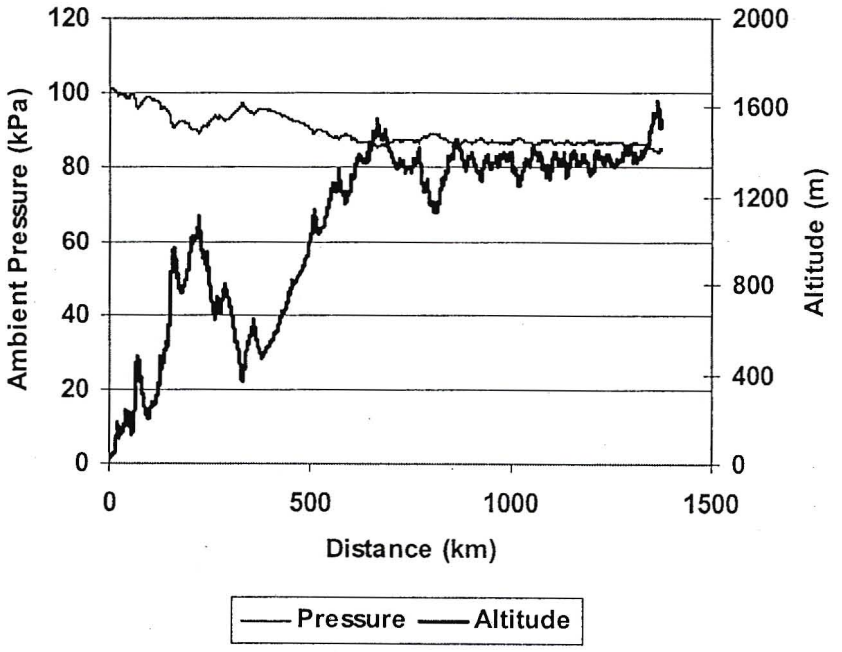

Figure 59 Altitude and ambient pressure across route from Cape Town to Johannesburg

The summary of emissions produced from Cape Town to Johannesburg is shown in table 14. As one would expect, the average values were similar for the Durban to Johannesburg. This was due to the fact that the same vehicle was used for both routes. The total emissions again were much lower for the unloaded vehicle. Difference in total emissions for NOx, HC, particulates and CO were in the order of 0.4%, 2%, 7% and 4% respectively for the 2 months. These differences were less compared with the previous route and can be attributed to the smaller difference in temperatures between the 2 simulations. The Cape Town to Johannesburg route was also, for a larger part of the route at lower altitudes than the Durban to Johannesburg route.

Table 14 Summary of emissions results for Cape Town to Johannesburg route.

		January	July	Unloaded-Jan
NOx	Total (g)	36321	36156	2213
	Average (g/s)	0.45	0.45	0.06
	Average (g/km)	29.5	29.4	3.09
	Average (g/l)	31.4	30.9	4.32
HC	Total (g)	1062	1086	62
	Average (g/s)	0.01	0.01	0.002
	Average (g/km)	0.86	0.88	0.09
	Average (g/l)	0.91	0.92	0.12
Particulates	Total (g)	776	827	48
	Average (g/s)	0.01	0.01	0.001
	Average (g/km)	0.63	0.68	0.09
	Average (g/l)	0.68	0.72	0.10
CO	Total (g)	1893	1978	129
	Average (g/s)	0.02	0.02	0.003
	Average (g/km)	1.56	1.63	0.18
	Average (g/l)	1.82	1.87	0.30

The largest source of pollution was Nox and it received the most attention from researchers. Particulate emissions appear to be small, however they were on a microscopic scale and are a significant pollutant.

6. CONCLUSIONS

As South Africa comes under increasing pressure to conform to the rest of the world in terms of emissions regulations, the need arises for a tool to assess emissions production in the country. Predicting emissions using SimTrans will go a long way in achieving this objective.

Diesel combustion, which is associated with compression ignition engines, is a very complex phenomenon and is highly dependent on the design of the combustion chamber and fuel injection parameters such as pressure, timing and injection rate. The accuracy of a combustion-emissions model to predict emissions will thus be very sensitive to these parameters. However, combustion-emissions modelling is very complex is usually restricted to a qualitative analysis.

A neural network model was included in SimTrans to provide a more accurate estimation of emissions. Simple back propagation architecture was chosen to train the neural network as it is an effective method to use. The results from the neural network showed good correlation with actual measurements provided from the Centre for Automotive Engineering (CAE) in Stellenbosch. These results also compare well with other studies found in the literature. The emissions of NOx, HC, particulates and CO were chosen, as they are the pollutants that cause the greatest concern.

There are large variations in altitude across South Africa, and an algorithm that caters for the effects of ambient conditions on the output of the engine was also included in SimTrans. This algorithm included ambient pressure, which is directly influenced by altitude as well as ambient temperature.

The sensitivity analysis showed the effect of ambient conditions on the engine output. This was significant at high altitudes and lower ambient temperatures. The sensitivity of emissions to ambient conditions was performed at five different speed and torque settings.

The routes from Durban to Johannesburg and Cape Town to Johannesburg were chosen to illustrate the usefulness of the model. The investigation showed a substantial difference in the emissions produced form a loaded vehicle compared to an unloaded one. The model also indicates that there is a difference in emissions that are generated at different temperatures.

The inclusion of the emissions prediction algorithm in the SimTrans model provides useful information for transport managers and environmentalists. Although the model was developed for one engine, a fair estimation can be made if the model is extended to different vehicles that use a similar engine. An intercooled turbocharged engine was chosen for this study as it was representative of the modern engines that are in common use.

6.REFERENCES

Amsden, A. A., P. J. O' Rourke and T. D. Butler. 1989. KIVA-II: A computer program for chemically reactive flows with sprays. Los Alamos National Laboratory Report No. LA-11560-MS.

Atkinson, M. A., T. W. Long and E. L. Hanzevack. 1998. Virtual sensing: a neural network-based intelligent performance and emissions prediction system for on-board diagnostics and engine control. SAE Technical Paper No. 980516. Reprinted from: *Electronic Engine Controls 1998: Diagnostics and Controls* (SP- 1357): 39-52.

Balles, E. N. and J. B. Heywood. 1988. Fuel-air mixing and diesel combustion in a rapid compression machine. SAE Technical Paper No. 880206.

Bazari, Z. 1992. A DI diesel combustion and emission predictive capability for use in cycle simulation. SAE Technical Paper No. 920462. In *Reducing Emissions from Diesel Combustion* (SP-895): 37-61.

Bazari, Z. 1994. Diesel exhaust emissions prediction under transient operating conditions. SAE Technical Paper No. 940666.

Chaffin, C. A. and T. L. Ullman. 1994. Effects of increased altitude on heavy-duty diesel engine emissions. SAE Technical Paper No. 940669.

Choi, C. Y. and R. D. Reitz. 1999. A numerical analysis of the emissions characteristics of biodiesel blended fuels. *Journal of Engineering for Gas Turbines and Power.* 121(1): 31-37.

Clark, D. J. 1996. Model for simulating on-road vehicle performance. Unpubl. MScEng thesis, Dept. of Agric. Eng., Univ. Natal, Pietermaritzburg, R.S.A.

Clark, N. N., C. M. Atkinson, G. J. Thompson and R. D. Nine. 1999. Transient emissions comparisons of alternative compression ignition fuels. SAE Technical Paper No. 1999-01-1117. Reprinted from: *Alternative Fuels for CI Engines* (SP-1412).

Edwards, J. B. 1977. Combustion: The formation and emission of trace species. Ann Arbor Science Publisher Inc., Ann Arbor, Michigan U.S.A.: 21-78.

Fomunung, I., S. Washington and R. Guensler. 1999. A statistical model for estimating oxides of nitrogen emissions from light duty motor vehicles. *Transportation Research Part D* 4(5): 333-353.

Gardner, T. P. 1992. Investigation of the effects of Engine design parameters on diesel combustion and emissions using Taguchi methods. SAE Technical Paper No. 920116.

Han, Z. H., A. Uludogan, G. J. Hampson and R. D. Reitz. 1996. Mechanism of soot and NOx reduction using multiple-injection in a diesel engine. SAE Technical Paper No. 960633.

Hansen, A.C. 1989. A diagnostic quasidimensional model of heat transfer and Combustion in compression ignition engines. Unpubl. PhD thesis, Dept. of Agric. Eng., Univ. Natal, Pietermaritzburg, R.S.A.

Hansen, A. C., R. W. Haines, P. W. L. Lyne and P. Meiring. 1990. Variation in cetane requirements of diesel fuels with altitude. *Journal of Energy R and D in Southern Africa*. 1(1): 7-16.

Haurwitz, B and J. M. Austin. 1944. *Climatology*. USA: McGraw-Hill, Inc.

Heywood, J. B. 1978. Engine combustion modelling-an overview. In *Combustion Modelling in Reciprocating Engines*, ed. J. N. Mattavi and C. A. Amann, 1-39. Plenum Publishing Co. New York, U.S.A.

Heywood, J. B. 1988. *Internal Combustion Engine Fundamentals*. USA: McGraw-Hill, Inc.

Hou, Z.-X and J. Abraham. 1995. Three-dimensional modelling of soot and NO in a direct-injection diesel engine. SAE Technical Paper No. 950608.

Kamimoto, T. and H. Kobayashi. 1991. Combustion processes in diesel engines. *Prog. Energy Combust. Sci* 17: 163-190.

Kouremenos, D. A., C. D. Rakopoulos and D. T. Hountalas. 1997. Multi-zone combustion modelling for the prediction of pollutants emissions and performance of DI diesel engines. SAE Technical Paper No. 970635.

Lilly, L. R. C. 1984. *Diesel Engine Reference Book*. London: Butterworths and Co.,Ltd.

Lipkea, H. L. and A. D. DeJoode. 1994. Direct injection diesel engine soot modelling: formulation and results. SAE Technical Paper No. 940670.

Lipkea, H. L., A. D. DeJoode and S. R. Christenson. 1987. The relationship between nitric oxide and work as influenced by engine operating conditions and combustion system parameters for a direct injection diesel engine. SAE Technical Paper No. 870269.

Logical Designs Consulting, Inc. 1991-1994. Thinks – Neural Networks for Windows Version 1.03dp, La Jolla, CA.

Montgomery, D. T. and R. D. Reitz. 1996. Six-mode cycle evaluation of the effect of EGR and multiple injections on particulate and NOx emissions from a DI diesel engine. SAE Technical Paper No. 960316.

Mullins, P. 1991. New emissions standards: The search for solutions continues. In *High Speed Diesels & Drives*.

Mundt, D. J., K. M. Nauss, A. J. Cohen, D. S. Greenbaum and M. Stilwell. 1999. Diesel emissions and lung cancer: Epidemiology and quantitative risk assessment. *Health Effects Institute. A Special Report of the Institute's Diesel Epidemiology Expert Panel*, Cambridge, MA, U.S.A.

Nauss, K. 1995. Diesel exhaust: A critical analysis of emissions, exposure, and health effects. Summary of a Health Effects Institute (HEI) special report, Cambridge, MA, U.S.A.

Newhall, H. K. 1978. Modelling of engine exhaust emissions-an introductory overview. In *Combustion Modelling in Reciprocating Engines*, ed. J. N. Mattavi and C. A. Amann, 1-39. Plenum Publishing Co. New York, U.S.A.

Norton, P., K. Vertin, N. N. Clark, D. W. Lyons, M. Gautam, S. Goguen and J. Eberhardt. 1999. Emissions from buses with DDC 6V92 engines using synthetic diesel fuel. SAE Technical Paper No. 1999-01-1512.

Rakopoulos, C. D. 1991. Influence of ambient temperature and humidity on the performance and emissions of nitric oxide and smoke of high speed diesel engines in the Athens/Greece region. *Energy conversion and management* 31(5): 447-458.

Reynolds, W. C. 1978. Modelling of fluid motions in engines. In *Combustion Modelling in Reciprocating Engines*, ed. J. N. Mattavi and C. A. Amann, 1-39. New York: Plenum Publishing Co.

SAE, 1990. Measurement of carbon dioxide, carbon monoxide, and oxides of nitrogen in diesel exhaust – SAE Standard J177 APR82. SAE Handbook, Vol. 3. SAE, Warrendale, PA.

SAE, 1992. Engine power test code - spark ignition and compression ignition - gross power rating - SAE Standard J1995. SAE Handbook, Vol. 3. SAE, Warrendale, PA.

Scholl, K. W. and S. C. Sorenson. 1993. Combustion of soybean oil methyl ester in a direct injection diesel engine. SAE Technical Paper No. 930934.

Schulze, R. E. 1997. *South African Atlas of Agrohydrology and -Climatology.* Water Research Commission, Pretoria, Report TT82/96.

Sears, F. W., M. W. Zemansky and H. D. Young. 1987. *University Physics.* 7 th edition. USA: Addison-Wesley Publishing Company.

Takeda, Y. and K. Niimura. 1995. Characteristics of diesel combustion and emissions with a multi-injector system. SAE Technical Paper No. 952511.

Taylor, A. B. 1987. Combustion quality of selected compression-ignition fuels. Unpubl. MScEng thesis, Dept. of Agric. Eng., Univ. Natal, Pietermaritzburg, R.S.A.

Taylor, C. F. 1979. The internal combustion engine in theory and practice. The MIT Press. Chambridge, Massachusetts, U.S.A.: 86-113.

Thinks™. 1994. Logical Designs Consulting Inc. 2015 Olite Court, La Jolla, CA 92037. (858) 459-6236. v1.03.

Uchida, N., Y. Daisho and T. Saito. 1992. The control of diesel emissions by supercharging and varying fuel-injection parameters. SAE Technical Paper No. 920117.

Weidmann, K. and H. Menrad. 1984. Fleet test, performance and emissions of diesel engines using different alcohol-diesel fuel blends. SAE Technical Paper No. 841331. Reprinted from: *Alternative Fuels for Compression and SI Engines* (SP-587).

Xin, J., D. Montgomery, Z. Han and R. D. Reitz. 1997. Multidimensional modelling of combustion for a six -mode emissions test cycle on a DI diesel engine. *Journal of Engineering for Gas Turbines and Power.* 119: 683-692.

Appendix A. Emissions data obtained from engine testing.

Table A-1. Average emissions data accumulated from engine testing.

Speed	Load	Torque	CO	Hcn	NOx	Part. Mass	NOx	CO	HCn	Parts
rpm	%	N.m	ppm	ppm	ppm	mg	g/kW.hr	g/kW.hr	g/kW.hr	g/kW.hr
602.2	25	221.95	268.36	279.53	618.25	1.57	17.85	4.54	2.37	0.8279
599.0	50	447.58	203.99	270.35	1108.61	1.00	15.87	1.68	1.15	0.4337
609.1	75	664.84	169.21	199.96	1562.12	0.65	15.42	0.92	0.57	0.3297
610.4	100	880.32	1358.06	186.53	1826.98	2.1	14.28	6.04	0.41	0.8933
799.8	20	209.86	260.31	262.21	440.21	1.48	14.41	5.09	2.56	1.0991
800.5	40	416.75	197.34	253.50	729.34	1.5	12.32	1.91	1.26	0.5743
800.4	60	637.33	147.89	156.88	1179.10	1.14	13.71	0.94	0.51	0.4116
800.2	80	839.46	203.04	142.21	1740.36	2.3	15.84	1.02	0.36	0.7581
798.6	100	1053.99	590.22	148.08	1958.94	1.45	15.57	2.63	0.32	0.5453
1001.6	20	330.75	246.69	227.60	574.73	3.87	11.01	2.90	1.34	0.6493
999.6	40	675.11	121.35	142.99	1296.26	1.14	13.52	0.69	0.42	0.2586
1009.2	60	983.17	96.76	119.41	1948.99	1.04	15.03	0.40	0.26	0.2408
1006.2	80	1278.77	156.94	124.15	2118.56	1.22	15.76	0.63	0.25	0.2572
995.8	100	1396.67	293.11	144.60	1969.93	1.89	15.70	1.28	0.32	0.5104
1203.1	20	326.24	258.71	174.49	442.88	2.8	8.34	2.94	0.97	0.4824
1201.7	40	651.98	105.42	153.87	952.18	2.52	10.70	0.64	0.50	0.2686
1200.6	60	979.47	64.49	126.18	1706.59	1.96	14.97	0.27	0.30	0.2064
1201.5	80	1302.81	80.28	138.22	2111.89	1.59	16.27	0.30	0.29	0.2114
1199.2	100	1628.60	178.56	122.83	1858.38	2.58	13.74	0.70	0.24	0.2531
1399.87	20	308.83	283.35	271.45	418.45	4.1	8.00	3.37	1.63	0.7164
1401.05	40	623.48	92.46	146.86	920.15	2.02	10.55	0.57	0.49	0.2894
1399.87	60	932.89	77.89	108.00	1332.02	1.34	12.55	0.36	0.27	0.1977
1400.26	80	1249.97	88.27	113.78	1635.82	1.61	13.47	0.36	0.25	0.1613
1401.0	100	1634.46	136.74	138.75	1558.78	2.52	11.98	0.54	0.29	0.2279
1465.47	100	1582.49	154.88	117.05	1454.26	2.23	11.72	0.65	0.25	0.2511
1532.53	100	1559.46	155.00	111.10	1418.39	1.68	11.27	0.66	0.24	0.2398
1601.72	20	315.49	245.19	193.30	457.15	3.18	9.61	2.96	1.15	0.5130
1601.85	40	623.25	113.04	117.97	933.16	1.8	11.24	0.72	0.38	0.2295
1599.74	60	937.54	83.34	106.36	1482.46	1.2	13.95	0.39	0.26	0.1730
1599.52	80	1242.67	82.12	105.78	1844.15	1.34	15.54	0.34	0.23	0.1607
1599.3	100	1564.2	134.90	90.75	1597.89	1.69	12.96	0.57	0.19	0.2102
1799.04	20	296.15	248.02	163.58	402.60	2.22	8.76	3.13	1.00	0.5212
1798.67	40	582.44	134.21	131.58	807.34	1.88	10.59	0.96	0.47	0.3029
1799.04	60	879.24	92.91	135.92	1194.29	2.04	12.31	0.50	0.39	0.1890
1798.46	80	1177.31	89.16	120.46	1459.12	1.64	13.16	0.41	0.29	0.1575
1789.6	100	1474.8	131.45	105.16	1406.60	2.31	12.18	0.59	0.24	0.1969
2008.0	100	1336.5	185.40	154.73	1092.81	1.48	9.85	0.93	0.40	0.2630
2099.1	100	1272.7	197.90	141.82	1036.05	2.18	9.40	1.01	0.36	0.2665

Appendix B. Calculation of gaseous and particulate emissions.

The final reported test results of the gaseous emissions are derived through the following steps:

- The exhaust gas mass flow rate G_{exh} is determined by the following equation:

$$G_{exh} = G_{air} + G_{fuel} \quad \text{(B-1)}$$

where : G_{fuel} is the fuel flow (kg/h)

G_{air} is the air flow (kg/h)

- When applying G_{exh} the measure concentrations are converted to a wet basis according to the following relationship:

$$\text{ppm (wet basis)} = \text{ppm (dry basis)} \times (1\text{-}1.85\ G_{fuel}/\ G_{air}) \quad \text{(B-2)}$$

- To correct for humidity the values of the oxides of nitrogen shall be multiplied by the following humidity correction factor:

$$\frac{1}{1 + A(7H - 75) + 1.8B(T - 302)} \quad \text{(B-3)}$$

where :

$$A = 0.044\frac{G_{fuel}}{G_{air}} - 0.0038$$

$$B = -0.116\frac{G_{fuel}}{G_{air}} + 0.0053$$

T = temperature of the air in K

H = humidity of the inlet air in grams of water per kilogram of dry air in which:

$$H = \frac{6.211 \cdot R_a \cdot P_d}{P_B - P_d \cdot R_a \cdot 10^{-2}} \quad \text{(B-4)}$$

where : R_a = relative humidity of the ambient air expressed in %

P_d = saturation vapour pressure at ambient temperature expressed in kPa

P_B = atmospheric pressure expressed in kPa

- The pollutant mass flow for each test point is calculated as follows:

$$NOx_{mass} = 0.001587 \times NOx_{conc} \times G_{exh} \quad \text{(B-5)}$$

$$CO_{mass} = 0.000966 \times CO_{conc} \times G_{exh} \quad \text{(B-6)}$$

$$HC_{mass} = 0.000478 \times HC_{conc} \times G_{exh} \quad \text{(B-7)}$$

Particulate mass flow for each test point is calculated in the following manner:

$$Parts_{mass} = Parts_{fil} \times q \times G_{exh} \times M_{sam} \quad \text{(B-8)}$$

where :

$Parts_{fil}$ = mass of particulates as measured from the filters (mg)

M_{sam} = total mass of exhaust gas (kg)

$q = (CO_{2\ raw} - CO_{2\ amb})/(CO_{2\ tunnel} - CO_{2\ amb})$

where :

$CO_{2\ raw}$ = CO_2 measured at the point where NOx and HC was analysed

$CO_{2\ amb}$ = CO_2 measured from the ambient air

$CO_{2\ tunnel}$ = CO_2 measured in the dilution tunnel

Appendix C. Regression results for boost pressure used in SimTrans.

Table C-1. Speed, torque and boost pressured data used for regression analysis.

Speed (rpm)	Torque (Nm)	Boost Pressure (kPa)
602.2	221.95	0.59
599.0	447.58	3.27
609.1	664.84	7.21
610.4	880.32	12.65
799.8	209.86	1.64
800.5	416.75	5.81
800.4	637.33	11.75
800.2	839.46	17.93
798.6	1053.99	25.64
1001.6	330.75	5.95
999.6	675.11	15.55
1009.2	983.17	31.50
1006.2	1278.77	47.65
995.8	1396.67	61.97
1203.1	326.24	5.72
1201.7	651.98	21.74
1200.6	979.47	39.81
1201.5	1302.81	62.53
1199.2	1628.60	87.70
1399.87	308.83	6.94
1401.05	623.48	25.60
1399.87	932.89	42.04
1400.26	1249.97	66.22
1401.0	1634.46	97.27
1465.47	1582.49	99.38
1532.53	1559.46	101.34
1601.72	315.49	10.66
1601.85	623.25	25.80
1599.74	937.54	46.64
1599.52	1242.67	71.47
1599.3	1564.2	103.4
1799.04	296.15	14.18
1798.67	582.44	30.51
1799.04	879.24	53.60
1798.46	1177.31	78.11
1789.6	1474.8	107.6
2008.0	1336.5	109.4
2099.1	1272.7	107.9

To obtain a better regression, higher order variables were introduced. The results of the regression analysis are shown in table C-2.

Table C-2 Results of regression analysis

Variable	Coefficient	Std.error of Coefficient	Number of Observations
Constant	2.849244	7.544678	38
Speed	0.000417	0.01342	38
Torque	-0.03164	'0.012616	38
$Speed^2$	-2.4E-06	5.59E-06	38
$Torque^2$	3.6E-05	8.51E-06	38
Speed*Torque	2.52E-05	1.55E-05	38
$Speed^2$*Torque	1.09E-08	5.94E-09	38
$Torque^2$*Speed	-9.7E-09	6.11E-09	38

An R Squared of **0.997806** was achieved with the above regression variables.